Epicardium-derived matricellular protein SPARC as a potential mediator of the switch from sprouting angiogenesis to arterialisation in coronary vessels



Polen Bareke

Linacre College, University of Oxford

Department of Physiology, Anatomy and Genetics

A thesis submitted for the degree of
MSc by Research

Trinity 2025

Table of Contents

Acknowledgements *12*

Abstract *13*

1 Introduction *15*

1.1 Coronary artery disease and the need for novel therapies **15**

1.2 Overview of murine coronary vessel development **16**

1.3 Origins of the primary coronary plexus endothelium **17**

1.4 Development of coronary arteries from a vein: the sinus venosus **21**

1.5 Role of cell cycle control in arteriovenous specification **22**

1.6 Epicardial cues in regulating the development of sinus venosus-derived coronary vasculature **25**

1.7 Myocardial infarction **26**

1.8 Neovascularisation following myocardial infarction **28**

1.9 Preliminary findings from the Smart laboratory **29**

1.10 SPARC **31**

1.11 SPARC in angiogenesis **32**

1.12 SPARC in myocardial infarction **36**

1.13 SPARC and VEGF-A **38**

1.14 SPARC and TGF-β **40**

1.15 Thesis rationale **42**

2 Methods & Materials *51*

2.1. Animal husbandry 51

2.1.1 Mouse lines 51

2.1.2 Myocardial infarction by permanent ligation of the left anterior descending coronary artery in mice 51

2.2 Cell culture 52

2.2.1 Maintenance of mouse epicardial cell line 52

2.2.2 Epithelial-to-mesenchymal transition assay 53

2.3 Molecular techniques 54

2.3.1 Reverse-transcription quantitative PCR 54

2.3.2 Western Blot 56

2.4 Primary cell culture 57

2.4.1 Explant culture 57

2.4.2 Explant treatment 58

2.5 Imaging sample preparation, acquisition and analysis 59

2.5.1 Immunocytochemistry 59

2.5.2 Immunofluorescence on SV explants 59

2.5.3 Cryosections 60

2.5.4 Immunohistochemistry (IHC) 60

2.5.5 Masson's Trichrome staining 61

2.5.6 Whole-mount tissue clearing and immunostaining 61

2.5.7 Microscopy 64

2.5.8 Image analysis 65

2.5.9 Statistical analysis 66

3 Results 68

3.1 SPARC is expressed in regions of actively remodelling coronary arteries 68

3.2 SPARC expression in the epicardial lineage positively correlates with coronary endothelial cells 70

3.3 SPARC is synthesised and accumulated in the epithelial state before its secretion in mesenchymal derivatives 71

3.4 SPARC augments VEGF-A-induced angiogenesis, while antagonising arterialisation, in sinus venosus-derived coronary endothelial sprouts 73

3.5 SPARC and TGF-β1 bias sinus venosus-derived endothelial cells towards an arterial identity 75

3.6 Epithelial cues induce angiogenesis in sinus venosus-derived endothelial sprouts 77

3.7 Acute delivery of SPARC and TGF-β1 post-MI may increase arterialisation and mature arterial coverage in the infarct/border zone 78

4 Discussion 98

4.1 Epithelial epicardial state favours SPARC synthesis and intracellular accumulation, priming for secretion and proteolytic activation 99

4.2 SPARC may promote VEGF-A-driven angiogenesis 102

4.3 SPARC promotes arterial specification via TGF-β1 during coronary vessel development and may support vessel growth and arterialisation post-myocardial infarction 106

4.4 Limitations and future directions 112

5 Conclusions 115

6 Supplementary materials 121

7 References 126

List of Tables

Table 1. Summary of studies examining the effects of SPARC on angiogenesis across developmental, tumour, injury, and immune-mediated contexts 36

Table 2. Primers used for RT-qPCR.....55

Table 3. Primary antibodies..... 62

Table 4. Secondary antibodies.....63

Appendix Table 1. Primers used for testing housekeeping genes for RT-qPCR.....121

List of Figures

Figure 1. Preliminary findings from the Smart laboratory……..…46

Figure 2. Structural domains of SPARC and its peptides, and proposed mechanisms by which they modulate angiogenesis……..…..…49

Figure 3. Characterisation of SPARC expression in the developing heart and embryo at E11.5-E15.5……..……..……82

Figure 4. SPARC closely associates with remodelling coronary arteries……..……84

Figure 5. SPARC expression in the epicardial lineage positively correlates with coronary endothelial cells……..……..……..……86

Figure 6. SPARC is synthesised and accumulated in the epithelial state before its secretion in mesenchymal derivatives……..……88

Figure 7. SPARC augments VEGF-A-induced angiogenesis, while antagonising arterialisation, in sinus venosus-derived coronary endothelial sprouts……..……91

Figure 8. SPARC and TGF-β1 cooperate to bias sinus venosus-derived endothelial cells towards an arterial identity……..……..……93

Figure 9. Epithelial epicardial cues induce angiogenesis in sinus venosus-derived endothelial sprouts……..……95

Figure 10. Acute delivery of SPARC with TGF-β1 post-MI increases arterialisation and mature arterial coverage in the infarct/border zone……..……97

Figure 11. Proposed model of SPARC and TGFβ-1-induced arterialisation of sinus- venosus-derived coronary vessel sprout……..……117

Figure 12. Summary of current evidence on the role of SPARC in cardiac repair post-myocardial infarction and proposed model of SPARC and TGFβ-1-induced arteriogenesis in the infarcted heart……120

Appendix Figure 1. Expression profiles of candidate housekeeping genes in the mouse epicardial cell (MEC1) line during epicardial epithelial-to-mesenchymal transition.....122

Appendix Figure 2. 123

List of abbreviations

aa – amino acid

AKT – RAC (Rho family)-alpha serine/threonine-protein kinase

ALK – activin-like kinase

Apj – apelin receptor

Apln – apelin receptor

AVM – arteriovenous malformation

BMI – body mass index

BMP – bone morphogenetic protein

BSA – bovine serum albumin

CAD – coronary artery disease

CAM – chorioallantoic membrane

CANX – calnexin

CCBE1 - calcium-binding EGF- like domain 1

CD31 (PECAM-1) – platelet endothelial cell adhesion molecule 1

CD4 – cluster of differentiation 4

CD68 – cluster of differentiation 68

CD8 – cluster of differentiation 8

cDNA – complementary DNA

CEC – coronary endothelial cell

COUP-TFII – COUP transcription factor 2

CT – cycle threshold

CTNI – cardiac troponin I

CUBIC – clear, unobstructed brain/body imaging cocktails and computational analysis

CVP – coronary vascular population

CX37 – connexin-37

CX40 – connexin-40

CXCR4 – C-X-C chemokine receptor 4

CYR61 – cysteine-rich angiogenic inducer 61

DAPI – 4', 6-diamidino-2-phenylindole

Dll4 – delta-like canonical Notch ligand 4

DMSO – dimethyl sulfoxide

DPX – dibutylphthalate polystyrene xylene

E – embryonic day

EBM – endothelial basal medium

EC – endothelial cell

ECM – extracellular matrix

EGM – endothelial growth medium

ELA – elabela

EMT – epithelial-to-mesenchymal transition

EPDC - epicardium-derived cells

Ephb2 – ephrin B2

Ephb4 – ephrin type-B receptor 4

EPI – epithelial

epiEMT – epicardial epithelial-to-mesenchymal transition

ER – endoplasmic reticulum

ERG – E26-transformation-specific-related gene

ERK - extracellular signal-regulated kinase

EV – extracellular vesicle

FBS – foetal bovine serum

FGF-2 – fibroblast growth factor 2

GAPDH – glyceraldehyde-3-phosphate dehydrogenase

HRP – horseradish peroxidase

HUVECs – human umbilical vein endothelial cells

iDISCO – immunolabelling-enabled three-dimensional imaging of solvent-cleared organs

JNK – c-Jun N-terminal kinase

LAD – left anterior descending artery

LFQ – label-free quantification

MAPK - mitogen-activated protein kinase

MEC1 – mouse epicardial cell line

MEF2 – myocyte-specific enhancer factor-2

MES – mesenchymal

MI – myocardial infarction

MMP – matrix metalloproteinase

mTOR – mammalian target of rapamycin

NFATC1 – nuclear factor of activated T-cells 1

NPR3 – natriuretic peptide receptor 3

NR2F2 – nuclear receptor subfamily 2, group F, member 2

NRP – neuropilin

OCT – optical cutting temperature compound

P – postnatal day

P/S – penicillin/streptomycin

PBS – phosphate-buffered saline

PBS-T - phosphate-buffered saline with Triton X-100

PDGFB – platelet-derived growth factor subunit B

PEO – proepicardial organ

PI3K – phosphatidylinositol 3-kinase

PPIA – peptidyl-prolyl cis–trans isomerase A

PVDF – polyvinylidene fluoride

RBPJ – recombination signal binding protein for immoglobulin kappa J region

RN18 – 18S ribosomal RNA

RT – room temperature

RT-qPCR – reverse transcription-quantitative polymerase chain reaction

SAPK – stress-activated protein kinase

scRNA-seq – single-cell RNA sequencing

SD – standard deviation

SHP-1 – Src homology 2 domain–containing protein tyrosine phosphatase 1

SM-MHC – smooth muscle-myosin heavy chain

SMAD – mothers against decapentaplegic homolog 2

SMC - smooth muscle cell

SPARC – secreted protein, acidic and rich in cysteine

STAT3 – signal transducer and activator of transcription 3

SV – sinus venosus

TENA – tenascin-C

TGF-β – transforming growth factor-β

TβR – TGF-β type receptor

VE-cadherin – vascular endothelial cadherin

VEGF-A – vascular endothelial growth factor A

VEGFR1 - vascular endothelial growth factor A receptor 1

VEGFR2 - vascular endothelial growth factor A receptor 2

YWHAZ - tyrosine 3-monooxygenase/tryptophan 5-monooxygenase activation protein zeta

ZEB – zinc finger E-box-binding homeobox

αSMA or **ACTA2** – alpha-smooth muscle actin

Acknowledgements

Firstly, I would like to thank my primary supervisor, Professor Nicola Smart, for giving me the opportunity to undertake this research in her lab and for bringing Dr Jacinta Kalisch-Smith on board for my project as a secondary supervisor. I am especially grateful to them both for teaching me embryonic heart dissections, a skill which I have come to greatly enjoy, and for their supportive supervision style, which encouraged independence while providing intellectual guidance through my Master's project.

I would also like to thank the members of the Smart Group, particularly Lili, for her generosity with her time in teaching me molecular biology techniques and guiding me through experimental design. Outside the lab, she, together with Esra and Konstantinos, has been very kind, enthusiastic and supportive of me. I am also grateful to the other members of the Cardio Floor at the IDRM, particularly those who kindly offered academic advice or shared reagents whenever I needed.

I would also like to extend my thanks to the patients I have met during my pre-clinical medical training, whose experiences have been a constant reminder of the importance of research in improving human health.

Finally, I owe all the accomplishments in my life to my parents, Çiğdem and Hüray, for supporting my choices, even if it meant they had to make immense financial and emotional sacrifices. I am also thankful to my partner, Ethan, and my friends for their encouragement and consistent support throughout this degree.

My master's degree was funded by the A.G. Leventis Foundation and Linacre College, of which I was a proud member, whilst this work was funded mainly by the British Heart Foundation through my supervisors, whose contributions to cardiovascular research I deeply value.

Abstract

The survival of ischaemic cardiomyocytes following myocardial infarction relies on new coronary vessel formation, in which the epicardium plays a central role. Between embryonic day (E) 11.5 and E13.5, the epicardium undergoes epithelial-to-mesenchymal transition (EMT), giving rise to mural cells and adventitial fibroblasts and acting as a source of growth factors and matrix proteins that facilitate coronary vessel formation. This begins at E11.5 with EC sprouting from the sinus venosus, ultimately giving rise to coronary arteries and veins. Given that SV sprouting and epicardial EMT coincide, their developmental transitions may be temporally coordinated.

Mass spectrometry analysis of EMT-conditioned media performed in our group from mouse epicardial cells identified several matricellular proteins to be upregulated in the mesenchymal state, with SPARC (Secreted Protein, Acidic and Rich in Cysteine) showing the most significant differential expression. SPARC is implicated in cellular processes such as angiogenesis, proliferation and migration, which are essential for proper coronary vasculature formation and maturation. Yet, its role in coronary vessel development remains unexplored. The activity of SPARC relies on its ability to modulate growth factor receptor availability and receptor activation, such as VEGF-A and TGF-β1, both of which are likewise upregulated in mesenchymal epicardial cells and are known to regulate EC proliferation, angiogenesis and arterialisation. We therefore hypothesised that SPARC facilitates the transition from angiogenesis to arterialisation in coronary vessels by modulating these signalling pathways.

To address this, we have characterised SPARC expression between epithelial and mesenchymal states of the developing epicardium using both *in vitro* and *in vivo* approaches and found that it is transcriptionally upregulated and accumulates intracellularly in epithelial cells, priming its secretion upon transition to the mesenchymal state. Here, it modulates VEGF-A and TGF-β1 signalling to promote coronary angiogenesis and arteriogenesis,

respectively, as demonstrated using an *in vitro* model of coronary angiogenesis from E11.5 connexin-40-EGFP mouse SV explants. The arteriogenic effect from the combined treatment of TGF-β1 and SPARC was beneficially recapitulated in an *in vivo* murine model of myocardial infarction, without inducing excessive fibrosis.

Taken together, these findings reveal a novel mechanism of arterial specification involving SPARC–TGF-β1 signalling in coronary vessels during development and after myocardial injury. By coupling epicardial EMT to the switch from angiogenesis to arteriogenesis in sinus-venosus-derived coronary vessels, this work provides a conceptual framework for harnessing extracellular cues to augment neovascularisation post-infarction, where pro-angiogenic therapies have so far shown limited success.

1 Introduction

1.1 Coronary artery disease and the need for novel therapies

The vasculature is among the first organ systems to become functional during vertebrate development, rendering its correct formation essential for continued embryogenesis [1]. Most cells in our body reside within a few hundred micrometres of a blood vessel, reflecting its crucial role as a conduit for oxygen, nutrients, and immune cells to vital organs [2]. In the heart, this distance reduces to as little as 2 µm between cardiomyocytes and neighbouring capillaries of the coronary circulation [3], owing to the high metabolic demand of the myocardium, which can only be met through its dedicated vascular network. As such, vascular dysfunction is a central feature of many chronic diseases, most notably coronary artery disease (CAD) [4].

CAD is the leading cause of mortality worldwide, characterised by the accumulation of atherosclerotic plaques capped by a fibrous layer, the rupture of which exposes thrombogenic material to the circulation, leading to a thrombus and the subsequent occlusion of a coronary artery [5]. Given that coronary blood flow accounts for 5% of total cardiac output and is coupled to the metabolic requirements of the myocardium [6], complete occlusion of a CA induces myocardial infarction (MI) and the loss of approximately one billion cardiomyocytes [7, 8].

Early reperfusion therapies, involving angioplasty and thrombolysis, can effectively re-establish the coronary blood flow to major coronary vessels during acute MI [9]. Yet, 30% of patients may still develop the 'no-reflow' phenomenon, to which embolisation of atherosclerotic debris leading to occlusion of the downstream microvasculature is a contributing factor [10, 11]. With prolonged ischaemia and reperfusion injury further impacting endothelial cell (EC) survival within the ischaemic core, patients bear an increased risk of subsequent major adverse cardiac events, including progression to heart failure [12, 13]. Although the heart induces an intrinsic neovascularisation response upon ischaemia, its speed and magnitude are insufficient to prevent extensive myocardial injury following coronary artery occlusion, necessitating the development of novel therapeutic strategies to revascularize the ischaemic

human heart [14].

To date, phase II and III clinical trials evaluating the efficacy of human recombinant pro-angiogenic growth factors, including vascular endothelial growth factor A (VEGF-A) and fibroblast growth factor 2 (FGF-2), have failed to improve coronary perfusion and cardiac function in patients with CAD [15, 16]. These therapies were developed on the assumption that their intramyocardial infusion, as well-established pro-angiogenic factors, would drive angiogenesis in coronary vessels, defined as the formation of new vessels from pre-existing ones. However, even if sufficient angiogenesis were achieved, it is unlikely to re-establish the hierarchical vascular network necessary for adequate myocardial perfusion without accompanying arteriogenesis, the maturation and remodelling of nascent vessels into fully developed arteries [14]. This gap may reflect our incomplete understanding of the mechanisms underlying coronary vessel development, which can be advanced based upon insights from the developing embryo, the blueprint for establishing a functional coronary vascular network.

1.2 Overview of murine coronary vessel development

During early embryogenesis, the primitive heart tube consists solely of an inner endocardial and outer myocardial layer, allowing its thin myocardial wall to be sufficiently oxygenated by simple diffusion across the endocardial layer. As the myocardium increases in size, however, diffusion becomes impractical, initiating the formation of its coronary vasculature at embryonic day (E) 11.5 in the widely studied mouse [17, 18], which corresponds to approximately seven to eight weeks of gestation in humans [19].

The development of coronary vessels follows the same pattern as systemic vasculature, beginning with vasculogenesis, the *de novo* assembly of endothelial tubes from mesoderm-derived EC progenitors [1]. Initially, coronary vessels consist of a single endothelial layer, the tunica intima, which forms a primitive vascular plexus, a highly branched network of similarly sized vessels [20]. This plexus subsequently expands over the ventricles through angiogenesis, achieved either by intussusception, to divide the vessel into two, or by sprouting to form new

branches, ultimately invading the underlying myocardium. For this vascular network to be functional, heterogeneous EC subpopulations must then emerge, which involves the acquisition of arterial and venous identities, termed arteriovenous specification. Shear stress resulting from the onset of blood flow subsequently induces vessel remodelling [21], which includes modifications to the vessel diameter, branching or wall thickness. Next, the vessels mature and stabilise, which can be achieved via the deposition of extracellular matrix (ECM) proteins to form a basement membrane [22]. Then, further structural support is provided through the recruitment of mural cells, including smooth muscle cells in arteries and pericytes in capillaries, forming the middle layer of the coronary vessels, the tunica media [23]. The outermost layer, the tunica externa, of larger arterial conduits also becomes surrounded by adventitia composed of connective tissue and fibroblasts [24, 25], remodelling the plexus into a hierarchical coronary vascular network comprising arteries, veins and capillaries. The importance of vascular remodelling is reflected in the embryonic lethality that is consistently observed with vascular patterning defects [26].

Coronary endothelial cells (CECs) form a distinct endothelial population in the developing heart, rendering an understanding of their developmental origins essential. Although structural differences in coronary vasculature exist between rodents and humans, such as the coronary arteries being intramyocardial in mice but subepicardial in humans, many processes underlying coronary vessel formation observed in these model systems appear to be largely conserved in humans [27, 28].

1.3 Origins of the primary coronary plexus endothelium

The embryonic origins of the coronary endothelium have been debated for over a century, particularly as new experimental techniques and models have emerged. Traditionally, it was believed that the coronary endothelium formed through angiogenic sprouting from the aorta [29]. However, subsequent quail-chick transplantation studies have supported a reverse model in which coronary vessels arise from the primitive coronary plexus of the developing heart and

subsequently connect to the aorta, initiating blood flow only after formation of the primitive coronary network [30-33]. Several years after these avian studies, the lack of mammalian data on whether coronary orifice formation occurs through coronary vessels growing into the aortic wall was addressed [34]. This gap largely reflected the absence of genetic tools capable of distinguishing coronary from aortic endothelium, which was overcome through the use of an inducible Cre-based lineage-tracing strategy. Using this approach, the authors demonstrated that coronary artery stems and orifices are predominantly derived from CECs that invade the aorta to communicate with the systemic circulation [34].

Later, studies using retroviral labelling and fluorescent cell tracking were the first to suggest an extracardiac source for CECs. Heterotopic transplantation of the proepicardial organ (PEO), a transient protrusion of coelomic mesothelium near the septum transversum, in quail-chick chimeras later implicated the PEO as a contributor to the coronary endothelium [35, 36]. While these studies were seminal in defining the PEO as the progenitor of the epicardium, outer layer of the heart, the proepicardial origin model was challenged upon the introduction of Cre recombinase-mediated progenitor cell lineage tracing [37, 38], suggesting that CECs originate from sources other than the aorta or the PEO/epicardium.

Using whole-heart histological analysis of *Apelin-nLacZ* knock-in mice between E11.5 and E15.5, in which nuclear β-galactosidase is selectively expressed in CECs but not in the endocardium, Red-Horse et al. [17] proposed that CECs originate from the sinus venosus (SV), a primitive vein located on the dorsal surface of the embryonic heart, and invade the myocardium in an ‘outside-in’ manner. At E11.5, the coronary plexus first appeared on the dorsal surface of the heart and expanded circumferentially around the atrioventricular canal to reach the outflow tract. Between E12.5 and E14.5, this plexus expanded caudally to populate the entire dorsal surface, including the interventricular groove by E13.5. By E15.5, the coronary plexus also covered the ventral surface of the heart. The authors further performed clonal analysis using an EC-specific *VE-cadherin*^{CreER} transgene, demonstrating that the majority of coronary artery cells were clonally related to SV-derived ECs. This established the SV as the principal contributor to coronary vessels and arteries during E13.5–E14.5. In

addition, the endocardium was identified as a minor secondary source of CECs, based on the observation that endocardial buds penetrate the myocardium and subsequently integrate into the coronary plexus at E14.5 [17].

Similarly, endocardial-derived blood islands were shown to penetrate the myocardium and merge with the SV-derived plexus, a contribution supported by *Nfatc1*^{Cre} mouse reporter line labelling the murine endocardium [39]. Here, endocardial-derived ECs were shown to populate the ventricular septum and ventral portions of the heart in an 'inside-out' pattern at E11.5-E13.5, complementing the SV-derived contribution to the coronary plexus.

A subsequent study by Chen et al. [40] refined the model that the coronary vasculature arises from two developmental origins, demonstrating that the sinus venosus and endocardium contribute to complementary regions of the coronary network in an inversely proportional manner along the dorsal–ventral axis. By combining whole-mount imaging across five cardiac domains at E15.5-E16.5, with fate mapping using *Nfatc1*^{CreER} and *Apj*^{CreER} mouse lines, marking SV- and endocardium-derived ECs, respectively, they quantified the relative contributions of each source to the developing coronary endothelium. This revealed that SV-derived CECs predominate on the dorsal and right lateral surfaces of the heart, whereas endocardium-derived CECs contribute most prominently to the left lateral, ventral, and septal regions.

Extending these findings, Tian et al. [41] proposed that coronary vasculature forms through successive phases, with ECs arising at distinct developmental time points contributing to different regions of the coronary plexus, which they called coronary vascular populations (CVP). Using tamoxifen-inducible *Apln*^{CreER} lineage tracing, a single tamoxifen administration at E10.5 was shown to label early coronary sprouts and their progeny, defining a first CVP, which contributed to nascent coronary vessels by E15.5 and, postnatally (P3–P7), remained largely confined to the outer myocardial wall. During this period of myocardial compaction, additional coronary vessels lacking *Apln*^{CreER} labelling emerged within the inner myocardial wall, indicating a distinct CEC origin. Consistent with this, tamoxifen administration at E13.5 revealed a second CVP, which contributed disproportionately to vascularisation of the

interventricular septum during postnatal myocardial compaction, with further expansion evident at P3 and P7. A third wave was subsequently identified in the neonatal period and was similarly associated with trabecular compaction and inner myocardial vascularisation. Complementary lineage tracing using *Nfatc1*^{CreER} mice, with tamoxifen administered at E8.0–E8.5 to label pre-coronary endocardial cells, demonstrated that the second CVP was predominantly endocardium-derived. Together, these data suggested that coronary vascular development proceeds through multiple waves, whose contributions remain spatially segregated in the adult heart, with postnatal coronary expansion driven largely by the later-arising endocardial-derived population.

However, interpretation of these findings was complicated by the expression of *Nfatc1* in the SV at E8.0-E8.5 [42], such that tamoxifen induction at this stage could not distinguish embryonic from neonatal coronary progenitors [41]. More recent work addressed this limitation using *Npr3*^{CreER}, as it is predominantly expressed in endocardial cells at birth or postnatal day 0 [43], thereby allowing temporal restriction of SV labelling. Using this approach, Lu et al. [43] demonstrated that ventricular endocardial cells present at E17.5–P0 do not serve as progenitors for postnatal coronary vessels, thereby excluding de novo angiogenesis from ventricular endocardium as the mechanism underlying neonatal coronary expansion. Instead, they showed that augmentation of the coronary vasculature occurs during the perinatal period (E16.5–P2) through angiogenic expansion of pre-existing coronary plexuses within the inner myocardial wall, a capacity that is lost prior to birth [43].

Collectively, these studies outline a model in which SV-derived ECs dominate early coronary plexus formation on the dorsal and right lateral surfaces of the heart, whereby these nascent endothelial populations retain the potential to differentiate into coronary arteries, as well as other CEC subtypes. Hence, it is important to understand the developmental pathways of SV sprouting, which may directly influence the mechanisms underlying the specification of coronary vessels into arteries.

1.4 Development of coronary arteries from a vein: the sinus venosus

Following the formation and expansion of the primitive coronary plexus, CECs must undergo arteriovenous specification to match the metabolic demands of the myocardium. Studies from multiple organ systems have consistently shown that arteries arise from venous ECs [22], rendering arterial-venous plasticity a common theme in development, including during murine CA formation [17, 44, 45].

Single-cell RNA sequencing (scRNA-seq) of SV–derived ECs isolated from E12.5 mouse hearts using *Apj*^{CreER} lineage tracing enabled Su et al. [46] to characterise the transcriptional programmes underlying the venous-to-arterial fate transition in developing coronary sprouts. Earlier work by Red-Horse et al. had shown, using *ephrinB2*-lacZ and other arterial markers, that as endothelial sprouts emerge from the sinus venosus at E11.5, expression of venous markers progressively declines, indicating loss of venous identity, and that by E12.5, upon invasion of the myocardium, these vessels begin to express arterial markers such as *ephrinB2* and subsequently assemble into mature coronary arteries [17]. The novelty of the study by Su et al. [46] lay in demonstrating that scRNA-seq can resolve the dynamic transcriptional states associated with venous dedifferentiation and arterial redifferentiation at single-cell resolution, transitions that had previously been obscured by bulk analyses of heterogeneous endothelial populations.

Gene set enrichment analysis revealed that as the SV-derived angiogenic sprouts migrate across the dorsal ventricular surface, they gradually downregulate venous markers such as *Ephb4* (Ephrin type-B receptor 4), while upregulating arterial markers including *Efnb2* (Ephrin B2). A subset of these CECs then surpasses a transcriptional threshold, giving rise to ‘pre-arterial’ cells that display a transcriptional profile resembling that of fully mature coronary arteries, including *Connexin-40* (*Cx40*) [46]. *Notch1*, the expression of which is induced by blood flow [47], was not expressed in pre-arterial cells [46], confirming that the acquisition of an early arterial fate occurs prior to the onset of coronary blood flow. Together, these findings indicate that the venous-to-arterial switch in CECs occurs via a plexus intermediate, as corroborated by an arterial transcriptional enhancer-reporter mouse model demonstrating that a distinct

arterial transcriptional programme becomes activated during the venous-to-arterial fate transition [48].

Further analysis of the E12.5 mouse *Apj*^{CreER}-lineage traced cells identified two main subpopulations: one forming a continuum between SV progenitors and coronary vessels, and another linking venous valves to coronary vessels [46]. The SV progenitor-coronary vessel population showed higher expression of proliferation-associated genes relative to the valve-like cluster, implicating cell-cycle activation in the loss of venous identity during arterial specification [46]. In addition, overexpression of *Nr2f2* (encoding for COUP-TFII, a master regulator of venous identity) inhibited pre-artery specification, not by directly repressing arterial markers or inducing venous markers, but by upregulating the expression of cell cycle genes [46]. This role of the cell cycle in regulating arteriovenous identity has also been observed in other vascular beds [49-51], implying a general mechanism for the specification of arterial endothelium from a venous origin.

1.5 Role of cell cycle control in arteriovenous specification

Increased Notch signalling in arterial relative to non-arterial ECs, which culminates in the activation of several artery-enriched genes, has long supported a model in which Notch signalling drives the transcriptional specification of arterial ECs [52, 53]. However, the direct binding of its downstream effectors, *Rbpj* or *Hey2*, to regulatory regions of arterial or venous genes has not yet been demonstrated, raising questions about whether Notch signalling directly induces arterial gene expression.

Fang et al. [50] first challenged this model by identifying a signalling pathway in which fluid shear stress of arterial magnitude activates Notch signalling, leading to the upregulation of *Cx37* and the downstream cyclin-dependent kinase inhibitor p27. This cascade subsequently promotes endothelial G1 arrest, which in turn enables the expression of arterial genes, suggesting that Notch governs arterial specification indirectly through modulation of the EC cycle state rather than through direct transcriptional activation. Building on this concept, Luo et al. [51] used a

mosaic genetic model, allowing differential Notch activation within individual CECs, and found that ECs with high Notch activity could still contribute to veins. In contrast, those with low Notch activity could form arteries. Together, these studies challenged the idea of a hard-wired Notch-driven transcriptional programme that predetermines CECs to an arterial identity. Although artery formation was impaired in *Rbpj*-knockout mice, a subset of *Rbpj*-deficient ECs still generated coronary and retinal arteries, indicating that Notch biases but does not determine arterial fate. Instead, *Rbpj*-deficient ECs regained the ability to form arteries once Myc, a cell cycle checkpoint regulator, was suppressed, suggesting that Notch indirectly favours arterial specification by downregulating Myc-dependent proliferation and metabolism-related genes [51], suggesting that Notch signalling is not the sole driver of arterial specification of ECs.

In addition to Notch, VEGF-A is also required for arterialisation in coronary vessel development [39]. Traditionally viewed as pro-mitogenic, VEGF-A was shown by Pontes-Quero et al. [54] to exert a bell-shaped dose-response, whereby high VEGF-A-MAPK (mitogen-activated protein kinase) activity induces p21-dependent cell cycle arrest in mouse retinal angiogenesis. Supporting this, Luo et al. [51] have shown that overexpression of VEGFR2 increases extracellular signal-regulated kinase (ERK) activity, which, in turn, upregulates Notch signalling through its ligand, Dll4. This pathway suppresses Myc expression, which would otherwise be promoted by only modest ERK activation [55], thereby coupling high VEGF-A-VEGFR2 signalling to the inhibition of CEC cycle progression and ultimately their arterial differentiation [51].

Although dysregulation of transforming growth factor-β (TGF-β) and bone morphogenetic protein (BMP) signalling has long been implicated in the development of arteriovenous malformations (AVMs) [56, 57], the mechanism by which these pathways are coordinated to establish arterial–venous identity remained unclear. Addressing this gap, Chavkin et al. [49] provided the first direct evidence linking EC cycle state to arterial-venous propensity. Using FUCCI-labelled human umbilical vein ECs (HUVECs) sorted into early or late G1 phases and stimulated with TGF-β1 or BMP4 under conditions that did not alter cell-cycle progression, the authors showed that TGF-β1 selectively induced arterial gene expression (*Efnb2*) exclusively

in ECs in late G1/G0, while BMP4 induced venous genes (*Ephb4*) only in early G1. These transcriptional responses were conserved in human arterial ECs. Mechanistically, siRNA-mediated knockdown of SMAD2/3, transcription factors that mediate canonical TGF-β signalling, abolished TGF-β1-induced *Efnb2* expression in late G1/G0, whereas knockdown of SMAD1/5 prevented BMP4-induced *Ephb4* expression in early G1, demonstrating that canonical SMAD signalling underlies this arterial specification restricted to the G0 state of the cell cycle [49].

Therefore, EC cycle arrest emerges as a prerequisite for the acquisition of arterial identity, consistent with earlier findings that forced overexpression of COUP-TFII blocks arterial identity in SV-derived ECs by upregulating positive regulators of proliferation [46]. Importantly, these insights were derived from E12.5-15.5 mice [51], during which coronary plexus expansion and arteriovenous specification occur, directly coupling cell cycle arrest to coronary artery formation *in vivo*.

Complementing these, an *in vitro* differentiation study has highlighted the importance of temporal regulation of extracellular signalling in arterial–venous fate decisions. Loh et al. [58] demonstrated that the generation of arterial or venous cells from human pluripotent stem cells depends on the temporally dynamic activation and repression of certain signalling pathways, involving VEGF-A and TGF-β1. In this model, TGF-β1 first induced-mid primitive streak, then repressed lateral mesoderm on day 2, and ultimately induced arterial ECs on day 3. In contrast, VEGF-A induced lateral mesoderm on day 2 and subsequently induced venous ECs on day 3, before inhibiting venous differentiation by day 4 [58]. Together, these findings suggest that EC cycle arrest is a prerequisite for the acquisition of arterial identity, which depends on the temporally regulated activation and repression of endothelial signalling pathways, which are partly mediated by paracrine cues, including those secreted by the epicardium.

1.6 Epicardial cues in regulating the development of sinus venosus-derived coronary vasculature

Recent lineage tracing, combined with scRNA-seq analyses, have shown that complementary SV- and endocardial-derived CECs converge transcriptionally and functionally by late embryonic development (E17.5), and are indistinguishable in their responses following ischemia - reperfusion injury [28]. Nonetheless, CECs of different origins are regulated by distinct pathways: hypoxia induced by the rapid growth of the compact myocardium in the first few days after birth drives VEGF-A-mediated endocardial sprouting [39], whereas SV-derived CECs rely on non-hypoxic, developmentally regulated cues from the epicardium [40].

By E8.5, the PEO, located near the septum transversum between the SV and the liver, becomes evident, giving rise to cells that migrate over the myocardium to form the epicardium [59-61]. In mice, this process culminates by E11.5 in the formation of an epicardial monolayer, whereas in humans, the ventricular epicardium develops as multiple cell layers [62-64]. From this stage onwards, the epicardium begins to actively secrete growth factors and ECM components that support coronary vessel expansion and maturation [65, 66]. Among these factors, deletion of the epicardial gene *Vegf-c* (vascular endothelial growth factor C), which encodes a ligand for VEGFR2 expressed in the SV, a receptor that strongly stimulates vascular growth [67], stunted the outgrowth of SV-derived subepicardial vessels along the dorsal and lateral surfaces towards the apex of the heart [40]. VEGF-C can also signal through VEGFR3, a receptor classically associated with lymphangiogenesis and not expressed in the SV [68]; however, VEGFR3 expression was induced in coronary endothelial sprouts after they emerged from the SV. In contrast, *Apj* was already highly expressed in the SV endothelium, leading to the hypothesis that *Apj* signalling, activated by its epicardial ligand Elabela (*Ela*), initiates SV sprouting [40]. However, heterozygous and homozygous deletion of *Apj* or *Ela* did not impair sprout initiation at E11.5 but instead delayed coronary vessel growth at E13.5 and later stages of plexus formation due to defective migration of coronary sprouts along the dorsal heart [69]. Collectively, these findings establish the epicardium as a dynamic signalling hub that coordinates SV-derived coronary endothelial sprouting.

As coronary development advances, the epicardium undergoes epithelial-to-mesenchymal transition (EMT) from E11.5, during which a subset of epicardial cells loses epithelial (EPI) characteristics, such as apical-basal polarity and intercellular adhesion, characterised by the expression of adhesion molecules like β-catenin [70]. The upregulation of mesenchymal (MES) genes, such as alpha-smooth muscle actin (*αSMA* or *ACTA2),* then occurs, conferring the cells with migratory and invasive capabilities, as well as an increased ability to produce ECM components [71, 72]. This process enables cells to detach from the epicardial layer and invade the myocardium, resulting in epicardium-derived cells (EPDCs) that can subsequently differentiate into multiple lineages, including fibroblasts, pericytes, and smooth muscle cells (SMCs) [14, 73, 74], which are essential for coronary maturation. The signalling cues that trigger sprouting from the SV remain unknown. Interestingly, these sprouts first form beneath the epicardium [17, 18, 75, 76] the onset of epicardial EMT (epiEMT), which peaks between E12.5 and E14.5, coinciding with the emergence of 'pre-arterial' cells in SV-derived endothelium [46]. Hence, epiEMT might act as a developmental switch, linking sprouting angiogenesis to arteriogenesis in coronary vessels, which has not been previously investigated.

Beyond its cellular contributions to the maturing coronary vasculature, the epicardium remodels the subepicardial ECM throughout coronary vessel development [73], suggesting the influence of the ECM on CEC fate. For instance, loss of collagen- and calcium-binding EGF-like domain 1 (*Ccbe1)*, which is expressed by the epicardium and SV at the stage of its contribution to the coronary endothelium, was shown to inhibit coronary sprouting from the SV. *Ccbe1* mutants further displayed delayed and mispatterned coronary artery stem formation, demonstrating its importance in coronary artery development [77, 78]. Notably, the dynamic changes in ECM observed during coronary development are mirrored in the coronary collateral arteries undergoing active remodelling in the infarcted adult heart [79], highlighting that the role of ECM in coronary artery formation persists post-MI.

1.7 Myocardial infarction

MI typically occurs when a coronary artery becomes occluded following rupture of an

atherosclerotic plaque, resulting in ischaemic injury to the downstream myocardium normally oxygenated by this vessel [80]. Within minutes of injury, a highly coordinated cardiac repair programme is initiated, characterised by the release of pre-formed granules from resident mast cells and the production of inflammatory cytokines and chemokines by resident macrophages and cardiomyocytes, which together trigger the acute inflammatory response [81]. This initial inflammatory trigger produced by resident cells promotes the recruitment of neutrophils and a pro-inflammatory subset of monocytes from the circulation within the first 24 hours after injury [81].

Recruited innate immune cells contribute to the phagocytosis of dead and dying cardiomyocytes and secrete more inflammatory cytokines, further amplifying the pro-inflammatory response. Neutrophils are rapidly cleared from the myocardium, with numbers declining after approximately three days and a complete absence by seven days. During their resolution, apoptotic neutrophils release TGF-β, lactoferrin, and annexin A1, which promote the emergence of anti-inflammatory, reparative macrophages with an M2-like phenotype [81, 82]. In contrast, monocytes persist within the injured tissue and continue to accumulate; however, as the response transitions from the inflammatory to the reparative phase around day seven, monocyte populations with reduced inflammatory activity and enhanced reparative capacity predominate and differentiate into M2-like macrophages [81].

In parallel, adaptive immune cells also contribute to post-MI repair. During the early inflammatory phase, $CD4^+$ helper T cells and $CD8^+$ cytotoxic T cells accumulate and exacerbate inflammation, whereas during the reparative phase, regulatory T cells become dominant, secreting interleukin-10 and TGF-β to facilitate inflammatory resolution and reinforce macrophage polarisation towards the reparative M2-like phenotype [81].

M2-like macrophages are a major source of TGF-β and VEGF-A, thereby promoting fibrosis and angiogenesis within the infarcted myocardium [81]. Fibrosis, driven by fibroblast proliferation and ECM deposition, is required for the formation of a collagen-rich scar that can stabilise the injured tissue, although this process increases the physical load on the neighbouring viable myocardium [81]. Therefore, neovascularisation is required to ensure adequate perfusion of peri-infarct regions and to mitigate the adverse functional consequences of scar formation.

1.8 Neovascularisation following myocardial infarction

Despite advances in reperfusion therapies that enable rapid restoration of blood and have dramatically reduced early mortality following acute MI, reperfusion itself can paradoxically trigger ischaemia–reperfusion injury, thereby promoting adverse remodelling and the development of heart failure in patients who initially survive the infarction [83]. In addition, imaging studies have estimated that in over half of these patients, the coronary microvasculature remains incompletely reperfused [9, 13], highlighting the need for therapeutic strategies that can promote the revascularisation of the ischemic heart. Nevertheless, clinical trials aimed at stimulating neovascularisation post-MI through exogenous administration of angiogenenic growth factors to a degree that improves cardiac function have thus far yielded limited success [15, 84-87]. In light of this, research has shifted towards elucidating the endogenous mechanisms underlying coronary neovascularisation post-MI, which necessitates an understanding of its cellular origins.

Several potential cellular origins of post-infarction coronary neovascularisation have been proposed, including bone marrow-derived endothelial progenitor cells, cardiac fibroblasts, endocardial and venous cells, and pre-existing CECs. These have been extensively reviewed elsewhere [14, 88, 89], A growing body of evidence, however, supports the latter as the dominant contributor. Following coronary artery occlusion, EC proliferation peaks within four days of infarction in the murine heart and is mainly localised to the infarct border zone [90], which is the interface between the infarcted and viable tissue. Lineage-tracing using three independent EC-specific inducible Cre mouse lines to achieve inducible labelling of the coronary endothelium demonstrated that the proportion of labelled CECs remains unchanged following ischaemia–reperfusion injury, indicating that the majority of newly formed coronary vessels arise from pre-existing CECs, with minimal contribution from alternative lineages [91].

More recently, clonal analysis using multi-spectral reporter systems, to enable the tracking of individual endothelial clones, has revealed that adult coronary angiogenesis post-MI occurs through contribution and incorporation of multiple EC populations, rather than through clonal

expansion of individual clones [92-95]. In contrast, angiogenesis under pathological hypoxic conditions across multiple tissues, including the heart, was found to be characterised primarily by clonal expansion of a subset of ECs [95]. Consistently, a separate study has identified large endothelial clones comprising more than 50 cells within the infarct border zone following MI [93], supporting clonal expansion as a principal mechanism of neovascularisation in the adult ischaemic heart.

Although pre-existing CECs appear to be the dominant source of post-infarct neovascularisation, several studies have proposed alternative contributions from non-endothelial sources, which have been extensively reviewed elsewhere [14, 88, 89]. Of these, Dubé et al reported indirect evidence of *de novo* vessel formation using pulse-chase lineage tracing with *Pdgfb*^{CreERT2} of murine hearts to label existing ECs prior to MI, showing contributions from the endocardium and coronary sinus [90]. Through a systematic analysis of these hearts over 14 days in response to MI, they identified a greater proliferative capacity in venous compared with arterial and capillary CECs. In particular, overt endothelial sprouting was observed at seven days post-MI from the coronary sinus, the adult derivative of the embryonic sinus venosus, which substantially contributes to the coronary endothelium during development. Since comparable sprouting was not detected from major coronary arteries or veins, these findings suggest the specific reactivation of venous-derived developmental programmes following MI [90]. Together, these observations reinforce the importance of understanding the developmental mechanisms underlying SV-derived coronary vessel formation, which can be leveraged to drive neovascularisation following MI.

1.9 Preliminary findings from the Smart laboratory

The importance of VEGF-A–VEGFR2 signalling in coronary vessel development has become increasingly apparent, which has, however, primarily been characterised in relation to the endocardium, owing to evidence demonstrating that loss of either myocardial VEGF-A or endocardial VEGFR2 abolishes angiogenic sprouting [39]. More recent work has confirmed that

VEGF-A-dependent angiogenesis is largely confined to endocardium-derived coronary vessels during development [48]. This was demonstrated in embryonic hearts of mice carrying a vascular enhancer–*lacZ* transgene under the control of myocyte-specific enhancer factor-2 (MEF2) proteins, where *lacZ* was expressed upon angiogenesis directly downstream of active VEGF-A–VEGFR2 signalling. Knowing that VEGFR2 is also expressed in the SV endothelium [40], VEGF-A-driven angiogenic enhancers were further shown to be transiently active within the SV-derived vascular plexus soon after sprouting [48], suggesting an additional role for VEGF-A signalling in this endothelial population prior to arteriovenous specification.

Building on this, our group performed ligand–receptor inference analysis using CellChat [96] on an in-house-generated E13.5 scRNA-seq whole-heart dataset, supplemented with literature-based ligand–receptor interactions. Focusing on signals from the epicardium, in both its epithelial and mesenchymal states, to the SV endothelium, this analysis revealed high communication between epicardium-derived VEGF-A, particularly from EPDCs, and VEGFR2 expressed on SV-derived CECs at E13.5 **(Fig. 1A)**. This coincides with the onset of arterialisation in SV-derived coronary vessels, suggesting a possible role for epicardial VEGF-A–VEGFR2 signalling not only in the angiogenic expansion of SV-derived sprouts but also in initiating their arteriogenesis.

It is worth noting that the strong VEGF-A-VEGFR2 signalling observed in SV-derived CECs in our analysis was accompanied by weaker, yet significant, communication of VEGF-A with VEGFR1 and neuropilins (NRPs). VEGFR1 acts as a decoy receptor, binding VEGF-A to limit its availability to VEGFR2 in neighbouring ECs, and NRPs, particularly NRP1, can form complexes with VEGFR2, upon binding of VEGF-A to both receptors simultaneously, to mediate VEGF-A-driven angiogenesis [97]. Therefore, these receptors may collectively fine-tune VEGF-A–VEGFR2 signalling to drive SV-derived coronary vessel sprouting and subsequent arterial specification during development.

Having established the epicardium as an important source of growth factors during SV-derived coronary vessel formation and arterialisation, both of which take place over the time window of epiEMT, our group next examined the secretory profile of the epicardium in its epithelial and

mesenchymal states. Therefore, they performed mass spectrometry on conditioned media from a mouse epicardial cell line (MEC1) [69] at 48 hours following EMT induction. Our data revealed the differential secretion of epicardial-derived ECM proteins between epithelial and mesenchymal states, among which the secreted protein, acidic and rich in cysteine (SPARC) protein, showed the most significant difference, with higher expression in the mesenchymal state **(Fig. 1B)**.

1.10 SPARC

SPARC, also known as osteonectin or basement membrane-40, is a matricellular protein, a class of ECM proteins that do not serve structural roles, in contrast to the classical ECM proteins such as collagens and laminins [98]. The gene encoding SPARC produces a 33 kDa protein consisting of 298-304 amino acids (aa), which undergoes post-translational glycosylation to yield a secreted 43 kDa protein [99]. Structurally, this mature SPARC peptide consists of three domains with distinct modular functions: an acidic N-terminal, (aa: 1-52), a follistatin-like domain (aa: 52-137), and a calcium-binding extracellular C-terminal domain (aa: 137-286) that contains two EF-hands capable of binding calcium (aa: 222-235; 257-268). These are highly conserved across species, highlighting the physiological importance of SPARC [100, 101], which is further underscored by its *Sparc* expression in a wide range of cell types including osteoblasts, macrophages, fibroblasts, SMCs, and ECs [102-104].

Following synthesis and post-translational modification, SPARC is secreted into the extracellular space. Matricellular proteins use a diverse array of secretory mechanisms, which can vary by protein and cellular context. For example, cysteine-rich angiogenic inducer 61 (CYR61) has been reported to undergo caveolae-mediated secretion [105], while other matricellular proteins, such as tenascin-C (TENA), have been characterised as extracellular vesicle (EV) cargoes that undergo exosomal release [106]. In contrast, SPARC, owing to its N-terminal signal peptide that can direct its insertion into the endoplasmic reticulum (ER), can be trafficked via the canonical ER–Golgi pathway into secretory vesicles for exocytosis at the

plasma membrane [107-110].

Although SPARC has been detected in EV-enriched fractions across multiple systems [108-110], no evidence to date demonstrates sorting of SPARC into intraluminal vesicles or exosomal cargoes, which include the defining compartments of the exosomal secretory pathway [111]. Instead, a recent high-resolution fractionation study has shown that SPARC co-purifies with EV fractions without necessarily being integrated into EV membranes [109]. Accordingly, the authors suggested that the abundant expression of SPARC in the extracellular space and basement membrane likely underpins its presence in these fractions, rather than supporting an unconventional EV-dependent secretory pathway [109].

Interestingly, peptidyl-prolyl cis–trans isomerase A (PPIA; cyclophilin A) was also detected as an abundant matricellular protein in our mass spectrometry analysis of epicardial cell conditioned media, but showed the opposite pattern to SPARC, being upregulated in the epithelial rather than mesenchymal state **(Fig. 1B)**. In vascular SMCs, PPIA is known to be released in response to defined stimuli, specifically oxidative stress via vesicular mechanisms that require actin remodelling [112]. While SPARC and PPIA may employ distinct secretory routes, the stimulus-dependent release of PPIA may provide precedent for the regulated release of matricellular proteins such as SPARC. Accordingly, its increased expression in mesenchymal epicardial conditioned media **(Fig. 1B)** may reflect regulated or temporally enhanced release coupled to epiEMT.

It is important to note that the abundance of extracellular SPARC reflects not only the rate of secretion but also its retention within, or release from, the ECM, which is in part modulated by its proteolytic processing, capable of generating bioactive fragments with distinct functional properties, including effects on angiogenesis [102, 107, 113].

1.11 SPARC in angiogenesis

Given that SPARC was first isolated from proliferating bovine aortic ECs undergoing

angiogenesis [102], it is not surprising that several studies have implicated SPARC in the regulation of angiogenesis, albeit with highly context-dependent outcomes **(Table 1)**. In fact, the initial study describing SPARC in angiogenesis demonstrated that it promotes endothelial cord formation and vessel sprouting, while paradoxically suppressing endothelial proliferation when administered exogenously to bovine aortic ECs [102].

Across tumour models, there is a consistent pattern in which *Sparc* overexpression suppresses tumour angiogenesis [114-119], whereas its genetic deletion [120, 121] or knockdown [117] augments vascular density, supporting an overall anti-angiogenic role for full-length SPARC in pathological angiogenesis. In contrast, developmental angiogenesis models, particularly the chick and quail chorioallantoic membrane (CAM), have revealed pro-angiogenic activities associated with specific SPARC-derived peptides rather than the full-length protein [102, 107, 113, 122]. Peptides encompassing the Cu^{2+}-binding motif KKGHK (amino acids 119–123) within the follistatin-like domain of SPARC promoted angiogenesis in CAM assays, whereas its full-length version in the same context had either an inhibitory or no effect on angiogenesis [102, 107, 122]. Interestingly, in a choroidal neovascularisation model, endogenous SPARC levels were insufficient to induce angiogenesis, yet exogenous SPARC administration post-choroidal injury promoted neovascularisation [123]. Taken together, these findings suggest that SPARC predominantly suppresses angiogenesis in tumour contexts, whereas its pro-angiogenic effects are largely restricted to developmental and post-injury settings, in which SPARC expression is transiently elevated [102, 107, 122]. Importantly, the effect of SPARC on angiogenesis is further complicated by its extracellular proteolytic processing, which generates bioactive peptides with opposing effects on angiogenesis **(Fig. 2A)**.

For example, Lane et al. [102] demonstrated that SPARC is transiently and selectively expressed in nascent capillaries during periods of rapid angiogenesis in the embryonic brain. *In vitro*, SPARC increased endothelial cord formation, an effect recapitulated by synthetic peptides spanning amino acids 113–130 (peptide 2.3), with both peptide 2.3 and smaller derivatives potently stimulating angiogenesis *ex vivo*. Importantly, proteolytic cleavage of SPARC or overlapping synthetic peptides released the bioactive peptide KGHK, which were shown to

arise following plasmin-mediated cleavage. The authors further proposed that thrombin, a potent activator of ECs and platelets, may generate intermediate cleavage products that are subsequently processed by additional proteases in the extracellular space [102].

Consistently, Iruela-Arispe et al. [122] demonstrated that plasmin, which was present at sites of SPARC expression in the CAM, can cleave SPARC to generate angiogenic peptides spanning amino acids 119–122, whereas intact SPARC failed to elicit an angiogenic response. Extending these observations, Sage et al. [107] showed that SPARC is selectively cleaved by matrix metalloproteinase-3 (MMP-3), but not by MMP-1 or MMP-9, yielding three major fragments (aa 2–87, 88–237, and 150–237). To dissect functional domains within these fragments, the authors employed synthetic peptides Z1 (aa 50–85), Z2 (aa 149–198), and Z3 (aa 220–239). Peptides Z2 and Z3 inhibited endothelial proliferation and angiogenesis in a concentration-dependent manner, whereas Z1 exhibited a biphasic effect dependent on peptide concentration. Notably, Z2 and Z3 lacked angiogenic activity in CAM assays, while Z1 retained a biphasic angiogenic response *ex vivo* [107]. Together, these findings point to proteolytic processing of SPARC in the extracellular space, as well as its concentration and tissue context as determinants of its effect on angiogenesis.

In addition to its effects on proliferation and angiogenesis, SPARC also exhibits anti-adhesive properties, facilitating cell migration [98], which are all essential for the proper formation of coronary vessels. Despite this, SPARC expression and function within the coronary vasculature have not yet been directly examined. Nevertheless, plasma SPARC concentrations were found to be elevated in patients with CAD than in age- and BMI-matched controls [124], highlighting its potential relevance in coronary pathologies that may predispose to MI.

Study	Angiogenesis model	SPARC manipulation	Direction of angiogenic effect	Molecular mediators implicated

Lane 1994 [102]	Bovine aortic ECs; chick CAM	Exogenous full-length SPARC; synthetic SPARC peptides	↑ sprouting ↓ proliferation	-
Iruela-Arispe 1995 [122]	Chick CAM	Exogenous full-length SPARC; synthetic SPARC peptides	– (native) ↑ (fragments)	-
Kupprion 1998 [113]	Human microvascular ECs (HMECs)	Exogenous full-length SPARC; synthetic SPARC peptides	↓	VEGF-A–**VEGFR**1–ERK
Sage 2003 [107]	Bovine aortic ECs; quail CAM	Exogenous full-length SPARC; MMP-3–cleaved SPARC peptides; synthetic peptides	↑ / ↓ (fragment-specific) – / ↓ with full-length SPARC	-
Chlenski 2006 [114]	Matrigel tumour plug injected into mice	*Sparc* overexpression	↓	FGF
Nozaki 2006 [123]	Choroidal neovascularisation	Exogenous full-length SPARC	↑	VEGF-A–VEGFR2
Yunker 2008 [115]	Glioma xenograft	*Sparc* overexpression	↓	VEGF-A–VEGFR2
Arnold 2008 [120]	Orthotopic murine model of pancreatic carcinoma	Sparc KO	↑	-
Bhoopathi 2010 [116]	HMEC–medulloblastoma co-culture	*Sparc* overexpression	↓	MMP-9–VEGF-A
Arnold 2010 [121]	Orthotopic murine model of pancreatic carcinoma	Sparc KO	↑	-

Zhang 2012 [117]	HUVEC-CM (gastric cancer cells); dorsal skinfold	*Sparc* overexpression / knockdown	↓ / ↑	VEGF–ERK–MMP7
Gorantla 2013 [118]	HMEC-CM (neuroblastoma cells); dorsal air sac	*Sparc* overexpression	↓	VEGFR2–PI3K–Akt–MTOR Notch-Stat3
Cydzik 2015 [125]	HUVEC; chick CAM	Exogenous full-length SPARC	↓	VEGFR2–ERK
Boyineni 2016 [119]	HUVEC-CM (neuroblastoma cells); dorsal air sac	*Sparc* overexpression	↓	miR-410–VEGF-A
Fu 2019 [126]	Human retinal capillary ECs (HRCECs)	*Sparc* knockdown	↑	-
Deng 2022 [127]	HUVEC-CM (M2 macrophages)	*Sparc* knockdown	↑ (indirect)	PI3K–Akt

Table 1. Summary of studies examining the effects of SPARC on angiogenesis across developmental, tumour, injury, and immune-mediated contexts.

1.12 SPARC in myocardial infarction

While mice lacking *Sparc* are viable, they have poor healing outcomes, consistent with SPARC expression in postnatal life becoming restricted to fibrotic tissues, including the infarcted heart [128-130]. SPARC has been shown to exert opposite effects during the inflammatory and maturation phases of cardiac repair following MI, a pattern that is reflected in its endogenous expression during both early and later stages of post-MI repair. This is unlike other matricellular proteins, such as thrombospondin-1, whose expression is confined to the early inflammatory phase [131, 132]. In both rodent and canine models, endogenous SPARC expression increased

significantly within the infarcted [133-135] and even remote [134] myocardium as early as 3 days post-injury compared with sham controls, with expression levels peaking around 14 days post-MI [133, 134, 136].

Beyond characterising its expression profile, several studies have investigated the functional role of SPARC during post-MI repair, primarily in relation to scar formation and cardiac remodelling, with more limited examination of its effects on leukocyte infiltration and neovascularisation [134, 135]. In *Sparc*-null mice, Schellings et al. [134] demonstrated a four-fold increase in post-MI mortality compared with wild-type controls, driven by a higher incidence of cardiac rupture and heart failure within 14 days of infarction. This phenotype was attributed to disorganised granulation tissue and impaired ECM maturation, evidenced by reduced collagen fibre diameter. Adenovirus-mediated SPARC overexpression rescued this phenotype, inhibiting adverse cardiac dilation and improving collagen maturation at 14 days post-MI [134]. In contrast, McCurdy et al. [135] examined SPARC function exclusively at an early point (3 days post-MI), revealing effects suggestive of its deleterious role during the inflammatory phase. *Sparc*-null mice exhibited attenuation of the decline in ejection fraction and the increase in end-diastolic volume observed in wild-type mice at this stage. The authors reported elevated connective tissue growth factor (CTGF) expression in cardiac fibroblasts of *Sparc*-null mice at baseline and at 3 days post-MI in the remote myocardium, suggesting altered basal ECM homeostasis and compensatory collagen synthesis and/or assembly in the absence of *Sparc* [135].

With respect to inflammation, Schellings et al. [134] reported SPARC colocalisation with CD45-positive leukocytes at both 3 and 14 days post-MI, with leukocyte expression being significantly higher in *Sparc*-null mice at the later time point. By contrast, McCurdy et al. [135] observed no difference in macrophage numbers between wild-type and *Sparc*-null mice at 3 days post-MI, although no later stages were examined. Regarding neovascularisation, Schellings et al. [134] found no significant difference in CD31-positive coronary vessel density between genotypes, whereas McCurdy et al. [135] later reported a reduction in CD31 levels in the wild-type left ventricle at 3 days post-MI, which was attenuated in *Sparc*-null mice. This suggested that

Sparc deletion may preserve existing vasculature during early infarct remodelling rather than actively promoting angiogenesis [135].

Collectively, these studies indicate that SPARC plays temporally distinct roles during post-MI repair, with evidence suggesting potentially adverse effects during early inflammatory phases and beneficial roles during later stages of matrix remodelling and scar stabilization [134, 135]. This duality parallels the well-described context-dependent functions of C-X-C chemokine receptor 4 (CXCR4) in myocardial ischaemia, where early CXCR4 blockade (3 days post-MI), at which its expression peaks, improves cardiac function at 8 weeks post-MI, an effect not observed when CXCR4 was blocked at later stages post-infarction [137]. Therefore, these observations underscore the importance of temporal context in determining the functional role of SPARC during cardiac repair, a principle that may also extend to developmental settings. Considering that SPARC, as a matricellular protein, interacts with and modulates various growth factor gradients and their receptors, including VEGF-A and transforming growth factor- β (TGF-β) [98], such interactions may underpin its context-dependent effects on angiogenesis and post-infarct remodelling.

1.13 SPARC and VEGF-A

Although SPARC has been shown to bind VEGF-A [113, 125], the outcome of this interaction for angiogenesis remains context-dependent and incompletely understood. Kupprion et al. [113] demonstrated that full-length SPARC co-immunoprecipitates with VEGF-A, with competition assays identifying peptide 4.2 (aa 254–273) within the EF-hand–containing C-terminal domain as a major VEGF-A–binding site. Despite reducing VEGF-A binding to its receptors by only ~70%, SPARC and peptide 4.2 abolished VEGF-A–induced DNA synthesis in human microvascular ECs, indicating potent downstream inhibition. Mechanistically, SPARC suppressed VEGF-A–mediated angiogenesis through inhibition of VEGFR1, but not VEGFR2, tyrosine phosphorylation, leading to reduced activation of ERK1/2 within the MAPK pathway [113]. Corroborating this, in a choroidal neovascularisation model, Nozaki et al. [123] also showed that VEGF-A administration prior to injury preferentially activated VEGFR1, promoting

expression of the VEGFR2 inhibitor SHP-1 (Src homology 2 domain–containing protein tyrosine phosphatase 1). Inhibiting SPARC via neutralising antibodies before injury suppressed VEGF-A-mediated choroidal neovascularisation, which was reversed upon recombinant SPARC administration post-injury. Therefore, this study suggested that SPARC promotes angiogenesis by inhibiting VEGF-A–VEGFR1 signalling while facilitating VEGF-A–VEGFR2 activation [123].

In contrast to the previous study, Yunker et al. [115] failed to detect direct co-immunoprecipitation between SPARC and VEGF-A, yet still observed marked inhibition of VEGF-A–driven angiogenesis in glioma cells *in vitro* expressing VEGFR2 but not VEGFR1, suggesting that SPARC can modulate VEGF-A signalling independently of stable ligand binding. Consistent with this, *Sparc* overexpression across multiple tumour contexts attenuated angiogenesis by limiting VEGF-A availability or downstream signalling, including suppression of MMP-mediated VEGF-A upregulation [116], reduced activation of MAPK family members (ERK1/2, p38, SAPK/JNK) [117, 118], and inhibition of VEGFR2-dependent PI3K–AKT–mTOR signalling [118]. In neuroblastoma models, *Sparc* overexpression further suppressed angiogenesis by disrupting Notch-STAT3 signalling downstream of VEGFR2, thereby reducing endothelial proliferation [118]. More recently, *Sparc* overexpression was shown to suppress tumour angiogenesis *in vivo* through induction of microRNA-410, which was shown to negatively regulate VEGF-A expression [119].

In contrast to earlier studies, Cydzik et al. [125]. provided the first direct evidence that SPARC and VEGF-A bind to each other, demonstrating a stable interaction characterised by slow association and dissociation kinetics. Functionally, co-treatment of HUVECs with SPARC and VEGF-A inhibited proliferation, adhesion, and migration of these cells, with immunoblotting showing this anti-angiogenic effect to be associated with reduced phosphorylation of VEGFR2 and its downstream effector ERK [125]. These findings were confirmed *in vivo* using a chorioallantoic membrane assay, where Matrigel (ECM) plugs containing both SPARC and VEGF-A failed to induce angiogenesis, yielding vessel morphology comparable to control or SPARC alone [125]. Together, these studies indicate that although SPARC can bind VEGF-A,

their combined effects on angiogenesis are context-dependent **(Fig. 2B)** and remain unexplored in coronary vessel development, arteriogenesis or neovascularisation following MI.

1.14 SPARC and TGF-β

TGF-β1 is a pleiotropic cytokine that plays a central role in connective tissue remodelling following injury [138]. Similar to SPARC, TGF-β1 exerts biphasic effects on cardiac repair following MI. Two independent studies showed that early inhibition of TGF-β1 signalling increased mortality and exacerbated left ventricular dilatation after MI [139], whereas blocking it later prevented adverse remodelling of the left ventricle [140]. Furthermore, studies have shown that TGF-β1 increases the level of *Sparc* mRNA in human fibroblasts through post-transcriptional mechanisms [141], and that SPARC can also increase TGF-β1 expression in cultured mouse mesangial cells [138], suggesting a positive feedback loop between the two factors. Given this reciprocal regulation and the important context-dependent roles of both factors in connective tissue remodelling following injury, the post-MI setting has provided a useful framework in which to interrogate the interaction between SPARC and TGF-β1.

Although the combined effect of SPARC and TGF-β1 in the infarcted heart has not been tested**,** Schellings et al. [134] demonstrated that *Sparc*-null mice have significantly impaired cardiac function post-MI compared to wild-type controls, owing to disorganised granulation tissue and immature collagenous ECM, as indicated by decreased collagen fibre diameter. However, this was reversed in *Sparc*-null mice infused with TGF-β1 at 7 days post-MI relative to untreated infarcted hearts. Therefore, the disorganised and immature collagen matrix in *Sparc*-null mice was associated with insufficient activation of TGF-β1 signalling [134]. *Sparc* knockdown by short-hairpin RNA was further shown to attenuate the TGF-β1-mediated increase in Smad2 phosphorylation, which was reversed upon exogenous administration of recombinant SPARC [134]. Collectively, these findings suggest that SPARC regulates infarct healing by promoting the post-translational maturation of collagen via TGF-β1–Smad2 signalling in cardiac fibroblasts.

SPARC has been shown to interact with the TGF-β1 receptor complex, but only in the presence of TGF-β1 bound to its cognate type II receptor (TβRII) [138]. In doing so, SPARC facilitates the activation of TGF-β1 signalling, as evidenced by significantly reduced Smad2 phosphorylation in primary mesangial cells derived from *Sparc*-null mice compared with wild-type controls [138]. Beyond their pro-fibrotic role, SPARC and TGF-β1 have been implicated in vessel maturation, although evidence is limited to one study, which was in an orthotopic model of pancreatic cancer [121]. Here, *Sparc*-null mice displayed a reduced number of pericyte-associated vessels, reflecting impaired blood vessel maturation and pericyte recruitment [121]. Consistent with this, Rivera et al. [142] proposed that SPARC supports angiogenesis indirectly by facilitating pericyte recruitment, a necessary step in vascular maturation whereby nascent endothelial tubes acquire mural cell coverage to stabilise newly formed vessels. In this study, SPARC was shown to bind endoglin, an accessory receptor of TGF-β1 expressed on ECs and pericytes. This interaction prevents endoglin from associating with αV integrins, which are known to promote the presentation of latent TGF-β1 to its receptors. In the absence of SPARC, αV integrins facilitate TGF-β1 activation and downstream SMAD2 phosphorylation, which maintains pericytes in an inactive, non-migratory state. By limiting integrin-mediated TGF-β1 presentation, SPARC is therefore proposed to attenuate TGF-β signalling, permitting pericyte recruitment to nascent vessels [142].

While these studies provide important mechanistic insight into SPARC–TGF-β1 interactions during vessel maturation **(Fig. 2B)**, they remain among the few examples directly addressing their combined roles in vascular biology. The paucity of studies examining the combined actions of SPARC and TGF-β1 in this context is surprising, given the well-established involvement of TGF-β signalling in angiogenesis and arteriovenous specification [49], as evidenced by vascular defects following the disruption of various components within this pathway (reviewed by [143, 144]).

Canonical TGF-β signalling involves the binding of TGF-β1 to TβRIII, facilitating its presentation to the constitutively active kinase TβRII, leading to the subsequent phosphorylation and activation of TβRI, which are also known as activin-like kinases (ALK) [145].

ECs express both ALK1 and ALK5, the latter of which forms a heterodimer with TβRII bound to TGF-β1. This activates the TβRII-ALK5 complex, propagating intracellular signalling through suppressor of Smad2 and Smad3 transcription factors. Once phosphorylated, these Smad proteins form a complex with Smad4, leading to nuclear translocation and initiation of transcription of genes promoting cell cycle arrest. Alternatively, TβRII bound to TGF-β can also activate the ALK-1 kinase domain, which signals through Smad1/5/8, ultimately stimulating cell cycle proliferation and angiogenesis [145]. *Alk1*-null embryos show excessive fusion of capillary networks and the major arteries and veins, resulting in AVMs [56, 57]. Likewise, mutations in endoglin cause hereditary haemorrhagic telangiectasia, a disorder characterised by microvascular overgrowth and large-calibre AVMs lacking clear arterial or venous identity [146]. Endoglin can bind TβRII, with which SPARC also associates, activating the downstream signalling pathways via Smad2/3 phosphorylation [138]. Knowing that TGF-β1 selectively induces arterial gene expression (*Efnb2*) exclusively in late G1/G0 ECs via Smad2/3 activation [49], SPARC and TGF-β1 may jointly influence arteriovenous specification. This is particularly relevant given our observations from mass spectrometry analysis of EMT-conditioned media from MEC1 epicardial cells, in which both SPARC and TGF-β1 were upregulated in the MES state (the latter based on unpublished observations).

1.15 Thesis rationale

The preceding sections highlight that while SPARC has been extensively studied in the context of angiogenesis and, more recently, linked to vascular remodelling, its role in coronary vessel development remains unexplored. Since SV sprouting coincides with epiEMT, with SPARC being upregulated in the mesenchymal state, the central hypothesis of this thesis is that epicardial-derived SPARC, as a mesenchymal-associated protein, mediates the switch from coronary angiogenesis to arteriogenesis through its interactions with VEGF-A and TGF-β1. Therefore, the primary aims of this thesis are:

1. **To characterise the expression profile of SPARC in epithelial versus mesenchymal states during coronary vessel formation**

We will map the spatiotemporal expression of SPARC between E9.5 and E16.5 using immunofluorescence staining of sagittal whole embryonic sections and frontal dissected hearts. This will be complemented by whole-mount immunofluorescence of optically cleared embryonic hearts at E17.5 to visualise SPARC three-dimensionally relative to the SV-derived coronary arteries. The latter will be visualised using a Cx40-EGFP reporter mouse line [147]. Differential expression of SPARC in epithelial versus mesenchymal states will be further validated using reverse transcription-quantitative polymerase chain reaction (RT-qPCR) and immunoblotting on MEC1 lysates and conditioned media at 24 and 48 hours post-EMT.

We hypothesise that Sparc is transcriptionally upregulated in the epithelial state, resulting in increased intracellular SPARC protein levels that are subsequently released upon transition to the mesenchymal state. The timely increase in SPARC secretion, as epiEMT coincides with SV-derived coronary vessel growth and arterialisation, may therefore increase SPARC availability in the extracellular milieu of epicardial cells, promoting its interaction with growth factors such as VEGF-A and TGF-β1, both of which are also upregulated in the mesenchymal state of MEC1-conditioned media (unpublished observations).

2. **To functionally assess the effects of SPARC on endothelial sprouting, proliferation and arterial specification**

We will use a well-established *in vitro* model of coronary angiogenesis [148], isolating the SV from Cx40-GFP reporter mice [147] at E11.5, which will be cultured with SPARC in combination with VEGF-A or TGF-β1. Angiogenesis will be quantified by CD31-positive vessel count normalised to explant area, arterial differentiation by Cx40-GFP expression, and proliferation via Ki67-positive ECs. Parallel experiments will use conditioned media from MEC1 cells in epithelial versus mesenchymal states at 48+8 hours post-EMT to assess angiogenic sprouting

from SV explants in a physiologically more relevant environment of epicardial signalling.

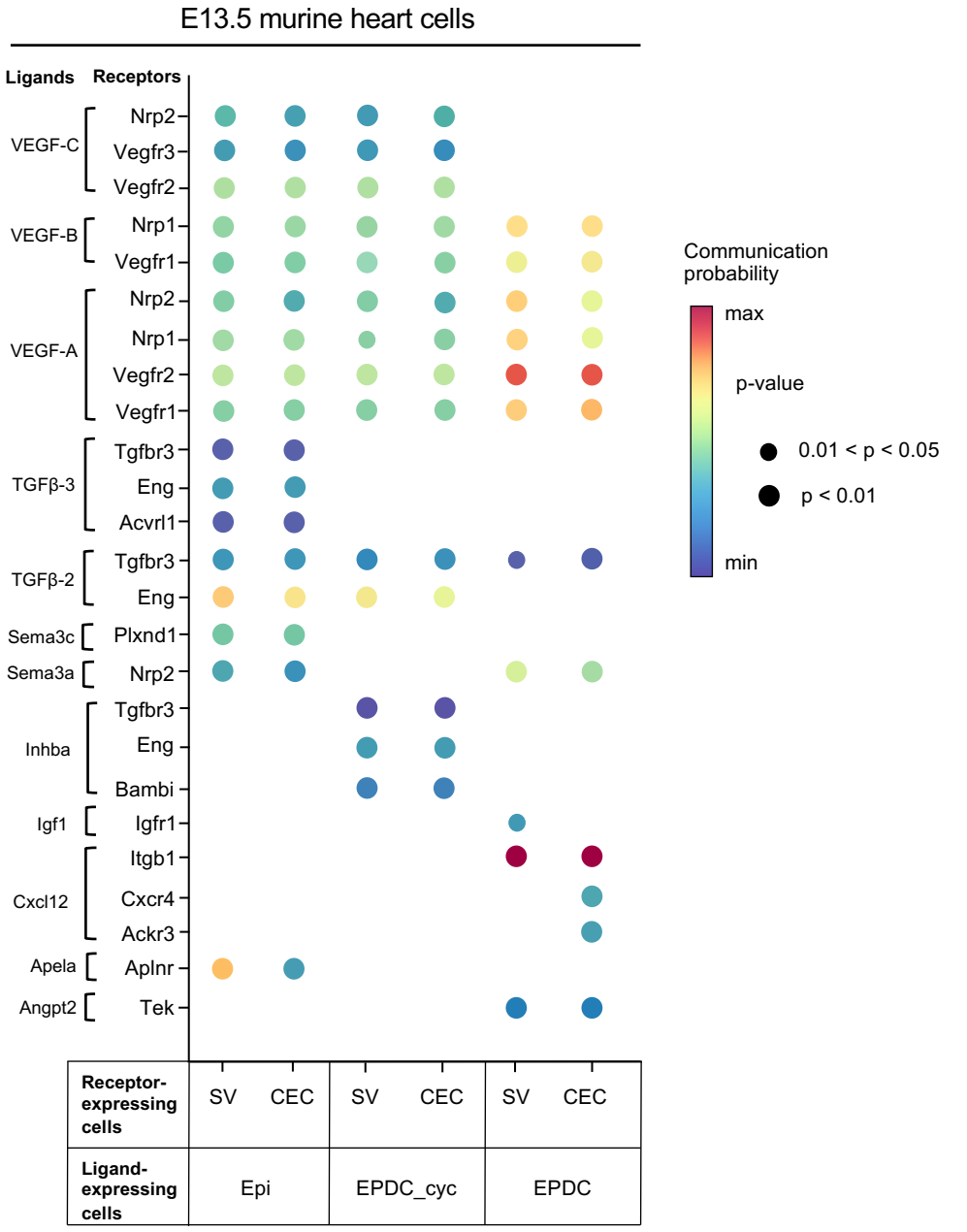
We hypothesise that SPARC, in combination with VEGF-A or TGF-β1, will promote arterialisation of SV-derived sprouts while suppressing EC proliferation and angiogenic expansion. Likewise, epithelial conditioned media will increase SV-derived EC proliferation and sprouting, whereas the mesenchymal conditioned media will exert the opposite effect.

3. To evaluate the potential for SPARC to promote neovascularisation

We will conduct a preliminary *in vivo* study on cryosections from previously collected infarcted murine hearts. Here, MI will be induced via the permanent ligation of the left anterior descending artery (LAD) [149]. These mice will receive four intramyocardial injections of SPARC alone or in combination with TGF-β1 into the infarct/border zone, and their hearts will be harvested at seven days post-injury. Immunofluorescence will be used to assess coronary vessel expansion and arteriogenesis, while Masson's trichrome staining will quantify fibrosis, enabling the correlation of vascularisation with tissue repair.

We hypothesise that infarcted hearts infused with SPARC, in combination with TGF-β1, will increase coronary vessel growth and arteriogenesis, which will be accompanied by an increase in collagen deposition at seven days post-MI.

A


E13.5 murine heart cells
Ligands
Receptors
VEGF-C
Nrp2
Vegfr3
Vegfr2
VEGF-B
Nrp1
Vegfr1
VEGF-A
Nrp2
Nrp1
Vegfr2
Vegfr1
TGFβ-3
Tgfbr3
Eng
Acvrl1
TGFβ-2
Tgfbr3
Eng
Sema3c
Plxnd1
Sema3a
Nrp2
Inhba
Tgfbr3
Eng
Bambi
Igf1
Igfr1
Cxcl12
Itgb1
Cxcr4
Ackr3
Apela
Aplnr
Angpt2
Tek
Communication probability
max
p-value
min
0.01 < p < 0.05
p < 0.01
Receptor-expressing cells
SV
CEC
SV
CEC
SV
CEC
Ligand-expressing cells
Epi
EPDC_cyc
EPDC

B

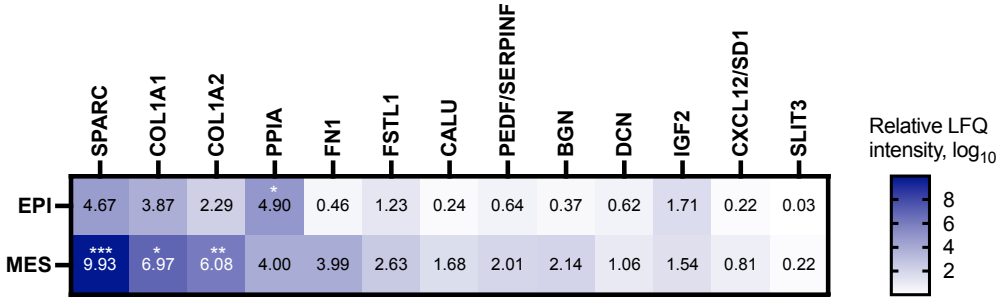

Epicardial secretory profile of matricellular proteins across epithelial and mesenchymal states
SPARC
COL1A1
COL1A2
PPIA
FN1
FSTL1
CALU
PEDF/SERPINF
BGN
DCN
IGF2
CXCL12/SD1
SLIT3
EPI
4.67
3.87
2.29
*
4.90
0.46
1.23
0.24
0.64
0.37
0.62
1.71
0.22
0.03
MES
***
9.93
*
6.97
**
6.08
4.00
3.99
2.63
1.68
2.01
2.14
1.06
1.54
0.81
0.22
Relative LFQ intensity, log10
8
6
4
2

Figure 1. Preliminary findings from the Smart laboratory

(A) Ligand–receptor inference analysis performed using CellChat [81] on in-house E13.5 murine whole-heart scRNA-seq dataset, supplemented with literature-based ligand–receptor interactions. Analysis focused on signals transmitted from the epicardium (Epi, EPDC_cyc, and EPDC clusters) to SV-derived and CECs. The results highlight significant communication between VEGF-A from EPDCs and VEGFR2 expressed on SV-derived CECs. The coloured scale indicates relative communication probability, with high communication probability indicated in red, while dot size reflects p-values.

(B) Heatmap showing relative label-free quantification (LFQ) intensities ($\log_{10}$) of selected extracellular and matricellular proteins secreted by the mouse epicardial cell line (MEC1) cultured in epithelial (EPI) and mesenchymal (MES) states for 48 h following EMT induction. Among differentially secreted proteins, SPARC exhibited the greatest upregulation in the mesenchymal state, consistent with its established role in collagen binding and ECM remodelling. Data are presented as the mean. Two-way ANOVA w/ Sidak multiple comparison test (*) P<0.05, (**) P<0.01, (***), P<0.001. E13.5 murine whole-heart scRNA-seq dataset was generated by Dr Andia Nicola Redpath, and the receptor-ligand inference, as well as mass spectrometry analyses, were undertaken by Dr Jacinta Kalisch- Smith.

SV, sinus venosus; CEC, coronary endothelial cell; Epi, epicardium; EPDC, epicardium-derived cell; EPDC_cyc, cycling epicardium-derived cell; VEGF, vascular endothelial growth factor; VEGFR, vascular endothelial growth factor receptor; TGFβ, transforming growth factor beta; NRP, neuropilin; ENG, endoglin; ACVRL1, activin receptor-like kinase 1; PLXND1, plexin D1; INHBA, inhibin subunit beta A; IGF, insulin-like growth factor; ITGB1, integrin beta-1; CXCL12, C-X-C motif chemokine ligand 12; ACKR3, atypical chemokine receptor 3; APLNR, apelin receptor; TEK, angiopoietin-1 receptor (Tie2); ANGPT2, angiopoietin-2; SPARC, secreted protein acidic and rich in cysteine; COL1A1, collagen type I alpha-1 chain; COL1A2, collagen type I alpha-2 chain; PPIA, peptidyl-prolyl cis-trans isomerase A; FN1, fibronectin-1; FSTL1, follistatin-like-1; CALU, calumenin; SERPINF1 (PEDF), pigment epithelium-derived factor; BGN, biglycan; DCN, decorin; IGF2, insulin-like growth factor-2; CXCL12/SD1, C-X-C

motif chemokine ligand 12 / stromal cell-derived factor-1; SLIT3, slit guidance ligand-3.

`

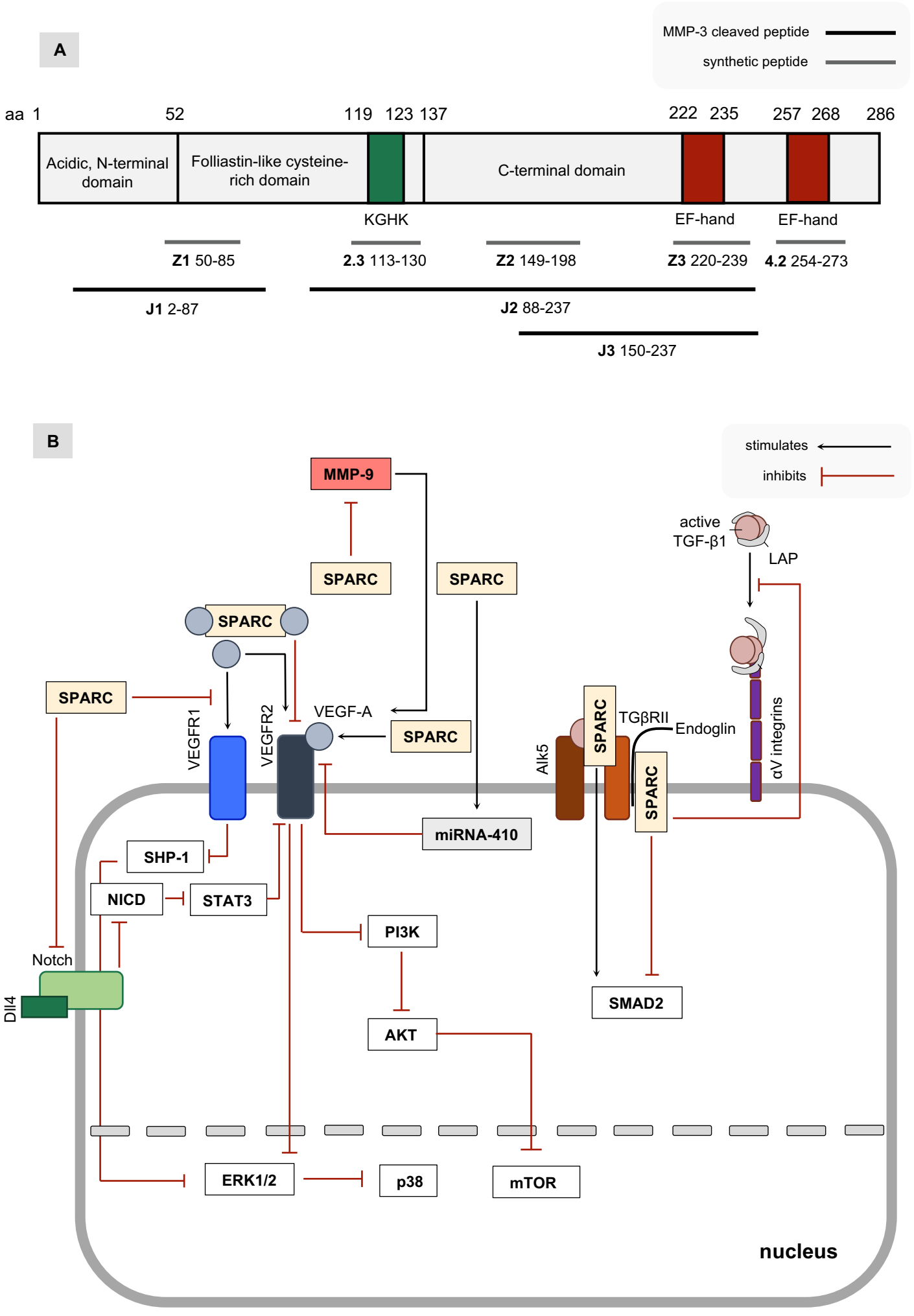

A
MMP-3 cleaved peptide
synthetic peptide
aa 1
52
119
123
137
222
235
257
268
286
Acidic, N-terminal domain
Folliastin-like cysteine-rich domain
C-terminal domain
KGHK
EF-hand
EF-hand
Z1 50-85
2.3 113-130
Z2 149-198
Z3 220-239
4.2 254-273
J1 2-87
J2 88-237
J3 150-237
B
stimulates
inhibits
MMP-9
SPARC
SPARC
SPARC
SPARC
SPARC
VEGF-A
VEGFR1
VEGFR2
miRNA-410
SHP-1
NICD
STAT3
PI3K
Notch
Dll4
AKT
ERK1/2
p38
mTOR
active TGF-β1
LAP
αV integrins
TGβRII
Endoglin
Alk5
SPARC
SPARC
SMAD2
nucleus

Figure 2. Structural domains of SPARC and its peptides, and proposed mechanisms by which they modulate angiogenesis.

(A) Schematic diagram of full-length SPARC protein, which contains three domains: (1) the N-terminal, acidic domain, (2) the follistatin-like, cysteine-rich domain, and (3) the C-terminal domain that contains two EF-hands. Synthetic peptides, as well as those cleaved by MMP-3, are also indicated.

(B) Summary model illustrating context-dependent mechanisms by which SPARC modulates angiogenesis. SPARC influences VEGF-A signalling by binding VEGF-A [113, 125] and modulating its interaction with VEGFR1 [113, 123] and VEGFR2 [115, 118, 123, 125], thereby affecting downstream ERK1/2, PI3K–AKT–mTOR, p38, and Notch–STAT3 pathways [117, 118, 125]. In tumour and endothelial contexts, SPARC suppresses angiogenesis through inhibition of VEGFR2 signalling, VEGF-A availability, and downstream mitogenic pathways, including via induction of miR-410 and suppression of MMP-mediated VEGF-A upregulation [116, 119]. SPARC has also been reported to modulate TGF-β signalling by binding endoglin, an accessory TGF-β receptor, thereby limiting αV-integrin-mediated activation of latent TGF-β1 and downstream SMAD2 phosphorylation [142]. Through this mechanism, SPARC is proposed to facilitate pericyte recruitment and vessel maturation by attenuating excessive TGF-β signalling. Arrows indicate stimulatory interactions, and blunt-ended lines indicate inhibitory effects. This schematic integrates findings from multiple studies and does not imply that all pathways operate simultaneously within a single cellular context.

aa, amino acids; SPARC, secreted protein acidic and rich in cysteine; MMP-3, matrix metalloproteinase 3; MMP-9, matrix metalloproteinase 9; VEGF-A, vascular endothelial growth factor A; VEGFR1, vascular endothelial growth factor receptor 1 (FLT1); VEGFR2, vascular endothelial growth factor receptor 2 (KDR); SHP-1, Src homology region 2 domain-containing phosphatase-1; NICD, Notch intracellular domain; STAT3, signal transducer and activator of transcription 3; Dll4, Delta-like ligand 4; PI3K, phosphoinositide 3-kinase; AKT, protein kinase B; ERK1/2, extracellular signal-regulated kinases 1 and 2; p38, p38 mitogen-activated protein

`

kinase; mTOR, mechanistic target of rapamycin; miRNA-410, microRNA-410; ALK5, activin receptor-like kinase 5 (TGF-β type I receptor); TGFβRII, transforming growth factor-β receptor type II; TGF-β1, transforming growth factor beta 1; LAP, latency-associated peptide; SMAD2, mothers against decapentaplegic homolog 2; αV integrins, alpha-V–containing integrins

`

2 Methods & Materials

2.1. Animal husbandry

2.1.1 Mouse lines

Mouse strains were generated on a C57/BL6 (Charles River Laboratories) genetic background and included Rosa26$^{tdTomato-}$; Wt1$^{CreERT2/+}$ (MGI: 137426 [38]) and Cx40$^{EGFP/+}$, the latter of which was kindly provided by Dr Lucile Miquerol [147]. Pregnant Rosa26$^{tdTomato-}$; Wt1$^{CreERT2/+}$ females were administered 40 mg/kg body tamoxifen by oral gavage at E9.5 and E11.5 for epicardial-lineage tracing, using a previously optimised regimen in the Smart Lab to achieve efficient recombination with minimal toxicity [38]. Experimental litters of Cx40$^{EGFP/+}$ mice were maintained by crossing with C57BL/6J females. For embryo collection, mice (8-12 weeks old) were paired overnight, and females were checked the following morning for the presence of a vaginal plug, which was designated as E0.5. Mice were culled at the stage of interest using CO_2 asphyxiation and confirmation by cervical dislocation. Mice were maintained in individually ventilated cages and ventilated racks at 22°C and 55% humidity in the Institute of Developmental and Regenerative Medicine Biomedical Services Unit under a 12-hour light-dark cycle, with *ad libitum* access to water and standard pellets for food. All procedures requiring a UK Home Office animal licence were performed by Professor Nicola Smart and Dr Jacinta Kalisch-Smith, who are licensed investigators. All animal procedures were approved by the University of Oxford Animal Welfare and Ethical Review Board and conducted in accordance with the Animals (Scientific Procedures) Act 1986 (Home Office, United Kingdom).

2.1.2 Myocardial infarction by permanent ligation of the left anterior descending coronary artery in mice

Permanent ligation of the LAD coronary artery was performed in 8-12-week-old male C57BL/6 mice, as previously described [149]. Mice were anaesthetised with inhaled isoflurane and intubated for ventilation. Body temperature was maintained using a heated pad. Following left thoracotomy at the fourth intercostal space, the pericardium was gently opened, and the LAD

was identified as coursing between the pulmonary artery and the left atrial appendage.

The artery was permanently ligated 1-2 mm below the tip of the left atrium. Immediately following LAD ligation, four intramyocardial injections were administered into the infarct and border zone using a Hamilton syringe. Mice received either human recombinant TGF-β1 (7.5 pmol) (Gibco, #100-21C) combined with human SPARC (R&D Systems, #941-SP-050) (7.5 pmol), SPARC alone or saline (vehicle control).

The chest wall was closed in layers, after which buprenorphine (0.1 mg/kg) was administered subcutaneously for analgesia peri-operatively. Mice were extubated once they regained autonomous, spontaneous breathing and recovered on a heated pad with supplemental oxygen before being returned to their home cage. Hearts were collected 7 days post-injury for downstream analysis. Since the experiment was conducted as a pilot study, the number of animals in each treatment group was two. All MI surgeries were performed by Dr Susanna Cooper (postdoctoral researcher, Riley Lab) and Sarah Sigal (research assistant, Riley Lab).

2.2 Cell culture

2.2.1 Maintenance of mouse epicardial cell line

The spontaneously immortalised mouse epicardial cell line, MEC1 [69], derived from E13.5 wild type hearts (ICR/CD1 strain background), was cultured in high-glucose DMEM (Gibco, #11965092) supplemented with 10% foetal bovine serum (FBS) (Gibco, #17593595) and 1% penicillin-streptomycin (P/S) (Gibco, #15140122) at 37°C, 5% CO_2 in a humidified incubator (Binder, model BD-56). Cells were routinely passaged upon reaching approximately 80% confluence, typically every four to five days, as monitored by a brightfield microscope (CarlZeiss, #12838065). MEC1 cells were used exclusively at early passages (p21–p26), as later passage numbers yielded a highly proliferative phenotype, which would have confounded the robustness and interpretability of our epicardial EMT assays and downstream readouts.

For passaging, the culture medium was aspirated, cells were washed twice in 1x Dulbecco's phosphate-buffered saline (PBS) (Gibco, #10010023), and then incubated with trypsin-EDTA

`

(Gibco, #25200072) for 2 minutes at 37°C and 5% CO_2. Cells were reseeded at a maximum of 1:12 seeding ratio, and when higher dilutions were required, a new frozen vial was thawed. Trypsin-EDTA was neutralised by adding three volumes of growth medium (high-glucose DMEM with 10% FBS, 1% P/S) relative to the volume of trypsin- EDTA used. The cell suspension was centrifuged (Eppendorf, 5804/5804R) at 64 RCF (g) for 4 minutes at room temperature (RT). Cell counts were determined using the Countess™ automated cell counter (Invitrogen) after diluting the cell suspension 1:1 with Trypan Blue (Invitrogen, #T10282), to assess viability, and loading it onto a chamber slide (Invitrogen, #C10228). The desired number of viable cells was plated into pre-coated flasks or assay plates for subsequent experiments. The pellet was resuspended in fresh growth medium for further culturing or assay seeding. The former uses T75 flasks (Corning, #430641U) coated with a 0.1% gelatin solution (STEMCELL Technologies, #07903), whereas assay plates, specified below, were coated with 1% gelatin (Sigma-Aldrich, #G1393) in ultrapure water (Invitrogen, #10977049) for at least 30 minutes at 37°C and 5% CO_2, followed by air drying before cell seeding.

For cryopreservation, MEC1 cells were resuspended in a freezing medium consisting of equal parts of high-glucose DMEM and FBS with 10% dimethyl sulfoxide (DMSO) (Sigma-Aldrich, #D8418), and then aliquoted into cryovials (Fisherbrand, #11787939) at 1×10^6 cells per vial. The vials were transferred to a Mr. Frostie container (Corning, #15542771) and stored at -80°C (Eppendorf, #FRE6202). For thawing, cryovials were rapidly thawed in a 37°C bead bath until only a small amount of ice remained. The suspension was then transferred immediately into a pre-coated T25 flask (Corning, #430639) containing pre-warmed growth medium. After incubation for 24 hours at 37°C and 5% CO_2, cells were washed in 1x PBS and the medium was replaced entirely to remove residual DMSO.

2.2.2 Epithelial-to-mesenchymal transition assay

MEC1 cells were seeded into plates of varying well numbers, depending on the downstream application (qPCR, immunoblotting, or immunofluorescence staining), and incubated overnight at 37°C, 5% CO_2 in growth medium consisting of high-glucose DMEM supplemented with 10%

FBS and 1% P/S. 24 hours later, EMT was induced with TGF-β1(10 ng/mL) and PDGF-BB (50 ng/mL) (Gibco, #100-14B) in high-glucose DMEM containing 2% FBS and 1% P/S. This condition was designated as the mesenchymal (MES) state. For the epithelial (EPI) state, the cells were incubated in high-glucose DMEM containing 2% FBS and 1% P/S without additional growth factors.

Following EMT induction, the culture medium in both EPI and MES conditions was left unchanged throughout the experimental period, except for conditioned media collection. In this case, the medium in both conditions was replaced 8 hours prior to collection with high-glucose DMEM supplemented with 2% FBS and 1% P/S, without additional growth factors, as described in Section 2.3.2.

2.3 Molecular techniques

2.3.1 Reverse-transcription quantitative PCR

RNA extraction

MEC1 cells were seeded in 6-well plates (Corning, #10578911) at densities of 2.27 x 10^4/cm^2 and 1.54 x 10^4/cm^2 for collection at 24 and 48 hours following EMT induction, respectively, with three technical replicates per condition. Total RNA was extracted using the RNeasy® Plus Micro Kit (Qiagen, #74034) according to the manufacturer's instructions, quantified with a NanoDrop™ 2000/2000c spectrophotometer (ThermoFisher Scientific) and stored at -80°C until use.

cDNA preparation

cDNA was synthesised from 500 ng RNA using the High-Capacity cDNA Reverse Transcription Kit (Applied Biosystems, #4368814) on a SimpliAmp™ Thermal Cycler (Applied Biosystems), following the manufacturer's instructions.

RT-qPCR

Relative gene expression was measured on the QuantStudio™ 5 system (ThermoFisher Scientific) using MicroAmp® Fast 384-well plates (Applied Biosystems, #4346907). Each 10

µL reaction contained 1x Fast SYBR™ Green Master Mix (ThermoFisher Scientific, #4385617), cDNA diluted 1:10 in ultrapure water, and 10 µM forward and reverse primers. Thermal cycling conditions were 50°C for 2 minutes, 95°C for 10 minutes during the hold stage, followed by 40 cycles of 95°C for 15 seconds and 60°C for 1 minute. All reactions were run in triplicate.

After testing a panel of five endogenous housekeeping genes (*β-actin, Gapdh, Rn18, Ywhaz, and Canx*) **(Appendix Table 1),** *Ywhaz* was selected for normalisation as having the most stable expression across treatments **(Appendix Fig. 1).** Samples for which melt curves peaked at unexpected temperatures were omitted from analysis to avoid the inclusion of nonspecific DNA products. Relative expression values were calculated using the $2^{-\Delta\Delta CT}$ method [150], where Δ cycle threshold (CT) values were normalised to *Ywhaz* and then expressed relative to the EPI control at 24 hours. Primer sequences for *Sparc* were obtained from a published study [151], while primers for other target genes were established primer sets that had been previously validated and routinely used in the Smart Lab. Primer sequences are listed in **Table 2**.

Gene	Forward sequence (5' → 3')	Reverse sequence (5' → 3')
Ywhaz	GAAAAGTTCTTGATCCCCAATGC	TGTGACTGGTCCACAATTCCTT
Sparc	AAACCGAAGAGGAGGTGGTG	GCAAAGAAGTGGCAGGAAGA
Wt1	TTCAAGGACTGCGAGAGAAG	GGGAAAACTTTCGCTGACAA
Acta2	TCCACGAAACCACCTATAACAGC	CGTTCTGGAGGGGCAATGAT
Tcf21	CGACAAGTACGAGAACGGTTA	TGTAGTTCCACACAAGCGGTT

Table 2. Primers used for RT-qPCR

`

2.3.2 Western Blot

Protein extraction from cells

For lysates, MEC1 cells (p21-26) were seeded in 6-well plates at densities of 2.27 x 10^4/cm^2 and 1.54 x 10^4/cm^2 for harvest at 24 and 48 hours post-EMT induction, respectively, with three technical replicates per condition. Cells were lysed in RIPA buffer (ThermoFisher Scientific, #89900) supplemented with protease (Roche, #118735800001) and phosphatase inhibitors (Roche, #4906845001), and the lysates were stored on ice prior to quantification.

Protein extraction from conditioned media

For secreted proteins, MEC1 cells were seeded in T75 flasks at densities of 1.87 x 10^5/cm^2 and 1.25 x 10^5/cm^2 for collection at 24h+8 and 48h+8 hours post-EMT induction, respectively. At 24 and 48 hours post-EMT induction, both EPI and MES wells were replaced with fresh growth medium of DMEM with 2% FBS and 1% P/S, which lacked additional growth factors to minimise carryover, so conditioned media were then collected 8 hours after this medium change, hereafter referred to as '24h+8h' and '48h+8h'. This step was implemented because, unlike cell lysates, which are washed with PBS before lysis to remove residual growth factors, conditioned media may retain traces of added growth factors from the EMT induction phase. Immediately upon collection, conditioned media (~10 mL) were centrifuged at 1000 RCF (g) for 10 minutes to remove cellular debris and concentrated using 10 kDa centrifugal filters (Sigma-Aldrich, #Z614467), which were pre-washed with 50 mM ammonium bicarbonate (ThermoFisher Scientific, #393212500) and, at pH 8, spun in 1-hour intervals until ~1mL was reached.

Electrophoresis and transfer

Protein concentrations were quantified using the Pierce™ BCA Protein Assay Kit (ThermoFisher Scientific, #23225). Equal amounts of protein (10 µg for lysates, 25 µg for conditioned media) were loaded on a 4-12% SDS-polyacrylamide gel (Invitrogen, #NW04120BOX) and transferred onto PVDF membranes using the Trans-Blot Turbo Mini 0.2 µm PVDF Transfer Pack (Bio-Rad, #1704156).

Immunoblotting

Membranes were blocked in 5% skimmed milk powder dissolved in TBS-T (20 mM Tris, pH 7.5, 150 mM NaCl, 0.1% Tween-20) (ThermoFisher Scientific, #28352) for 1 hour, followed by overnight incubation at 4°C with primary antibodies **(Table 3)**, while rotating. The next day, membranes were washed three times in PBS-T for 10 minutes, incubated for 1 hour at RT with HRP-conjugated secondary antibodies **(Table 4)** and washed again three times in TBS-T for 10 minutes. The protein bands were detected using the Immobilon Crescendo Western HRP substrate (Sigma-Aldrich, #WBLUR0100) and visualised with a ChemiDoc XRS+ Imaging Systems (Bio-Rad, #1708265).

Analysis

For lysates, protein expression was normalised to GAPDH. For conditioned media, Ponceau S (ThermoFisher Scientific, #A4000279) staining was performed to verify even protein loading across lanes **(Appendix Fig. 2A)**. Membranes were immersed in Ponceau S solution for 5 minutes and then rinsed with distilled water until the background was reduced and protein bands were clearly visible. Densitometry analysis [152] was performed in FIJI/ImageJ (version 1.54g) [153].

2.4 Primary cell culture

2.4.1 Explant culture

SV explants were isolated from E11.5 wild-type and Cx40$^{EGFP/+}$ C57BL/6 murine hearts, as previously described [148]. Some embryos were staged using the embryonic mouse ontogenetic staging system (eMOSS), which estimates developmental stage based on limb bud morphology with an accuracy of ± 2 hours [154]. After assessing approximately 14 embryos, it was observed that the developmental stage did not correlate with treatment effects on angiogenic sprouting or arterialisation. Therefore, subsequent experiments omitted embryonic staging, and vessel measurements were instead normalised to explant area. Briefly, embryos were dissected in ice-cold sterile PBS under a stereomicroscope (CarlZeiss, Stemi 305) and hearts were removed following decapitation and opening of the thoracic cavity. The lungs and atria were carefully removed to expose the SV, which was dissected away using fine forceps

(Sigma-Aldrich, #930229). The SV explants were then placed onto polyethylene terephthalate culture inserts (8.0 µm pore size) (Sigma-Aldrich, #PTEP24H48) that were fitted into 24-well plates (Corning, #3524). The inserts were pre-coated with Geltrex (Gibco, #A4000046703) diluted 1:2 in pre-cooled endothelial basal medium-2 (EBM-2) (Lonza, #CC- 3202, which did not include growth factors) and incubated for at least 30 minutes at 37°C, 5% CO_2 in a humidified incubator (PHC Holdings Corporation, MCO-170M-PE). Endothelial growth medium-2 (EGM-2) (Lonza, #CC-3202) supplemented with 10% FBS was then added to both the insert and the well, ensuring that the medium was in contact with the basal membrane of the insert. To facilitate attachment and prevent floating, each SV explant was gently pushed onto the Geltrex immediately after adding the EGM-2. Explants were cultured at 37°C, 5% CO2 in a humidified incubator, and assessed 24 hours later for attachment and spontaneous beating. The explants that failed to attach were discarded.

2.4.2 Explant treatment

On Day 2 (24 hours after plating), the SV explants were serum-starved by replacing EGM-2 with EBM-2 without FBS for 24 hours. Before adding EBM-2, the explants were washed twice with sterile PBS, gently tapping the plate to remove any residual medium. Serum starvation was performed to reduce the basal endothelial proliferation and GF signalling, thereby synchronising the explants and increasing their responsiveness to subsequent treatments. From Day 3 onwards, three treatment regimes were applied. In the first, explants were initially stimulated with human recombinant VEGF-C (100 ng/mL) (Gibco, #100-20CD-20UG) and VEGF-A (50 ng/mL) (R&D Systems, #293-VE-500/CF) on Day 3 to induce sprouting. After two PBS washes on Day 4, they received either EBM-2 as a control, SPARC (10 ng/mL), TGF-β1 (10 ng/mL), or a combination of SPARC and TGF-β1 (each at 10 ng/mL). The treatments were reapplied on Day 5, and explants were harvested on Day 6. In the second regime, explants were not pre-stimulated with VEGF-A/C but were instead treated directly from Day 3 to Day 4 with VEGF-A (100 ng/mL), SPARC (100 ng/mL), both SPARC and VEGF-A (at 100 ng/mL each), or control medium, before being collected on Day 5. The third regime likewise omitted

`

VEGF-A/C pre-stimulation, and explants were treated from Day 3 to 4 with either control medium or conditioned media (200 µg/mL) from MEC1 cells that were cultured in the EPI or MES states for 48 hours. These were also harvested on Day 5 for downstream immunofluorescence staining.

2.5 Imaging sample preparation, acquisition and analysis

2.5.1 Immunocytochemistry

MEC1 cells were seeded in pre-coated PhenoPlate™ 96-well microplates (Revvity, #6055302) at a density of 1,250 cells/cm^2 and harvested at 24, 24+8, 48 and 48+8 hours following EMT induction. Cells were washed twice in PBS and fixed in 4% paraformaldehyde (PFA) (Sigma-Aldrich, #158127) in PBS for 10 minutes at RT, then washed twice with PBS and stored in PBS at 4°C, if not stained immediately. Permeabilisation was performed with 0.5% Triton X-100 (Gibco, #HFH10) for 15 minutes at RT, followed by blocking for 1 hour at RT in PBS supplemented with 0.5% bovine serum albumin (BSA), 0.5% casein and 0.1% sodium azide (abcam, #ab64226). Cells were incubated overnight at 4 °C with primary antibodies **(Table 3)** diluted in blocking buffer. The next day, cells were washed three times in 0.1% Triton X-100 for 10 minutes/wash, incubated for 1 hour at RT with appropriate secondary antibodies **(Table 4)** diluted in blocking buffer, and washed again three times. Nuclei were counterstained with 4', 6-diamidino-2-phenylindole (DAPI) (Sigma-Aldrich, #28718-90-3) diluted in PBS for a final concentration of 250-300 nM, for five minutes before two final PBS washes for 10 minutes/wash. Plates were stored in PBS at 4°C for up to one week prior to imaging.

2.5.2 Immunofluorescence on SV explants

SV explants were fixed in 4% PFA/PBS for 20 minutes at 4°C, permeabilised with 0.5% Triton X-100/PBS at RT for 15 minutes and incubated overnight at 4 °C with primary antibodies **(Table 3)** diluted in blocking buffer. The following day, explants were washed 10-15 times in 0.1% Triton X-100/PBS for 10 minutes/wash, incubated with secondary antibodies **(Table 4)**

`

diluted in blocking buffer overnight at 4 °C and washed again 10-15 times. Nuclei were counterstained with DAPI for 10 minutes at RT, followed by three PBS washes for 10 minutes/wash. Explants were stored in PBS at 4 °C for 3-10 days to reduce background staining.

For mounting, membranes were carefully peeled off from the inserts with fine forceps and inverted onto slides with the explant surface facing upwards. Slides were then mounted in ProLong™ Gold antifade reagent (Invitrogen, #P36930) with coverslips and left at RT for 24 hours to cure before being stored at 4°C.

2.5.3 Cryosections

Embryos younger than E11.5 were fixed intact, whereas hearts were dissected from older embryos. Adult hearts collected 7 days post-MI were cut transversely. Samples were fixed overnight in 4% PFA/PBS at 4°C, washed twice in PBS, and optionally dehydrated in a series of increasing methanol (Sigma-Aldrich, #8222831000) concentrations (25%, 50%, 75%, 90% and 100% methanol/PBS). When ready to be stained, tissues were rehydrated in decreasing methanol concentration (100%, 90%, 75%, 50% and 25% methanol/PBS) and washed in PBS. All samples were washed for 5 minutes at each step, except for E12.5 embryos, which required 15 minutes per wash.

Samples were equilibrated overnight in 30% sucrose/PBS at 4°C, then rinsed in a 1:1 mixture of Tissue-Tek optical cutting temperature compound (OCT) (VWR, #361603E) and 30% sucrose/PBS, followed by two rinses in 100% OCT, before being embedded in 100% OCT, chilled to -80°C. Blocks were cryosectioned as 10 µm-thick sections using a cryostat (Bright Instrument Co. Ltd., OFT500), and mounted on SuperFrost Plus slides (VWR) for storage at -80°C until required.

2.5.4 Immunohistochemistry (IHC)

Cryosections were equilibrated to RT for 10 minutes, rehydrated in PBS, and permeabilised

with 0.5% Triton X-100/PBS for 15 minutes. After blocking for 1 hour at RT, sections were incubated overnight at 4°C with primary antibodies **(Table 3)** diluted in blocking buffer. Sections were then rinsed and washed three times with 0.1% Triton X-100/PBS for 10 minutes/wash, incubated with secondary antibodies **(Table 4)** for 1 hour at RT, and rinsed and washed again three times. Nuclei were stained with DAPI for 5 minutes at RT, followed by two PBS washes for 10 minutes/wash. Slides were mounted in ProLong™ Gold antifade reagent with coverslips and left for 24 hours at RT before storage at 4°C for future imaging. Negative controls (without primary antibody) were included for each secondary antibody to confirm signal specificity **(Appendix Fig. 2B)**.

2.5.5 Masson's Trichrome staining

Masson's Trichrome staining was performed using the manufacturer's protocol (abcam, ab150686). Briefly, cryosetions were incubated in pre-heated Bouin's solution for 60 minutes, cooled for 10 minutes, rinsed thoroughly in tap water, and processed sequentially through Weigert's iron haematoxylin solution, Acid Fuchsin, Phosphotungstic Acid and Aniline Blue solutions. Following incubation (3 minutes) in 1% acetic acid/ MilliQ®water, sections were rapidly dehydrated in 2 changes of 95% ethanol/ MilliQ® water (Supelco®, #1009831011), cleared in 1-butanol (Supelco®, #19422) and mounted in DPX mountant (Sigma®, 06522) with coverslips and left for 24 hours at RT before being stored at 4°C for future imaging.

2.5.6 Whole-mount tissue clearing and immunostaining

Embryonic hearts were fixed in 4% PFA/PBS overnight at 4°C, washed twice in PBS for 10 minutes/wash at RT before incubation in CUBIC-L (Tokyo Chemical Industry, #T3740) for delipidation and decolouring, at 37°C with shaking for at least three days, replacing CUBIC-L daily. E15.5 hearts and older remained in CUBIC-L for an additional two days, replacing CUBIC-L every other day. After three PBS washes at RT for 20 minutes/wash, samples were transferred to 1.5 mL tubes and permeabilised for three days at 4°C in PBS containing 0.1% Triton X-100, 0.2% glycine (Fisher BioReagents™, #BP381500), and 0.2% DMSO, followed

by three days in blocking buffer for three days at 4°C. Hearts were incubated with primary antibodies **(Table 3)** for 5 days at 4°C, washed five times in 0.1% Triton X-100, for 20 minutes/wash, incubated with secondary antibodies **(Table 4)** diluted in blocking buffer for 3 days at 4°C, and washed again five times. For refractive index matching, samples were incubated in a 1:1 solution of CUBIC-R2 (25% urea [Sigma-Aldrich, #U6504], 50% sucrose [Sigma-Aldrich, #S1888], 10% triethanolamine [Sigma-Aldrich, #T0449] and 15% MilliQ® water) and PBS for one day, followed by 100% CUBIC-R2 for at least five days at 37°C, replacing it every day. Before imaging, hearts were embedded in 2% agarose/CUBIC-R2 (Sigma-Aldrich, #A6013) in syringes and set overnight at 4°C.

Antigen	**Marker**	**Host species**	**Company (Catalogue number)**	**Dilution (application)**
ERG	EC nuclei	Rabbit	abcam (ab92513)	1:200 (IF-SV)
CD31 (PECAM-1)	EC surface	Goat	R&D Systems (AF3628)	1:50 (IF-SV, IF-Fr, IF-WM)
Ki67	All except for quiescent (G0) cell nuclei	Rabbit	abcam (ab16667)	1:200 (IF-SV)
Endomucin	EC surface (enriched in veins and capillaries)	Rat	Santa Cruz Biotechnology (sc- 53941)	1:50 (IF-Fr, IF-WM)
SM-MHC	Contractile SMCs	Rabbit	abcam (ab125884)	1:400 (IF-Fr, IF-WM)

`

SPARC	SPARC	Goat	R&D Systems (AF942)	1:100 (IF-Fr, IF-WM) 1:500 (WB)
CD68, clone FA-11	Macrophage / monocytes	Rat	Bio-Rad (MCA1957)	1:200 (IF-Fr)
Cardiac troponin I (cTnI)	Cardiomyocyte -specific contractile protein	Rabbit	abcam (ab47003)	1:100 (IF-Fr)
α-SMA-Cy3	SMCs / activated myofibroblasts (mesenchymal marker)	-	Sigma-Aldrich (C6198)	1:400 (IF-MEC1)
β-catenin	Cell-to-cell adherens junctions (epithelial marker)	Rabbit	abcam (ab32572)	1:250 (IF-MEC1)
GAPDH	Housekeeping protein (loading control	Rabbit	abcam (ab9485)	1:500 (WB)

Table 3. Primary antibodies

EC, endothelial cell; SMC, smooth muscle cell; IF-MEC1: immunofluorescence on MEC1 cells; IF-SV: immunofluorescence on SV explants; IF-Fr: immunofluorescence of cryosections; IF-WM: immunofluorescence of whole-mount tissue; WB: western blot

Fluorophore/ Conjugate	**Host species**	**Company (Catalogue number)**	**Dilution**
AlexaFluor-647	Donkey	Invitrogen (A21447)	1:200
AlexaFluor -546	Donkey	Invitrogen (A10040)	1:200
AlexaFluor -488	Donkey	Invitrogen (A21208)	1:200

`

AlexaFluor -488	Donkey	Invitrogen (A21206)	1:200
AlexaFluor -594	Donkey	Invitrogen (A21209)	1:200
AlexaFluor -555	Donkey	Invitrogen (A21432)	1:200
AlexaFluor -647	Donkey	Invitrogen (A31573)	1:200
HRP	Goat	R&D Systems (HAF017)	1:500
HRP	Rabbit	GeneTex (GTX628142-01)	1:500

Table 4. Secondary antibodies

2.5.7 Microscopy

Images of MEC1 cells and sinus venosus (SV) explants were captured using a Plan-Apochromat 20×/0.8 NA air objective, while images of embryonic and adult cryosections were acquired using a Plan-Apochromat 10×/0.3 NA M27 air objective. Emission detection wavelength windows for each fluorophore were set as follows: 409–516 nm for 405/DAPI, 410–696 nm for 488, 410–696 nm for 546 and 594, and 415–735 nm for 647 and 633.

Images covering an area of 2834.0 × 2834.0 µm were acquired at a spatial resolution of 512 × 512 pixels with a pixel dwell time of 4.10 µs. For all experiments, laser power was kept to a minimum (≤ 1%) to limit phototoxicity and photobleaching. Absolute laser power output was not measured. Detector gain was adjusted to avoid signal under- or over-saturation. Z-stack acquisition was used for all experiments, with the number of optical sections and z-depth adjusted for each sample to ensure complete coverage of the tissue or cells in the z-plane. Where applicable, tiled images were acquired and stitched with a 10% overlap.

Whole-mount hearts were imaged using a light-sheet microscope (CarlZeiss, Z.1) with a Lightsheet Z.1 detection optics 5×/0.16 objective by trained operators Konstantinos Mitis (DPhil student, Srinivas Lab) and Dr Shifaan Thowfeequ (postdoctoral researcher, Srinivas Lab). Confocal images were processed using AngioTool and/or FIJI/ImageJ, while whole-

mount datasets were processed using Imaris Viewer (v10.2.0). For SV explants, display settings were standardised relative to litter-matched controls. Masson's Trichrome–stained sections were imaged using an automated slide scanner (Hamamatsu NanoZoomer S210) by a trained operator (Dr Sophie Payne, Sarah De Val Lab) and analysed using NDP.view2 software.

2.5.8 Image analysis

SV explants

Explant areas were first outlined using the DAPI channel, after which the explant body was excluded to isolate vascular sprouts. The CD31 channel alone was exported as a .tiff file and used as input for AngioTool to quantify total vessel length and junction number, as previously described [155]. Prior to AngioTool analysis, images were pre-processed in FIJI/ImageJ to remove background staining, thereby improving vessel detection accuracy. Within AngioTool, vessel diameter and intensity thresholds were adjusted for each image, alongside parameters for small particle removal and hole filling, to optimise the segmentation of CD31-positive vessels. Based on these user-defined thresholds, AngioTool generates a skeletonised representation of the vascular network and outputs parameters including total vessel length and total number of junctions as a spreadsheet.

Junction number was defined as the total number of branch points within the skeleton, corresponding to areas where more than two vessel segments converge, as illustrated in Zudaire et al. (Fig 7A,C) [155]. Total vessel length (mm) was calculated as the sum of Euclidean distances between adjacent pixels along all skeletonised vessel segments, where a vessel segment is defined as the distance between two junctions or between a junction and an endpoint. As opposed to average vessel length, which represents total vessel length divided by the number of vessels, total vessel length was reported as it reflects the overall extent of vascular sprouting from the SV explants rather than the growth of individual sprouts.

Separately, binary masks were generated for DAPI and ERG channels using FIJI/ImageJ, and

`

ERG+ nuclei colocalising with CD31+ cells were quantified as endothelial sprouts normalised to explant area. Ki67+ ERG+ nuclei were expressed as a percentage of total ERG+ cells to quantify endothelial proliferation. Cx40-GFP+ ERG+ colocalisation identified arterial cells, and its proportion relative to total ERG+ nuclei was calculated as arterialisation. Data were processed into Excel® (version 16.100.3).

MI hearts

The infarct region was identified by cardiomyocyte loss ($cTnI^-$) and macrophage infiltration ($CD68^+$) and manually outlined using ImageJ. To ensure the inclusion of the adjacent border zone, the outlined infarct was enlarged by 20 µm, based on spatial transcriptomics data showing that the border zone spans several micrometres beyond the infarct core [156]. The defined infarct/border zone was mapped onto serial sections with different staining combinations from the same heart. The CD31 channel was exported for vessel length analysis on AngioTool, and binary masks for CD31 and SM-MHC were then used to quantify arterialisation as SM-MHC+ area expressed as a proportion of CD31+ area. Fibrosis was assessed on Masson's Trichrome sections using colour deconvolution in QuPath (version v0.6.0) to distinguish collagen (blue) from myocardium (red), as previously described [157]. The collagen channel was exported and thresholded in FIJI/ImageJ to generate a binary mask of collagen-positive pixels. Fibrosis was quantified as the percentage area occupied by collagen-positive signal relative to the total tissue area analysed and is reported as % fibrosis. Analyses of MI hearts were performed blinded to treatment.

2.5.9 Statistical analysis

All statistical analyses were performed using the GraphPad Prism software (version 10.0). The number of replicates and specific statistical tests used are provided in the corresponding figure legends. For each group, normality was assessed through an F-test. Where the sample size was insufficient for a normality test, data were assumed to follow a normal distribution. Given the small sample sizes used in this study ($n \leq 9$), formal statistical outlier tests were not applied, as these lack sufficient power to reliably identify outliers in small datasets. Instead,

explants deviating by more than ± 2 SD from the group mean were excluded for each outcome measure prior to statistical testing. Therefore, an explant excluded for one outcome measure could be retained for analysis of another, accounting for the differing n values reported across outcome measures within the same experimental condition. Comparisons between two independent variables (EPI vs MES) among two or more groups (24h vs 48h) were analysed by two-way ANOVA with uncorrected Fisher's LSD test or Šídák post-hoc correction for multiple comparisons. For comparisons involving more than two groups, one-way ANOVA or Kruskal- Wallis tests were applied for parametric and non-parametric data, respectively. Dunnett's or Dunn's post-hoc tests were used for pairwise comparisons against control groups, depending on whether the data were normally distributed or not, respectively. Data are presented as individual points with error bars indicating ± 2 SD, as indicated in the figure legends. Significant p-values are reported as * ($p<0.05$), ** ($p<0.01$) and *** ($p<0.001$). Non-significant p-values are provided to three significant figures.

`

3 Results

3.1 SPARC is expressed in regions of actively remodelling coronary arteries

Despite a growing body of evidence implicating SPARC in vascular remodelling [104], its expression in relation to the developing coronary vasculature has not yet been documented. While previous work noted SPARC expression in the embryonic murine heart (E14-E18), this was limited to a binary observation of its presence, without spatial information by imaging [130]. We, therefore, mapped SPARC expression *in vivo* from E11.5 to E16.5 to characterise its spatiotemporal distribution during coronary vessel development, from the earliest formation of an immature coronary plexus to its subsequent specification and remodelling into arteries.

At E11.5, SPARC was broadly distributed throughout the myocardium and endocardium, with enrichment in the right atrium. SPARC localised adjacent to endomucin$^+$ endocardial surfaces of atria and ventricles. During E12.5-E14.5, epicardial expression remained pronounced (**Fig. 3A**). By E15.5, SPARC became concentrated within the walls of the aorta, pulmonary artery and intramyocardial arteries, all of which were invested with SMCs (SM-MHC$^+$). Within the latter, it was expressed adjacent to CECs bearing arterial macrovascular identity, marked by vascular SMC coverage, particularly at the base of the heart (**Fig. 3B**), indicating SPARC availability in the ECM surrounding the CECs, thereby highlighting its proposed role in influencing endothelial functions via ECM interactions as a secreted glycoprotein.

Given the strong association of SPARC with endothelial compartments in the developing heart, we investigated whether its perivascular pattern extended to other embryonic vascular beds. Beyond the heart, SPARC was also observed at E9.5, surrounding endothelial networks in the head and pharyngeal arch vasculature, and by E12.5, its expression extended to mesothelia, paralleling the sinusoidal endothelium of the liver (**Fig. 3C**). The localisation of SPARC to vascular niches, therefore, represents a broader developmental phenomenon.

Complementing these observations in cryosections, we performed light-sheet fluorescence imaging on Cx40-EGFP whole-mount hearts to visualise the 3D spatial relationship between SPARC and coronary arteries. Imaging was carried out at E17.5, when Cx40 expression extends beyond atrial myocardium and ventricular conduction system to mark coronary arteries, as previously described [158] **(Fig. 4A)**.

The Cx40-EGFP reporter line was selected as a marker of coronary arterial identity based on transcriptional evidence from scRNA-seq of SV-derived endothelial populations at E12.5. SV progenitor, coronary plexus, and pre-arterial endothelial populations were projected onto a linear continuum, identifying a subset of ECs that had completed pre-arterial specification, which was characterised by a sharp downregulation of venous markers such as *Coup-Tf2* and the abrupt induction of arterial genes, including *Cx40* [46]. Consistently, single Cx40^{+} cells were detected using *Apj*^{CreER} and *Nfatc1*^{Cre} lineage-tracing models to mark SV- and endocardium-derived ECs within the immature coronary plexus, with tamoxifen induction at E11.5**,** prior to pre-artery specification [46], indicating that Cx40 expression marks early arterial specification rather than mature arteries alone. Therefore, the Cx40-EGFP mouse line can provide a sensitive readout of coronary arterial and pre-arterial endothelium.

By E17.5, when the coronary plexus had remodelled into a more hierarchical arterial tree, SPARC expression was prominent around arteries of smaller calibre **(Fig. 4B)** but was largely absent from Cx40-EGFP^{+} major coronary arteries **(Fig. 4C)**, indicating that SPARC expression during coronary artery development is spatiotemporally restricted to smaller, actively remodelling arteries. This pattern mirrors previous observations, where SPARC was transiently and specifically expressed in nascent, developmentally younger vessels, including in capillaries during periods of rapid angiogenesis in the embryonic brain [102]. In addition, significantly higher SPARC levels were found in smaller, newly formed vessels during CAM morphogenesis compared with larger, more mature vessels [122].

Nevertheless, we cannot exclude suboptimal antibody penetration as a potential confounder in our whole-mount preparations. The reduced definition of the endomucin signal, compared to cryosections, suggests limited antibody access through the thick myocardium. Thus, the

apparent SPARC signal within the compact myocardial layer may, at least in part, reflect a detection gradient rather than genuine enrichment of SPARC. Although cryosections confirm SPARC enrichment at the epicardial surface, we refrain from inferring its distribution within the deeper compact myocardium, except in the interventricular septum, where staining was consistently observed.

3.2 SPARC expression in the epicardial lineage positively correlates with coronary endothelial cells

Given that our proteomic screen identified SPARC as significantly upregulated in the mesenchymal state of epicardial cells *in vitro*, we next sought to determine whether this association was recapitulated *in vivo*. We utilised the epicardial-lineage tracing capabilities of the *Wt1*^{CreERT2}; Rosa26^{tdTomato} mice, in which tamoxifen administration before E11.5 labelled the newly formed epicardium while minimising labelling of SV-derived *Wt1*-expressing endothelium (**Fig. 5A**) [65, 159]. SPARC expression was examined at E14.5 and E16.5, capturing the progression of epiEMT. At E14.5, SPARC was prominent in the epicardial layer, and notably in a subset of EPDCs, identified as tdTomato^{+} cells detaching from the epicardial surface, within the subepicardial space and compact myocardium. With E14.5, following the most dynamic stage of the epicardium, undergoing extensive EMT when there is abundant production of factors to support coronary vessel development [65], SPARC was observed adjacent to EPDCs and ECs in the interventricular septum and the base of the heart. Considering the proximity of the latter to the SV, these ECs might be derived from the SV. By E16.5, SPARC localisation extended beyond the epicardium, colocalising with epicardial-derived mesenchymal cells in regions of high EMT activity such as the apical subepicardium. This expression remained adjacent to CECs invading the myocardium, consistent with the integration of EPDCs into mural compartments of the developing vasculature (**Fig. 5B**). Collectively, during the dynamic phase of epiEMT, SPARC is abundantly expressed in the epicardium, before shifting towards a close association with EPDCs, as well as neighbouring CECs and cardiomyocytes.

`

3.3 SPARC is synthesised and accumulated in the epithelial state before its secretion in mesenchymal derivatives

To further assess the regulation of SPARC during epiEMT, we utilised the MEC1 mouse embryonic epicardial cell line, derived from E13.5 ventricular epicardial explants, which is shown to accurately reflect the plasticity of the ventricular epicardium [160]. We quantitatively assessed the gene, intracellular and secreted protein expression of SPARC in MEC1 epicardial cells cultured in epithelial and mesenchymal states for 24 and 48 hours **(Fig. 6A)**. To confirm that treatment with TGFβ-1 (10 ng/mL) and PDGF-BB (50 ng/mL) appropriately induced EMT, we first examined established phenotypic markers of epiEMT, including β-catenin and α-smooth muscle actin (α-SMA). B-catenin is an intracellular component of adherens junctions that maintains epithelial cell integrity by linking cadherins to the actin cytoskeleton [161], which translocates into the cytosol (and even the nucleus upon active Wnt signalling). α-SMA, a canonical component of actin filaments, is characteristic of cells adopting a mesenchymal phenotype [162, 163]. Fluorescence imaging revealed morphological changes consistent with the adoption of a mesenchymal phenotype upon treatment with TGF-β1 and PDGF-BB. This included the disruption or complete loss of β- catenin-expressing cell-to-cell junctions, cytoplasmic or translocated β-catenin, and/or a clear upregulation of α-SMA expression with spindle-shaped morphology. These mesenchymal features became more evident with increased time in culture under EMT-inducing conditions **(Fig. 6B)**.

Recognising that morphological changes alone cannot definitively indicate epiEMT, or quantify the extent, we next sought to validate our assay at the transcriptional level **(Fig. 6C)**. At 24 hours, the levels of *Wilm's tumour 1 (Wt1)* transcription factor, a master regulator of epicardial identity [164], were reduced by 64% in the mesenchymal (MES) compared to epithelial (EPI) states, albeit non-significantly. However, by 48 hours, *Wt1* remained significantly lower in MES relative to EPI. Transcription factor 21 (Tcf21) is upregulated in epicardium-derived mesenchymal cells, particularly cardiac fibroblasts [65]. Therefore, as expected, *Tcf21* expression increased significantly in the MES relative to the EPI state, a difference that was maintained at 48 hours, with expression in the MES cells being 4.0-fold higher than in EPI

cells. The expression of *Acta2*, encoding α-SMA, was also significantly induced under mesenchymal conditions. At 24 hours, *Acta2* expression was 1.5-fold higher in MES compared with EPI cells, and further increased significantly by 48 hours, consistent with the progressive acquisition of mesenchymal identity with increasing time under EMT-inducing conditions. Taken together, these findings provide a molecular validation of epiEMT in our assay.

Having established the reliability of our epiEMT assay, we next examined how epiEMT influenced *Sparc* gene expression **(Fig. 6D)**. At both 24 and 48 hours, *Sparc* transcript levels were significantly higher in EPI cells compared to MES cells, with EPI cells expressing nearly twice as much as MES cells. Expression of *Sparc* remained stable within each state across the two time points, indicating that the transcriptional regulation of *Sparc* was determined primarily by EPI versus MES identity, rather than duration in culture.

We then assessed whether this transcript-level differential expression was reflected at the protein level **(Fig. 6E)**. At 24 hours, intracellular SPARC expression was modestly higher in EPI compared to MES cells, albeit without significance. By 48 hours, however, intracellular SPARC was significantly upregulated in EPI relative to MES cells, with levels almost double those in MES cells.

To explore how this translated to the secretion dynamics of SPARC, we measured secreted SPARC expression in conditioned media at 24+8 and 48+8 hours, where the media was refreshed 8 hours prior to collection to minimise growth factor carryover **(Fig. 6F, Appendix Fig. 2)**. At both timepoints, SPARC secretion was modestly higher in MES relative to EPI, although differences did not reach significance. This contrasts with our preliminary mass spectrometry analysis of EMT-conditioned media, which showed SPARC as significantly upregulated in the MES relative to the EPI state at 48 hours.

Considering previous reports describing SPARC predominantly within subcellular compartments such as the Golgi-ER complex rather than within the extracellular space [107], we next sought to confirm its lack of differential expression between EPI and MES states at the ECM level. In a preliminary attempt, we, therefore, localised SPARC *in vitro* by immunofluorescence **(Fig. 6G)**. Across both states and timepoints, SPARC was consistently

expressed in the cytoplasm, with little indication of ECM localisation, in line with the relatively faint bands from conditioned media immunoblots. Nevertheless, at 48+8 hours in the MES state, SPARC exhibited a more diffuse and fibrillar distribution extending into the extracellular space, indicative of its secretion following EMT. Taken together, our findings indicate that SPARC is primarily synthesised and accumulates intracellularly within the epithelial state, which initiates its subsequent secretion that increases with the transition to a MES state after 48 hours.

3.4 SPARC augments VEGF-A-induced angiogenesis, while antagonising arterialisation, in sinus venosus-derived coronary endothelial sprouts

SPARC and VEGF-A have both been reported to promote or inhibit angiogenesis [54, 107, 113, 165]. Yet, their investigation during vascular development has been limited to the CAM, in which angiogenic activity was inferred solely from morphometric measures [102, 107, 113, 125]. We combined these metrics with cellular readouts to provide greater resolution of how these factors interact to influence vessel sprouting using SV explants derived from E11.5 Cx40-EGFP murine embryos **(Fig. 7A-C)**.

After 24 hours of culture in endothelial growth medium supplemented with 10% FBS to promote initial sprouting, explants were transferred to basal medium lacking FBS for 24 hours to reduce basal endothelial proliferation and growth factor signalling. This serum-starvation step served to synchronise the explants and increase their responsiveness to subsequent treatments. Explants were then treated for 48 hours with SPARC (100 ng/mL), VEGF-A (100 ng/mL), or a combination of both in serum-free basal medium, with media refreshed every 24 hours and replenished with the corresponding factors **(Fig. 7A)**. Angiogenic sprouting was assessed by quantifying the number of ERG^+ vessels, as ERG is a nuclear marker of ECCs, allowing accurate identification of SV-derived sprouts. SPARC alone modestly suppressed sprouting, reducing it by approximately one-third compared to control, whereas VEGF-A

induced a significant angiogenic response, increasing EC sprouting by 6.4-fold relative to control **(Fig. 7D)**. In light of previous evidence that SPARC binds VEGF-A [125], inhibiting angiogenesis [113, 125], we hypothesised their combined application to reduce sprouting in our assay. We compared sprout numbers in SPARC and VEGF-A-treated explants, not only with the control but also with the VEGF-A-alone group, which served as the positive angiogenic control after demonstrating significant sprouting. Contrary to our hypothesis, this combined treatment in our assay yielded a significant increase in the number of ECs, indicating that SPARC does not antagonise VEGF-A-driven sprouting.

We next quantified total vessel length based on $CD31^+$ endothelial vessels, which showed a similar, albeit non-significant trend **(Fig. 7E)**. VEGF-A increased cumulative sprout length by 40% relative to control, whereas SPARC alone had minimal impact. Interestingly, the SPARC and VEGF-A combination yielded vessels that were shorter than those treated with VEGF-A alone and control, suggesting that while increasing sprouting, SPARC and VEGF-A may hinder sprout elongation, which could be due to increased branching. This led us to examine the number of branch points formed under SPARC and VEGF-A treatment **(Fig. 6F)**, particularly as VEGF-A is well-recognised for guiding the migration of endothelial tip cells at the forefront of the vessel sprouts, where they can join with neighbouring tip cells to generate branches [166, 167]. SPARC alone had a negligible effect on junction formation, while VEGF-A significantly increased junction density by 6.4-fold relative to control. Similarly, SPARC and VEGF-A increased junction density compared to control, which was lower relative to VEGF-A, albeit non-significantly.

The receptor-ligand inference analysis on E13.5 epicardial lineage-traced hearts in our group has predicted strong signalling between EPDC-derived VEGF-A and VEGFR2 expressed on SV-derived CECs. VEGF-A-VEGFR2 signalling has been shown to promote the arterial specification of CECs [51]. Together with the evidence that VEGF-A can upregulate SPARC expression in human microvascular endothelium [168], we reasoned that co-stimulating the SV-derived sprouts with these factors might contribute to their acquisition of arterial identity. We therefore quantified the proportion of ERG^+ sprouts co-expressing Cx40-EGFP, relative to the

total number of ERG$^+$ endothelial cells, under SPARC and VEGF-A treatment conditions **(Fig. 7G)**. VEGF-A significantly increased the proportion of arterialised ECs by 5.4-fold compared with control. On the other hand, SPARC alone, and combined with VEGF-A, each showed a trend towards increased arterialised EC count compared with control, yet these differences did not reach significance.

To explore whether these arterialisation effects were coupled to altered EC proliferation as previously suggested [46, 49, 51], we quantified the proportion of Ki67$^+$ ECs relative to total ECs. Ki67 labels cells engaged in the active phases of the cell cycle (G1–M) and is absent in quiescent (G0) cells**,** providing a measure of EC proliferation **(Fig. 7H).** SPARC treatment alone significantly reduced EC proliferation by 59% compared to control, correlating with its suppression of sprouting. In contrast, VEGF-A-induced arterialisation was not associated with reduced proliferation. The trend towards increased arterialisation observed in the SPARC and VEGF-A group was likewise not accompanied by a significant reduction in proliferation; in fact, the combined treatment yielded proliferation levels almost identical to control, indicating that VEGF-A may override the anti-proliferative effect of SPARC. Overall, SPARC alone decreased EC proliferation and, thereby, had a negligible effect on sprout formation, but did not antagonise VEGF-A-driven angiogenic sprouting, unlike arterialisation.

3.5 SPARC and TGF-β1 bias sinus venosus-derived endothelial cells towards an arterial identity

Although the interaction between SPARC and TGF-β1 has been examined across a variety of physiological and pathological contexts, this has not yet been explored in development. As our group demonstrated an upregulation of SPARC and TGF-β1 in the mesenchymal state of the epicardium, which temporally coincides with the arterial specification of SV-derived CECs *in vivo* [46], we anticipated that their combined administration would favour arterialisation over angiogenesis. Pilot experiments performed by Dr Jacinta Kalisch-Smith indicated that treating SV explants with SPARC and TGF-β1 alone did not induce endothelial sprouting under baseline conditions. Although explants were initially cultured in endothelial growth medium

containing 10% FBS, as in our other treatment regimens of SV explants, additional pro-angiogenic support was required to establish a consistent sprouting response. VEGF-A and VEGF-C, known to promote endothelial sprouting [40], with the latter at moderate levels [54], were hence introduced to promote endothelial sprouting, thereby providing baseline endothelial sprouting that enabled the subsequent assessment of how SPARC (10 ng/mL) and TGF-β1 (10 ng/mL) modulate sprouting and arterialisation **(Fig. 8A)**. With each factor reported to exert both pro- and anti-angiogenic effects, we asked whether SPARC and TGF-β1 combined would influence sprouting in SV explants **(Fig. 8B)**. Nevertheless, none of the treatments significantly altered EC sprouting relative to control, although SPARC and TGF-β1 combination produced the lowest sprouting, decreasing it by 42.5% compared to control **(Fig. 8C)**. Analysis of total vessel length further revealed a partially divergent pattern from sprout counts, whereby SPARC and TGF-β1 combination exhibited moderately longer vessels compared to control, despite the lower sprout count **(Fig. 8D)**. Since the SPARC and TGF-β1 combination did not favour angiogenic sprouting, further quantification of vessel branching was not undertaken.

To determine whether the absence of increased sprouting reflected arterial specification of SV- derived ECs, we next assessed their arterialisation under combined SPARC and TGF-β1 treatment. This significantly increased the proportion of arterialised sprouts by 3.7-fold, whereas SPARC and TGF-β1 each showed only an increasing trend towards arterialisation **(Fig. 8E)**. To determine whether these arterialisation effects were accompanied by changes in EC proliferation, we quantified Ki67-positive endothelial sprouts as a proportion of total ECs **(Fig. 8F)**. Consistent with the model that acquisition of arterial identity precedes the inhibition of cell cycle progression [51], SPARC and TGF-β1 combination reduced proliferating sprouts by 78.7% compared with control, though this decrease did not reach statistical significance. However, it is important to note that the proliferation analysis of this group is underpowered. SPARC alone also reduced proliferation, but, as in the SPARC and VEGF-A regime, this reduction was not significant, likely due to the ten-fold lower SPARC concentration used here compared with the VEGF-A regimen. Taken together, in our SV sprouting model, SPARC, in the presence of TGF-β1, biases endothelial sprouts towards an arterial identity, while trending

towards suppressing proliferation.

3.6 Epithelial cues induce angiogenesis in sinus venosus-derived endothelial sprouts

We demonstrated that SPARC decreases endothelial proliferation, thereby limiting sprouting, and that together with TGF-β1 biases these SV-derived endothelial sprouts towards an arterial phenotype. Considering that both SPARC and TGF-β1 are upregulated extracellularly in the MES state, we next asked whether the angiogenesis of SV sprouts is similarly influenced by the more physiologically relevant paracrine milieu of epithelial and mesenchymal epicardial cells. Therefore, we treated the SV explants with conditioned media derived from epicardial MEC1 cells cultured either in the EPI state or induced to the MES state with TGF-β1 and PDGF-BB for 48 hours to assess the effects of these paracrine signals on endothelial sprouting and proliferation **(Fig. 9A-B)**. Conditioned media were applied at a concentration of 200 µg/mL total protein, which is higher than the concentrations used for isolated growth factor treatments. This concentration was selected based on pilot experiments performed by Dr Jacinta Kalisch-Smith, which demonstrated that lower concentrations of conditioned media did not induce endothelial sprouting, indicating that higher levels of epicardial-derived factors in the conditioned media were required to elicit a measurable angiogenic response.

The EPI state elicited an angiogenic response, significantly increasing EC sprout number by 2.8-fold relative to the control **(Fig. 9C)**. By contrast, MES- conditioned media produced 16% fewer sprouts than the control, implicating an absence of pro-angiogenic, or even the presence of anti-angiogenic, activity. Analysis of total vessel length showed that EPI-conditioned media significantly increased cumulative vessel length by 4-fold compared to control, whereas the MES state induced only a modest 30.8% increase in total vessel length **(Fig. 9D)**. Therefore, in the EPI state, both sprout number and cumulative vessel length increased significantly relative to control, with the gain in length exceeding that in sprout number, indicating that epicardial EPI-associated factors preferentially promote sprout elongation over initiation.

Further assessment of proliferation revealed that EPI- conditioned media significantly doubled the proportion of proliferating sprouts, consistent with a significant increase in sprouting angiogenesis, whereas MES-conditioned media left proliferation essentially unchanged from control levels **(Fig. 9E)**. Taken together, these data show that paracrine factors secreted by the EPI state of epicardial cells stimulate both sprouting and elongation of SV-derived endothelial sprouts, associated with the significant increase in EC proliferation. Contrastingly, factors derived from the MES state of epicardial cells fail to support sprouting angiogenesis. This pattern complements our earlier observation that SPARC, in combination with TGF-β1, both of which are MES-associated factors, limits endothelial sprout expansion to favour arterialisation. Future studies should assess the potential for MES-conditioned media to promote arterialisation.

3.7 Acute delivery of SPARC and TGF-β1 post-MI may increase arterialisation and mature arterial coverage in the infarct/border zone

Having identified SPARC as a regulator of arterialisation during coronary vessel development, we next performed an *in vivo* pilot study to assess whether its pro-arteriogenic effect, when administered with TGF-β1, could be harnessed in the post-MI heart **(Fig. 10A)**. Hearts were harvested 7 days post-MI, guided by prior work showing a significant increase in endogenous SPARC expression in the infarcted left ventricles at 7- and 14-day post-injury [133, 134, 136]. For our pilot, we restricted the harvest of infarcted hearts to 7 days post-injury, which falls within the proliferative phase of cardiac repair, when optimal arteriogenesis can occur [169], thereby supporting the perfusion of the healing infarct and supplying the cells of the granulation tissue with oxygen and nutrients. This design parallels observations with other matricellular proteins, such as follistatin-like 1, where endogenous upregulation of the protein was insufficient for promoting significant regeneration, but instead was achieved with exogenous administration [170]. Considering the limited neovascularisation responses post-MI, we inferred that endogenous production of SPARC and pro-arteriogenic growth factors, such as TGF-β1, following MI would be insufficient or delayed in eliciting arteriogenesis, justifying our

exogenous delivery of SPARC and TGF-β1 at the time of injury. The infarct/border zone (I/BZ) was defined by cardiomyocyte loss ($cTnI^-$) and macrophage infiltration ($CD68^+$), considering that during the proliferation phase of cardiac repair, M2 macrophages are recruited to resolve inflammation in the I/BZ area following the removal of dead cardiomyocytes and other cell types [81] **(Fig. 10B)**. To ensure the inclusion of the adjacent border zone, the outlined infarct was enlarged by 20 μm, based on spatial transcriptomics data showing that the border zone spans several micrometres beyond the infarct core [156]. We then mapped this defined I/BZ area onto serial sections to quantify SPARC expression **(Fig. 10C)**, total vessel length (CD31+) (**Fig. 10D)**, arterialisation, mature arterial coverage (SM-MHC+) **(Fig. 10D)** and fibrosis (Masson Trichrome blue) **(Fig. 10H)**.

SPARC was endogenously expressed in the I/BZ area of control hearts and rose modestly with exogenous SPARC, the addition of TGF-β1 to which yielded a 3.4-fold higher SPARC expression compared to SPARC treatment alone **(Fig. 10E)**, consistent with evidence that TGF- β1 can induce SPARC [138]. Nevertheless, the lack of a TGF-β1-only group means that we cannot attribute the increase in SPARC within the I/BZ area to being driven solely by TGF-β1.

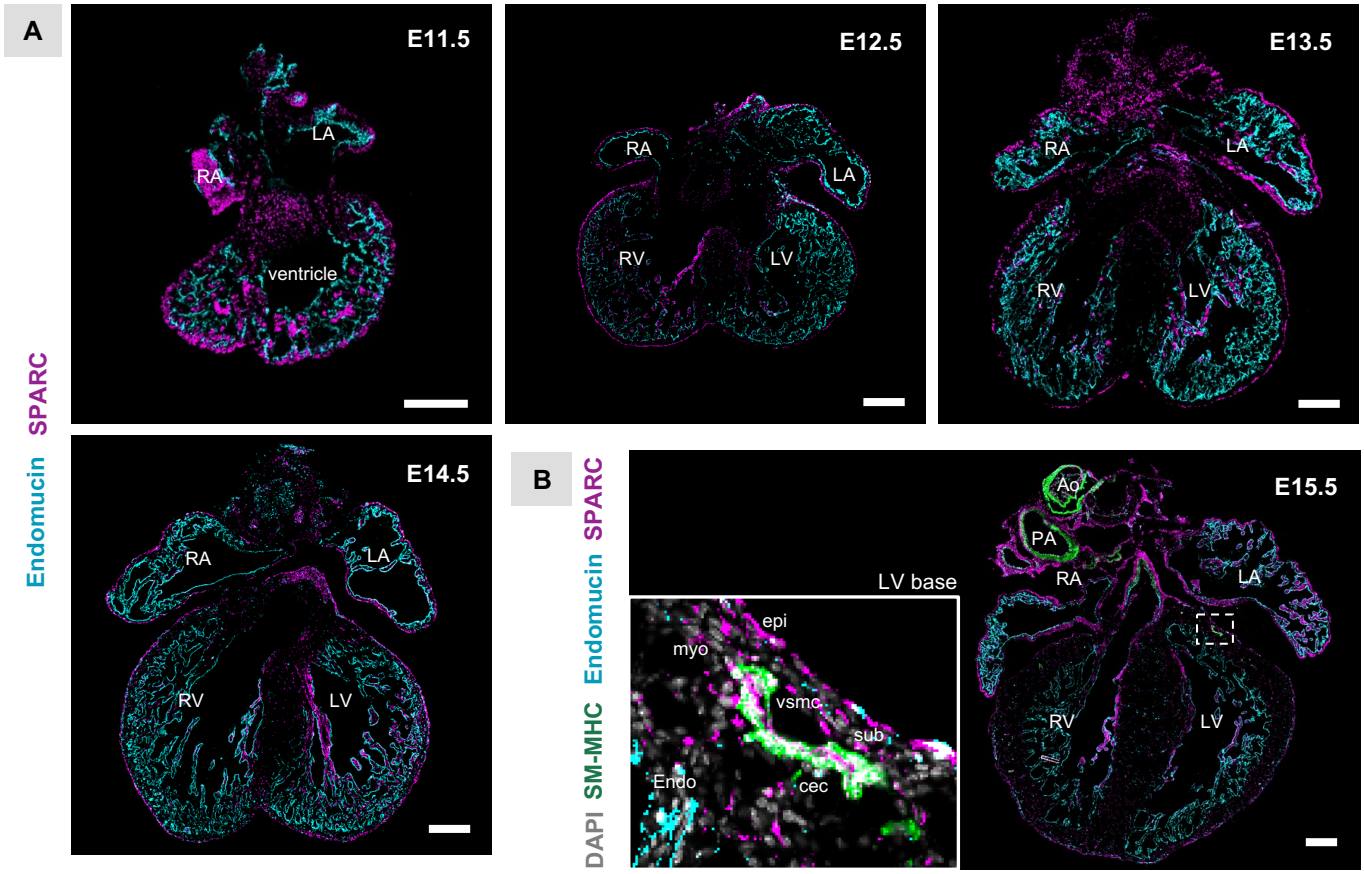
Vascularisation within the I/BZ was assessed by quantifying total vessel length based on the $CD31^+$ endothelium. Compared with control, SPARC alone modestly increased total vessel length, whilst SPARC and TGF-β1 induced a 5.2-fold increase **(Fig. 10F)**. Although this increase did not reach statistical significance, likely owing to the limited sample size, the magnitude of this response indicates that SPARC and TGF-β1 may promote vascular growth post-MI.

In parallel, arterialisation was assessed by quantifying $CD31^+$ endothelial vessels that were invested with SMCs ($SM\text{-}MHC^+$) expression and expressed as a proportion of total endothelial vessels. Importantly, SPARC and TGF-β1 significantly increased the proportion of mature arteries that occupied I/BZ by 3.1- fold compared to control **(Fig. 10G)** and further significantly raised the arterial coverage of the injured myocardium by 6.9-fold **(Fig. 10I)**. SPARC alone, on the other hand, showed only an increasing trend in both measures. Arterial coverage was

quantified as the percentage area of the I/BZ occupied by SM-MHC$^+$ signal. The finding that SPARC, in combination with TGF-β1 rather than alone, significantly improved arterialisation in the infarcted adult heart provides preliminary *in vivo* evidence that SPARC-mediated potentiation of TGF-β signalling promotes revascularisation post-MI, concordant with the reported ability of SPARC to modulate TGF-β signalling [138, 171].

Since both SPARC and TGF-β1 have established roles in collagen deposition in the infarct region [134, 135], the primary constituent of the fibrous scar that prevents cardiac rupture [172], fibrosis was assessed by Masson's Trichrome staining, in which collagen-rich regions are detected as a dark purple/blue signal. Collagen deposition was measured as the percentage area of Trichrome-positive signal within the defined I/BZ region **(Fig. 10H)**. This analysis revealed higher fibrosis with SPARC, alone and in combination with TGF-β1, the latter showing 24.5% higher fibrosis in the I/BZ area than SPARC alone **(Fig. 10J)**. Yet, these differences were not statistically significant in this underpowered pilot. Given that at seven days post-injury, scar formation has not yet entered its maturation phase [173], the higher collagen deposition in the I/BZ area with SPARC and TGF-β1 likely reflects early matrix laid down to replace the lost myocardium rather than maladaptive fibrosis.

`


A
E11.5
LA
RA
ventricle
E12.5
RA
LA
RV
LV
E13.5
RA
LA
RV
LV
Endomucin SPARC
E14.5
RA
LA
RV
LV
B
DAPI SM-MHC Endomucin SPARC
LV base
epi
myo
vsmc
sub
Endo
cec
E15.5
Ao
PA
RA
LA
RV
LV

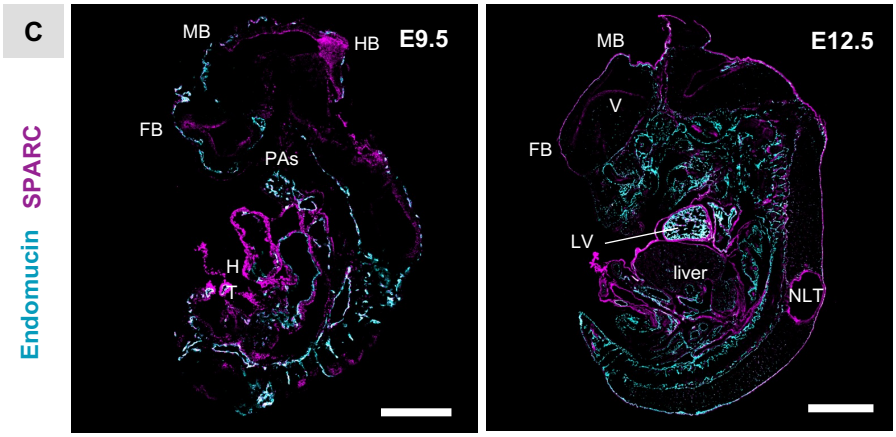

C
Endomucin SPARC
MB
HB
E9.5
FB
PAs
H
T
MB
E12.5
V
FB
LV
liver
NLT

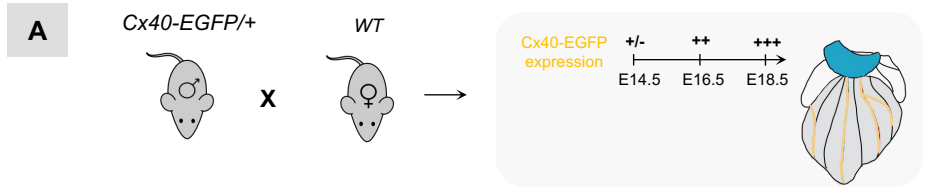
Figure 3. Characterisation of SPARC expression in the developing heart and embryo at E11.5-E15.5

(A) Immunofluorescence on frontal cryosections of E11.5-E14.5 hearts for endomucin and SPARC, showing the latter localised in the epicardium, myocardium and adjacent to endocardial/endothelial cells. Scale bars: 200 μm. Images representative of n=3 embryos for all stages.

(B) Immunofluorescence on a frontal cryosection of an E15.5 heart for SM-MHC, endomucin and SPARC, showing enrichment of SPARC around the aorta, pulmonary artery and intramyocardial arteries. White signal denotes co-localisation of SPARC (magenta) with endomucin marking the endothelium (cyan) and/or SM-MHC-positive SMCs (green), indicating CECs with arterial identity expressing SPARC. Scale bar: 200 μm. Images representative of n=3 embryos.

(C) Immunofluorescence on frontal cryosections of E9.5 and E12.5 sagittal whole-embryo sections for endomucin and SPARC, showing the association of SPARC with endothelial networks beyond those in the heart, including pharyngeal arch vasculature and sinusoidal endothelium of the liver. Scale bars: 100 μm. Images representative of n=3 embryos for both stages. All images shown represent either a single optical plane or a maximum-intensity projection of z-stacks.

HT, heart tube; RA, right atrium; LA, left atrium; RV, right ventricle; LV, left ventricle; PA, pulmonary artery; vsmc, vascular smooth muscle cell; cec, coronary endothelial cell; IVS, interventricular septum; FB, forebrain; MB, midbrain; HB, hindbrain; PAs, pharyngeal arches; SC, spinal cord; V, ventricle; NLT, neural tube; epi, epicardium; sub, subepicardium; myo, myocardium; Endo, endocardium


A
Cx40-EGFP/+
WT
X
Cx40-EGFP expression
+/-
++
+++
E14.5
E16.5
E18.5

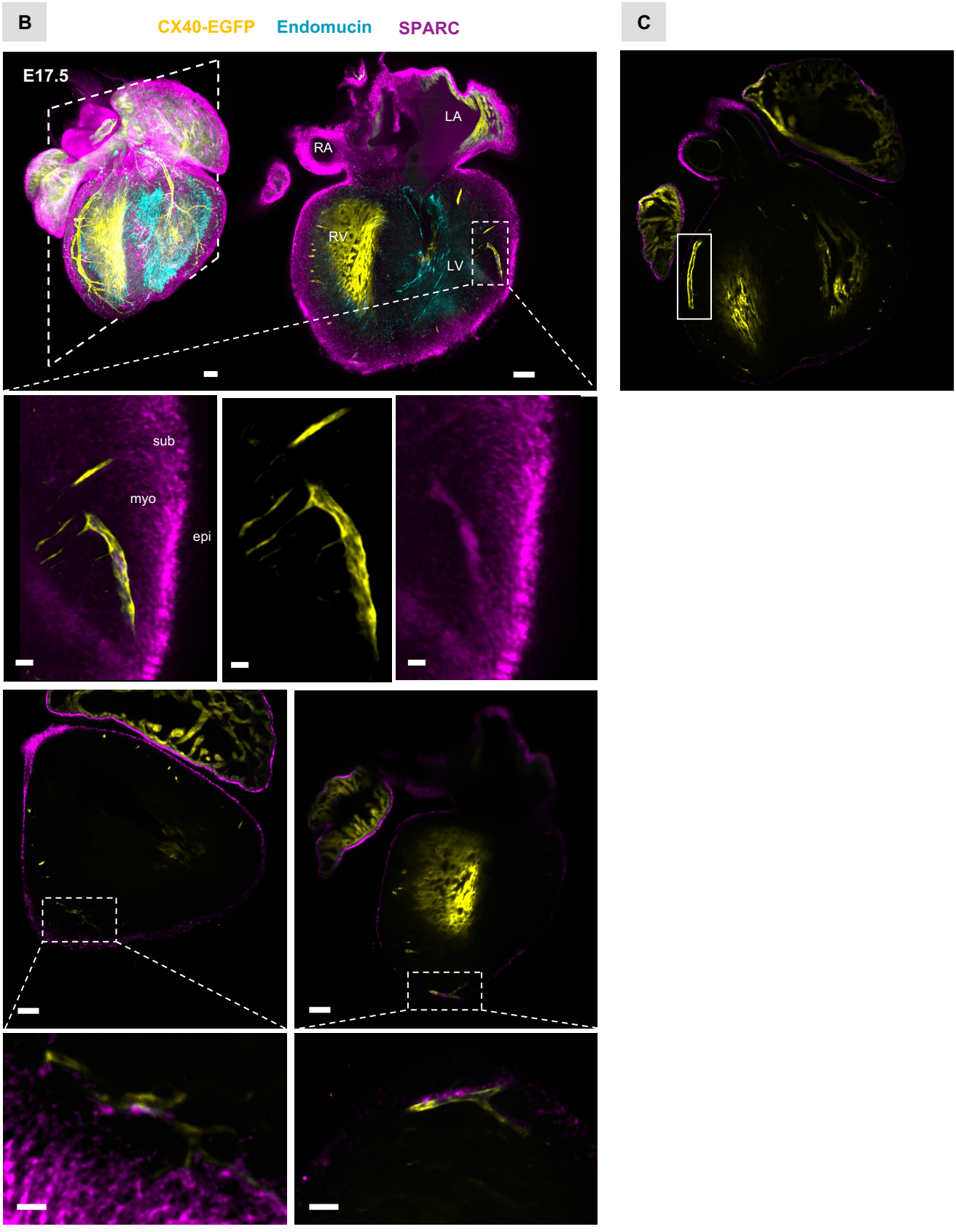

B
CX40-EGFP
Endomucin
SPARC
E17.5
LA
RA
RV
LV
sub
myo
epi
C

Figure 4. SPARC closely associates with remodelling coronary arteries

(A) Generation of Cx40-EGFP reporter mice [147], in which Cx40-EGFP becomes detectable in coronary endothelial arteries (CAs) from E14.5 onwards, as well as in the His-Purkinje system and atria [158].

(B–C) E17.5 whole-mount heart imaged by light-sheet fluorescence microscopy and corresponding coronal optical sections. **(B)** SPARC (magenta) is detected in smaller Cx40-EGFP-positive coronary arteries. **(C)** In contrast, SPARC is absent from a major coronary artery (white boxed region). Scale bars: whole heart, 200 μm; zoomed-in images, 50 μm (top) and 40 μm (bottom). Images of n=1 for both stages. Heart dissection was performed by Jacinta Kalisch-Smith and imaged by Shifaan Thowfeequ.

All images shown represent a maximum-intensity projection of z-stacks.

RA, right atrium; LA, left atrium; RV, right ventricle; LV, left ventricle; epi, epicardium; sub, subepicardium.

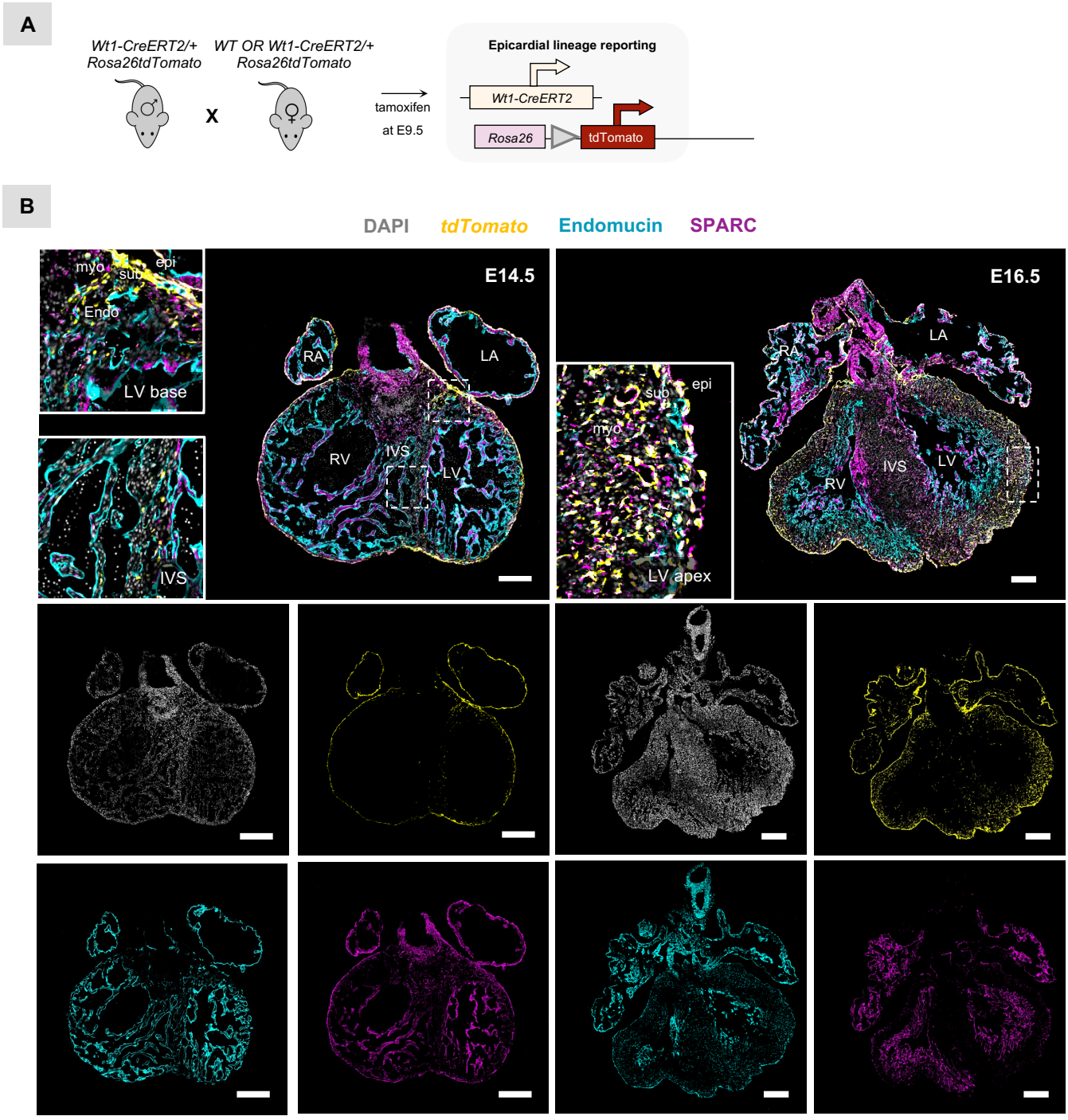

A
Wt1-CreERT2/+
Rosa26tdTomato
WT OR Wt1-CreERT2/+
Rosa26tdTomato
X
tamoxifen
at E9.5
Epicardial lineage reporting
Wt1-CreERT2
Rosa26
tdTomato
B
DAPI
tdTomato
Endomucin
SPARC
E14.5
E16.5
myo
sub
epi
Endo
LV base
IVS
RA
LA
RV
LV
LV apex

Figure 5. SPARC expression in the epicardial lineage positively correlates with coronary endothelial cells

(A) Generation of epicardial-lineage reporting hearts by crossing a heterozygous carrier of the $Wt1^{CreERT2}$ allele and $Rosa26^{tdTomato}$ allele. Pregnant females were induced with tamoxifen at E9.5 to label the newly formed epicardium and trace its derivatives.

(B) Immunofluorescence on frontal cryosections of E14.5 and E16.5 hearts stained for DAPI, tdTomato (labelling epicardial cells and their derivatives), endomucin and SPARC. SPARC expression was detected in epicardial cells and EPDCs, including those surrounding coronary arteries, identified from their round morphology and proximity to the epicardium. EPDCs were defined as $tdTomato^{+}$ cells that were detached or detaching from the epicardial surface. White signal indicates co-localisation of endomucin (cyan) with tdTomato (yellow), or co-localisation of SPARC (magenta) with tdTomato, indicating SPARC expression by EPDCs. Separate single-channel images (DAPI, tdTomato, endomucin and SPARC) are shown for clarity. Images representative of n=1 embryo for both stages.

All images shown represent maximum-intensity projection of z-stacks.

IVS, interventricular septum; myo, myocardium; sub, subepicardium; epi, epicardium; endo, endocardium; WT, wild type; RV, right ventricle; RA, right atrium; LA, left atrium; LV, left ventricle

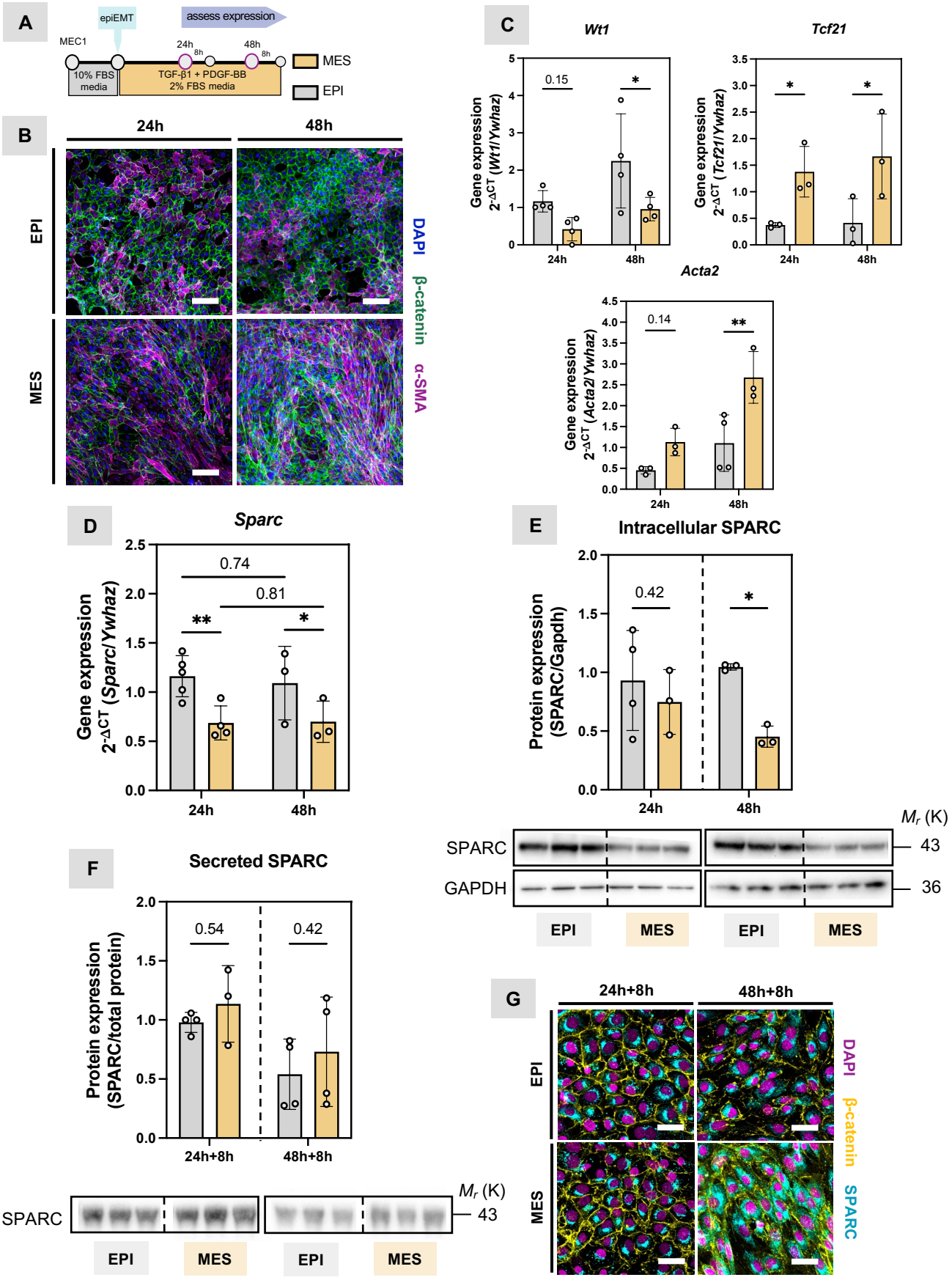

A
epiEMT
assess expression
MEC1
24h 8h
48h 8h
10% FBS media
TGF-β1 + PDGF-BB 2% FBS media
MES
EPI
B
24h
48h
EPI
MES
DAPI
β-catenin
α-SMA
C
Wt1
Tcf21
Gene expression 2-ΔCT (Wt1/Ywhaz)
Gene expression 2-ΔCT (Tcf21/Ywhaz)
0.15
*
*
*
24h
48h
Acta2
Gene expression 2-ΔCT (Acta2/Ywhaz)
0.14
**
24h
48h
D
Sparc
Gene expression 2-ΔCT (Sparc/Ywhaz)
0.74
0.81
**
*
24h
48h
E
Intracellular SPARC
Protein expression (SPARC/Gapdh)
0.42
*
24h
48h
Mr (K)
SPARC
43
GAPDH
36
EPI
MES
EPI
MES
F
Secreted SPARC
Protein expression (SPARC/total protein)
0.54
0.42
24h+8h
48h+8h
Mr (K)
SPARC
43
EPI
MES
EPI
MES
G
24h+8h
48h+8h
EPI
MES
DAPI
β-catenin
SPARC

Figure 6. SPARC is synthesised and accumulated in the epithelial state before its secretion in mesenchymal derivatives

(A) Mouse embryonic epicardial cell line (MEC1) treated under epithelial (EPI) conditions involving basal medium containing 2% FBS or mesenchymal (MES) conditions containing TGFβ-1 (10 ng/mL) and PDGF-BB (50 ng/mL) for 24 or 48 hours. Circles outlined with pink indicate the collection of samples 8 hours after the replacement of media, following treatment with growth factors for 24 or 48 hours, to prevent the carryover effect of growth factors in conditioned media**.**

(B) Immunofluorescence images showing β-catenin and α-SMA staining of epicardial cells treated either under EPI or MES conditions for 24 and 48 hours. Scale bars: 100 μm. Images representative of n=1 experiment.

(C) qRT-PCR quantification of *Wt1, Tcf21, Acta2* and relative expression in EPI and MES-treated epicardial cells. Relative expression was determined using the $2^{-\Delta\Delta Ct}$ method, normalised to *Ywhaz* and expressed relative to the EPI treatment at 24 hours. Data are presented as mean ± SD (n=3-4 experiments). Two-way ANOVA with Šidák multiple corrections tests (*) P<0.05, (**) P<0.01.

(D) qRT-PCR quantification of *Sparc* in EPI and MES-treated epicardial cells. Relative expression was determined using the $2^{-\Delta\Delta Ct}$ method, normalised to *Ywhaz* and expressed relative to the EPI treatment at 24 hours. Data are presented as mean ± SD (n=3-4 experiments). Two-way ANOVA with uncorrected Fisher's LSD test (*) P<0.05, (**) P<0.01.

(E) Western blot showing intracellular SPARC from lysates at 24 and 48 hours in EPI versus MES-treated MEC1 epicardial cells. Blots representative of n=3-4 experiments. Corresponding quantification of intracellular SPARC normalised to GAPDH and expressed relative to EPI treatment at 24 hours. Two-way ANOVA with Šidák multiple corrections tests (*) P<0.05.

(F) Western blot showing intracellular SPARC from conditioned media at 24+8 and 48+8 hours in EPI versus MES-treated MEC1 epicardial cells. Blots of n=3-4 experiments. Corresponding

quantification of intracellular SPARC normalised to total protein and expressed relative to EPI treatment at 24 hours. Two-way ANOVA with Šidák multiple corrections tests (*) $P<0.05$.

(G) Immunofluorescence images showing β- catenin and SPARC staining of epicardial cells treated either under EPI or MES conditions for 24+8 and 48+8 hours. Scale bars: 100 μm. Images of n=1 experiment. Corresponding quantification of the % proportion of epicardial cells with nuclear SPARC.

All images shown represent maximum-intensity projection of z-stacks. For qRT-PCR and immunoblotting, each biological replicate was analysed using a single technical replicate.

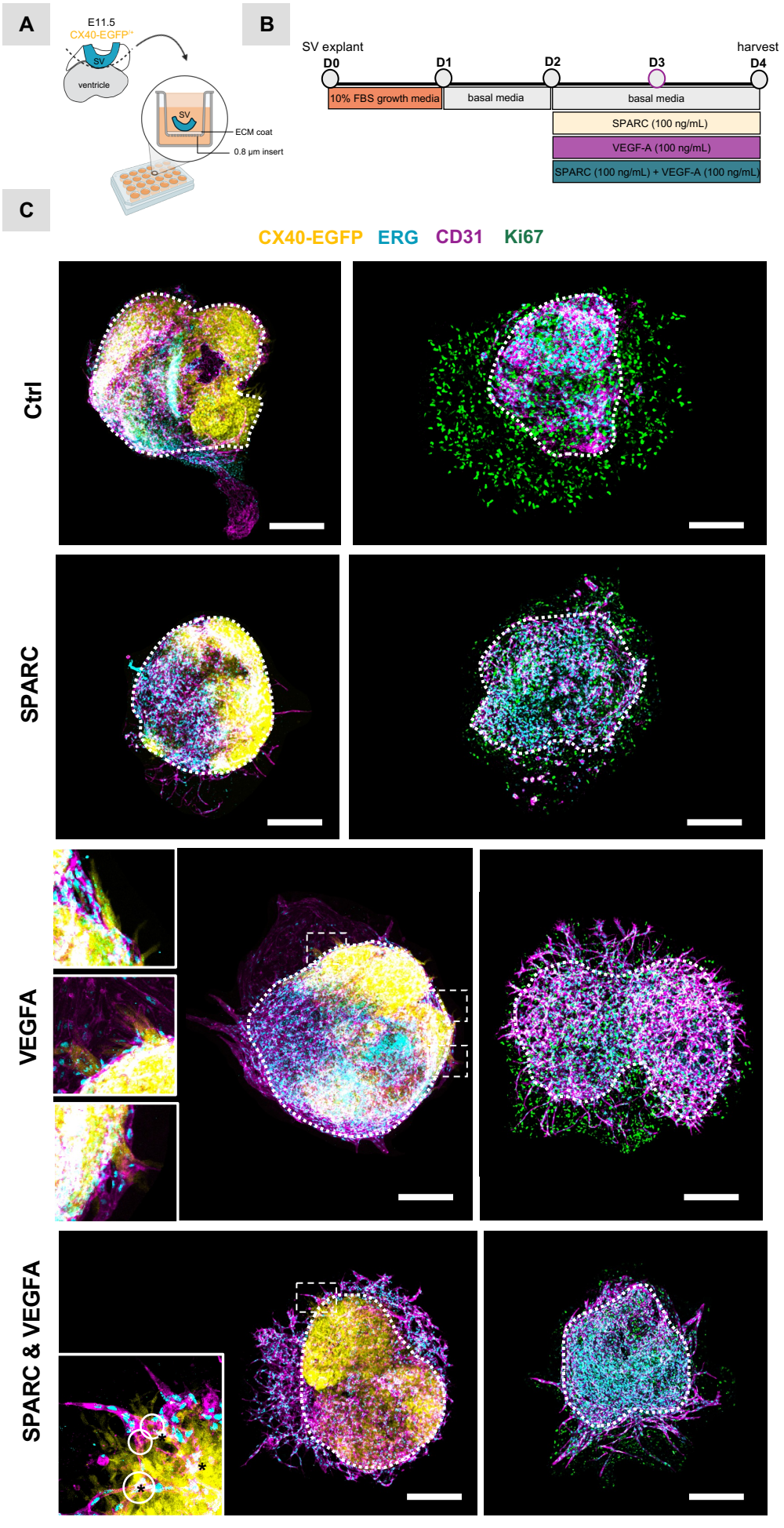

A
E11.5
CX40-EGFP+
SV
ventricle
ECM coat
0.8 µm insert
B
SV explant
harvest
D0
D1
D2
D3
D4
10% FBS growth media
basal media
basal media
SPARC (100 ng/mL)
VEGF-A (100 ng/mL)
SPARC (100 ng/mL) + VEGF-A (100 ng/mL)
C
CX40-EGFP ERG CD31 Ki67
Ctrl
SPARC
VEGFA
SPARC & VEGFA
D
EC sprout count
EC sprouts / explant area (n / µm²)
0.93
0.98
*
**
Ctrl
SPARC
VEGF-A
SPARC & VEGF-A
E
Total vessel length
Total vessel length / explant area (mm / µm²)
0.77
0.74
>0.99
0.31
F
Total junction number
Total junction number / explant area (n / µm²)
0.39
*
< 0.99
0.68
G
Arterialised EC sprouts
Cx40-EGFP+ sprouts / total EC sprouts (%)
0.48
*
0.22
H
Proliferating EC sprouts
Ki67+ sprouts / total sprouts (%)
0.86
0.69
*

Figure 7. SPARC augments VEGF-A-induced angiogenesis, while antagonising arterialisation, in sinus venosus-derived coronary endothelial sprouts

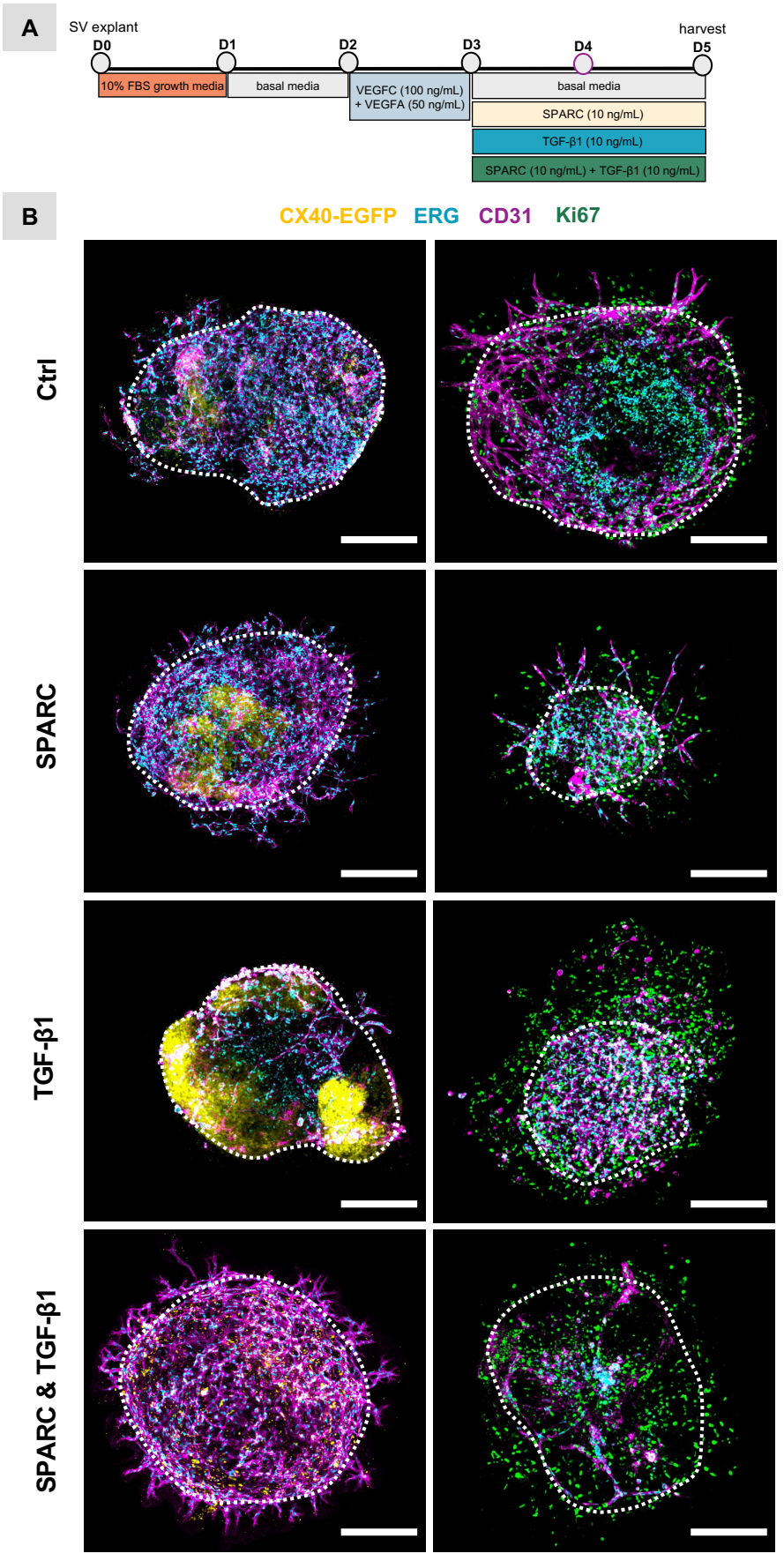
(A) Schematic of SV sprouting assay from E11.5 Cx40-EGFP embryos.

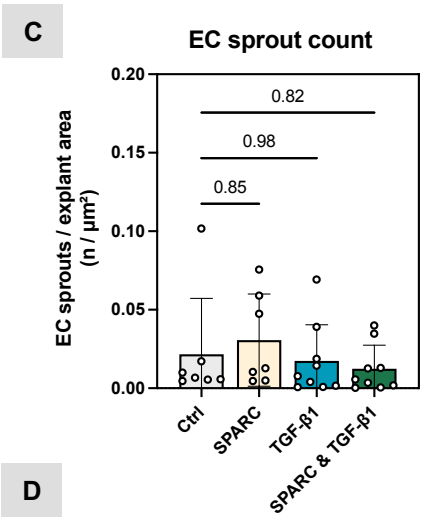
Explants were plated on an ECM coat on porous inserts.

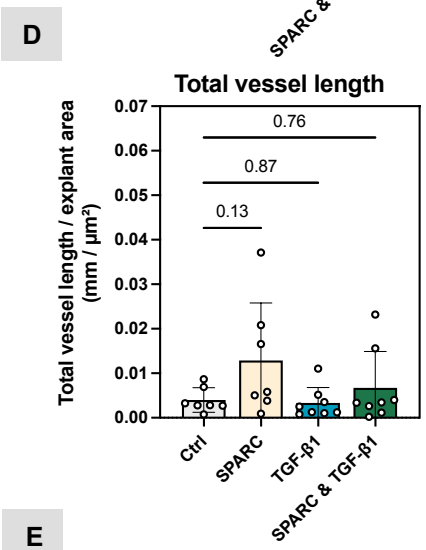
(B) Schematic of the culture timeline. After a day of culture in endothelial growth medium supplemented with 10% FBS to encourage sprouting, explants were switched to basal medium and treated for 48 hours with SPARC (100 ng/mL), VEGF-A (100 ng/mL) or both. Pink-outlined circle indicates reapplication of growth factors.

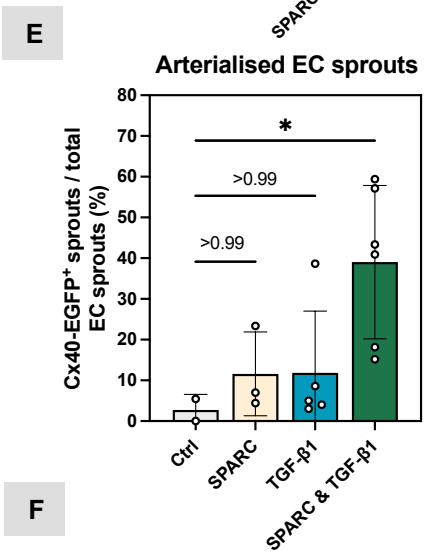
(C) Representative immunofluorescent images of explants stained with ERG, CD31, Cx40-EGFP and Ki67 to assess sprouting, arterialisation and proliferation, respectively. White dashed lines outline the explant area. Circles indicate vessel junctions, while the asterisk denotes an arterial endothelial cell, appearing white due to the co-localisation of ERG (cyan), Cx40-EGFP marking arterial identity (yellow), and CD31 (magenta). Scale bars: 200 μm. Two representative images per condition n=2-11 embryos. All images shown represent maximum-intensity projection of z-stacks.

(D-F) Quantification of **(D)** EC sprout number**, (E)** total vessel length, **(F)** total number of junctions normalised to explant area. Data are presented as mean ± SD (n=7-11 experiments). One-way ANOVA with Tukey's multiple corrections test (*) $P<0.05$, (**) $P<0.01$. **(G)** Quantification of Cx40-EGFP^{+} endothelial sprouts relative to total sprouts, normalised to explant area, showing a significant increase in arterialisation with VEGF-A. Data are presented as mean ± SD (n=4-6 experiments). One-way ANOVA with Dunnett's multiple corrections test (*) $P<0.05$. **(H)** Quantification of Ki67^{+} endothelial sprouts relative to total sprouts, normalised to explant area, showing a significant decrease in proliferation with SPARC. All measurements are normalised to the explant area. Data are presented as mean ± SD (n=2-8 experiments). One-way ANOVA with Dunnett's multiple corrections test (*) $P<0.05$. Experiments (n = 2) were conducted by Jacinta Kalisch-Smith but analysed by me.


A
SV explant
harvest
D0
D1
D2
D3
D4
D5
10% FBS growth media
basal media
VEGFC (100 ng/mL) + VEGFA (50 ng/mL)
basal media
SPARC (10 ng/mL)
TGF-β1 (10 ng/mL)
SPARC (10 ng/mL) + TGF-β1 (10 ng/mL)
B
CX40-EGFP ERG CD31 Ki67
Ctrl
SPARC
TGF-β1
SPARC & TGF-β1


C
EC sprout count
EC sprouts / explant area (n / µm²)
0.20
0.15
0.10
0.05
0.00
0.82
0.98
0.85
Ctrl
SPARC
TGF-β1
SPARC & TGF-β1


D
Total vessel length
Total vessel length / explant area (mm / µm²)
0.07
0.06
0.05
0.04
0.03
0.02
0.01
0.00
0.76
0.87
0.13
Ctrl
SPARC
TGF-β1
SPARC & TGF-β1


E
Arterialised EC sprouts
Cx40-EGFP⁺ sprouts / total EC sprouts (%)
80
70
60
50
40
30
20
10
0
*
>0.99
>0.99
Ctrl
SPARC
TGF-β1
SPARC & TGF-β1

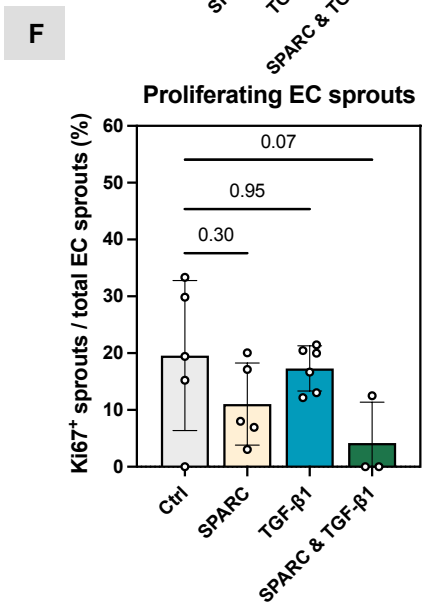

F
Proliferating EC sprouts
Ki67⁺ sprouts / total EC sprouts (%)
60
50
40
30
20
10
0
0.07
0.95
0.30
Ctrl
SPARC
TGF-β1
SPARC & TGF-β1

Figure 8. SPARC and TGF-β1 cooperate to bias sinus venosus-derived endothelial cells towards an arterial identity

(A) Schematic of the culture timeline. SV explants were initially stimulated with VEGF-C (100 ng/mL) and VEGF-A (50 ng/mL) for 24 hours to encourage endothelial sprouting then treated for 48 hours with SPARC (10 ng/mL), TGF-β1 (10 ng/mL) or both.

(B) Representative immunofluorescent images of explants stained with ERG, CD31, Cx40-EGFP and Ki67 to assess sprouting, arterialisation and proliferation, respectively. Pink-outlined circle indicates reapplication of growth factors. White dashed lines outline the explant area. Scale bars: 200 μm. Two representative images per condition n=2-9 embryos. All images shown represent maximum-intensity projection of z-stacks.

(**C-F)** Quantification of **(C)** EC sprout number, **(D)** total vessel length normalised to explant area. Data are presented as mean ± SD (n=7-9 experiments). One-way ANOVA with Dunnett's multiple corrections tests. **(E)** Quantification of Cx40-EGFP^{+} endothelial sprouts relative to total sprouts, normalised to explant area, showing a significant increase in arterialisation with SPARC and TGF-β1. Data are presented as mean ± SD (n=2-6 experiments). One-way ANOVA with Dunnett's multiple corrections test (*) $P<0.05$. **(F)** Quantification of Ki67^{+} endothelial sprouts relative to total sprouts, normalised to explant area, with SPARC and TGF-β1 resulting in a borderline non- significant decrease in proliferation. All measurements are normalised to the explant area. Data are presented as mean ± SD (n=3-6 experiments). One-way ANOVA with Dunnett's multiple corrections tests. Experiments (n = 2) were conducted by Jacinta Kalisch-Smith.

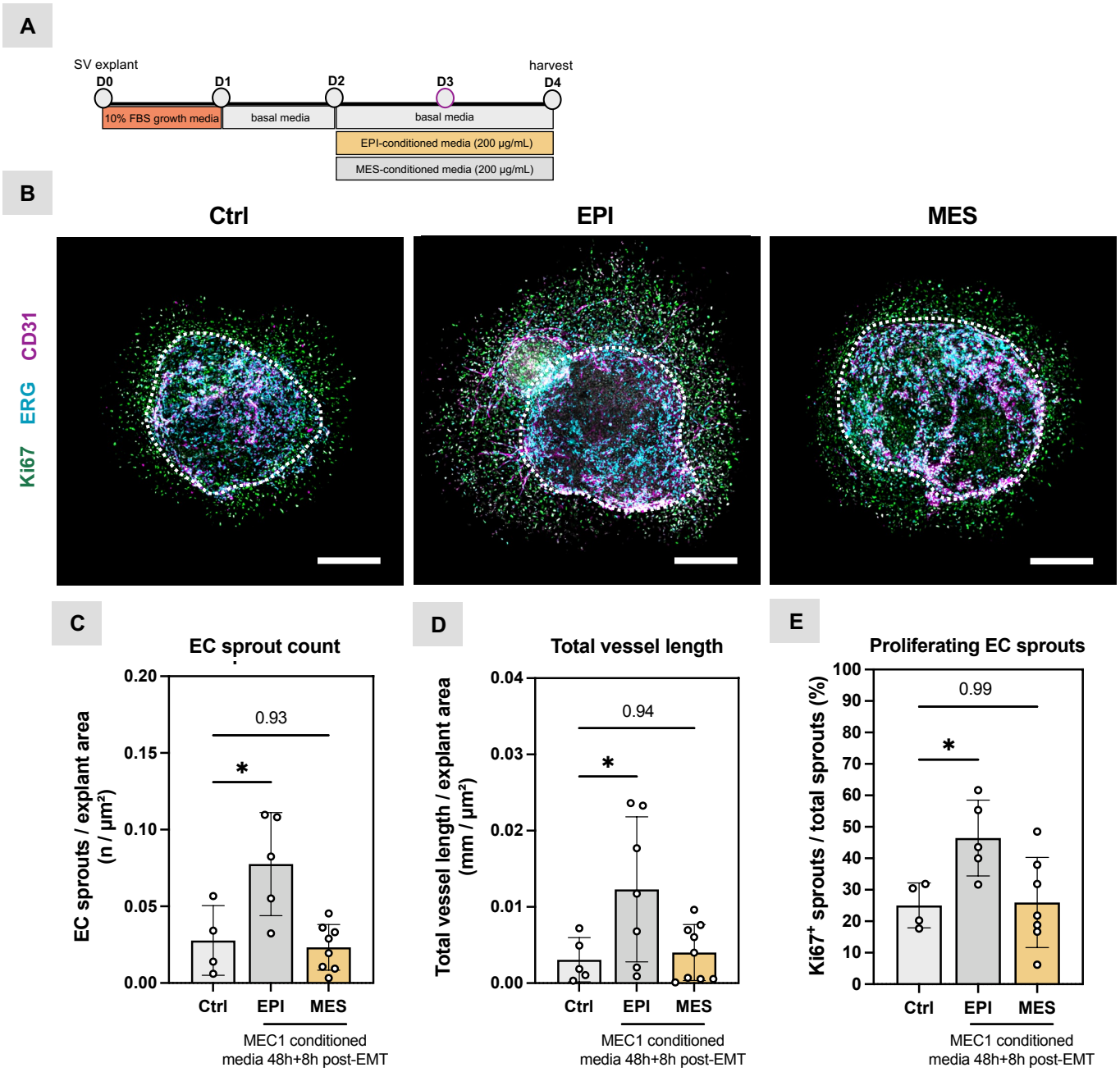

A
SV explant
harvest
D0
D1
D2
D3
D4
10% FBS growth media
basal media
basal media
EPI-conditioned media (200 µg/mL)
MES-conditioned media (200 µg/mL)
B
Ctrl
EPI
MES
Ki67 ERG CD31
C
EC sprout count
EC sprouts / explant area (n / µm²)
0.20
0.15
0.10
0.05
0.00
0.93
*
Ctrl
EPI
MES
MEC1 conditioned media 48h+8h post-EMT
D
Total vessel length
Total vessel length / explant area (mm / µm²)
0.04
0.03
0.02
0.01
0.00
0.94
*
Ctrl
EPI
MES
MEC1 conditioned media 48h+8h post-EMT
E
Proliferating EC sprouts
Ki67⁺ sprouts / total sprouts (%)
100
90
80
70
60
50
40
30
20
10
0
0.99
*
Ctrl
EPI
MES
MEC1 conditioned media 48h+8h post-EMT

Figure 9. Epithelial epicardial cues induce angiogenesis in sinus venosus-derived endothelial sprouts

(A) Schematic of the culture timeline. SV explants were treated for 24 hours either with EPI- or MES-conditioned media (200 µl/mL) derived from MEC1 epicardial cells at 48+8 hours.

(B) Representative immunofluorescent images of explants stained with ERG, CD31, Cx40-EGFP and Ki67 to assess sprouting, arterialisation and proliferation, respectively. Pink-outlined circle indicates reapplication of conditioned media. White dashed lines outline the explant area. Scale bars: 200 µm. Two representative images per condition n=4-8 embryos. All images shown represent maximum-intensity projection of z-stacks.

(C-E) Quantification of **(C)** EC sprout number, **(D)** total vessel length, **(E)** proliferating EC sprouts normalised to explant area. Data are presented as mean ± SD (n=4-8 experiments). One-way ANOVA with Dunnett's multiple corrections test (*) $P<0.05$. Experiments (n = 3) were conducted by Jacinta Kalisch-Smith.

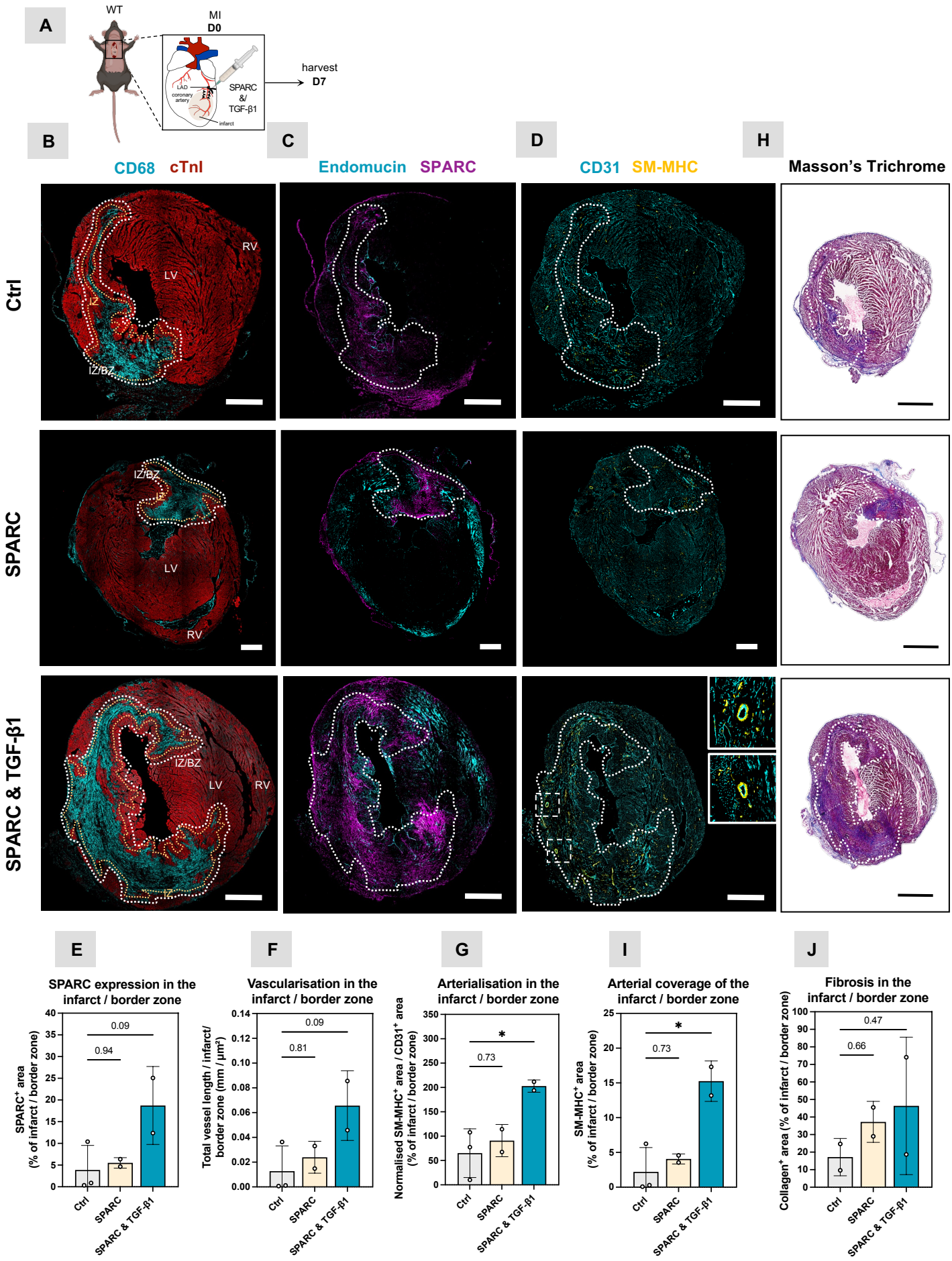

A
WT
MI
D0
harvest
D7
LAD coronary artery
SPARC &/ TGF-β1
infarct
B
CD68 cTnI
C
Endomucin SPARC
D
CD31 SM-MHC
H
Masson's Trichrome
Ctrl
SPARC
SPARC & TGF-β1
RV
LV
IZ
IZ/BZ
E
SPARC expression in the infarct / border zone
SPARC+ area (% of infarct / border zone)
F
Vascularisation in the infarct / border zone
Total vessel length / infarct/ border zone (mm / µm²)
G
Arterialisation in the infarct / border zone
Normalised SM-MHC+ area / CD31+ area (% of infarct / border zone)
I
Arterial coverage of the infarct / border zone
SM-MHC+ area (% of infarct / border zone)
J
Fibrosis in the infarct / border zone
Collagen+ area (% of infarct / border zone)
0.09
0.94
0.81
0.73
0.66
0.47
*
Ctrl
SPARC
SPARC & TGF-β1

Figure 10. Acute delivery of SPARC with TGF-β1 post-MI increases arterialisation and mature arterial coverage in the infarct/border zone

(A) Schematic of the experimental design for our pilot study. Permanent ligation of the left anterior descending coronary artery (LAD) was performed on adult wild-type mice to generate an *in vivo* model of myocardial infarction (MI). Mice received intramyocardial injections of saline (Ctrl) or SPARC, alone or in combination with TGF-β1, concurrent with LAD ligation surgery. Hearts were harvested 8 days post-MI (D7).

(B) Identification of the infarct border zone (I/BZ) by $cTnI^-$ and $CD68^+$ staining. Dashed yellow and white lines indicate the infarct area and IZ/BZ, respectively.

(C-D) The I/BZ area for each heart was mapped onto serial sections stained for **(C)** endomucin and SPARC, and (D) CD31 and SM-MHC to assess neovascularisation. Scale bars: 500 μm. Images representative of n=2-3 adult mice. All images shown represent maximum-intensity projection of z-stacks.

(E-G) Quantification of **(E)** total vessel length, **(F)** SM-MHC+ relative to CD31+ area within the I/BZ representing arterialisation, and **(G)** SM-MHC+ area within the I/BZ representing mature arterial coverage, all normalised to I/BZ area. Data are presented as mean ± SD (n=2-3 experiments). One-way ANOVA with Dunnett's multiple corrections test (*) $P<0.05$. **(H)** I/BZ area mapped onto hearts stained with Masson's Trichrome to assess scar size/fibrosis. Collagen-rich regions appear as dark purple/blue. Scale bars: 1 mm. Images representative of n=2 adult mice. **(I)** Quantification of fibrotic area within the I/BZ area showing SPARC and TGF-β1 trending towards increased fibrosis. All measures are normalised to the I/BZ area. Data are presented as mean ± SD (n=2 experiments). One- way ANOVA with Dunnett's multiple corrections tests.

4 Discussion

Despite extensive evidence implicating SPARC in angiogenesis across diverse contexts, including cancer [114-120], chorioallantoic membrane [102, 107, 122, 125], and post-injury choroidal neovascularisation [123], its role in coronary vessel formation has not previously been examined. Epicardial EMT, which begins around E11.5, temporally coincides with the expansion of sinus venosus–derived sprouts and the emergence of arterial ECs within these sprouts by E12.5 [46]. Building on our group's previous finding that secreted SPARC is significantly upregulated in the mesenchymal compared to the epithelial state, we show here that *Sparc* is paradoxically transcribed in the epithelial epicardial cells. We propose that this transcriptional upregulation in the epithelial state ensures the intracellular accumulation of SPARC, which is then increasingly secreted upon transition to the mesenchymal state, consistent with the *in vivo* developmental remodelling of the epicardial extracellular matrix that is proposed to drive coronary vessel growth [174].

As is characteristic of matricellular proteins, SPARC can bind to growth factors, modulating their availability and receptor activation [175]. Among these, VEGF-A has been shown by our group to be secreted by epicardium-derived mesenchymal cells and to then activate its VEGFR2 expressed on SV-derived CECs. While VEGF-A– VEGFR2 signalling has been well characterised in the endocardium [39] and has been shown to promote both angiogenic sprouting and arterial specification, depending on VEGFR2 activation levels [54], its contribution to SV–derived coronary vessels has remained largely overlooked. Here, we demonstrate that VEGF-A promotes both angiogenic sprouting and arterialisation in SV-derived coronary vessels, the former of which is further maintained in the presence of SPARC. Complementarily, we have shown that TGF-β1, a well- established regulator of arteriovenous specification [49, 143, 144], when co-administered with SPARC, augments TGF-β1-induced arterialisation in SV-derived coronary sprouts, potentially through EC cycle arrest, which is beneficially recapitulated following myocardial infarction.

Although SPARC has been studied extensively in the infarcted heart [133-136], most investigations

have focused on the inflammatory and maturation phases of cardiac repair, during the latter of which it promotes collagen fibre assembly, thereby facilitating infarct healing and preventing cardiac rupture [134]. Here, we examined the effect of SPARC, alone and in combination with TGF-β1, during the proliferative phase of post-MI repair, when neovascularisation predominates [81]. Co-infusion of SPARC and TGF-β1 promoted angiogenesis and arteriogenesis within the infarcted myocardium without inducing excessive fibrosis, albeit these findings were statistically underpowered. Taken together, these findings may reveal a novel role for SPARC, whose secretion is induced by epiEMT, contributing to the switch from coronary angiogenesis to arteriogenesis during development and repair, mainly via its interaction with TGF-β1.

4.1 Epithelial epicardial state favours SPARC synthesis and intracellular accumulation, priming for secretion and proteolytic activation

We have shown that *Sparc* is differentially upregulated in the epithelial epicardial cells, relative to their mesenchymal counterparts, at both 24 and 48 hours following EMT induction. This occurs without a further increase in its transcript levels between these timepoints, suggesting the lack of new SPARC mRNA synthesis, which is plausible given its long half-life of approximately 50 hours [141]. In contrast, a significant rise in intracellular SPARC protein was observed, albeit only at 48 hours, indicating a 24-hour lag between its transcription and protein accumulation in the epithelial state of the epicardium. This paradox is consistent with findings from the CAM, where a marked increase in SPARC protein, which correlated with maximal rates of CAM expansion, succeeded *Sparc* transcript induction by approximately 24 hours [122]. The absence of *de novo Sparc* transcription between 24 and 48 hours following EMT further suggests that this late-phase accumulation of intracellular SPARC is not transcription-driven. Instead, it may reflect post-transcriptional regulation that can either increase the translation efficiency of pre-existing *Sparc* mRNA or promote the stabilisation of its protein within epicardial cells, thereby allowing its build-up in the epithelial state. Supporting this, early work

in fibroblasts reported an increase in SPARC protein despite an absence of its *de novo* mRNA synthesis following exposure to TGF-β [141], implicating a TGF-β- mediated post-transcriptional regulation of SPARC. In our context, such a mechanism may promote the build-up of an intracellular SPARC reservoir in the epithelial state, priming it for release as epicardial cells undergo EMT, particularly given that TGF-β is a well-established inducer of this process [176].

Our *in vivo* observations from the epicardial-lineage traced embryonic hearts demonstrated that EPDCs express SPARC, which is further localised adjacent to ECs at the base of the heart, consistent with an SV origin. The proximity of SPARC-positive EPDCs and ECs reinforces the existence of paracrine interactions between the two, with the extracellular localisation of SPARC suggesting that such signalling likely involves its association with other matrix-bound or soluble factors. These observations were inferred from the E14.5 heart, which developmentally coincides with the arterial specification and remodelling of ECs, in which SPARC may play a spatiotemporal role. To exert its angiogenic or arteriogenic effects on CECs in said paracrine manner, SPARC must be secreted, prompting us to investigate whether the mesenchymal state acts as a switch for its secretion. Prior work in a similar developmental context reported higher SPARC expression in conditioned media derived from mesenchymal parietal endodermal cells compared to their epithelial counterparts: a transition required for cardiomyogenesis *in vitro* [177]. By contrast, we inferred that SPARC secretion occurs both in epithelial and mesenchymal states of the epicardium at 24+8 or 48+8 hours following EMT induction, with secretion increasing as epicardial cells transition towards a mesenchymal phenotype. A likely explanation of this lack of significance is that extracellular SPARC has a short half-life owing to its rapid proteolysis by several proteases [165, 178-180], including MMPs. This, therefore, prevents the accumulation of full-length SPARC in culture media, which is reflected in our immunoblots showing fainter bands of SPARC with increasing time in culture. Consistent with this, MMP-3 cleaves native SPARC within 16 hours [107], which is well before our first conditioned media collection timepoint at 24+8 hours. Notably, the study that reported higher SPARC in conditioned media derived from mesenchymal parietal endodermal cells used an antibody that was solely specific to an epitope within the C-terminal

domain of the mouse SPARC protein (Santa Cruz Biotechnologies, sc-13326) [177]. MMP-3 cleavage generates three fragments, two of which span the C-terminal region, indicating that the increase of secreted SPARC in the mesenchymal state reflects proteolysed SPARC peptides rather than the full-length protein [107]. As our antibody was raised against full-length SPARC and polyclonal, epithelial versus mesenchymal differences in secreted SPARC fragments would not likely have been captured in our WB analysis. This interpretation is further in line with our mass spectrometry analysis of conditioned media derived from mouse epicardial cells at 48+8 hours, which revealed significantly higher SPARC expression in the mesenchymal relative to epithelial state, contradicting our results from WB analysis. This discrepancy may be understood by considering the fundamental differences between the two techniques. In mass spectrometry, proteins are digested into shorter peptides before ionisation, required for the detection of these peptides, which are ultimately mapped onto their parent proteins [181]. As a result, mass spectrometry can capture cleaved SPARC peptides, whereas immunoblotting only detects full-length SPARC, suggesting that epiEMT may induce the secretion of SPARC, which is subsequently rapidly proteolysed in the extracellular space. Despite being exploratory, we also examined the intracellular distribution of SPARC in epicardial cells and found it predominantly localised to subcellular compartments, hinting at a secretory pathway that involves trafficking via the ER and Golgi complex into secretory vesicles for exocytosis at the plasma membrane. This is in line with reports identifying SPARC in the ER-Golgi apparatus [107], as well as within extracellular vesicles [108-110].

Taken together, we propose a model in which SPARC is transcribed and translated in the epithelial state of epicardial cells, establishing an intracellular reservoir. Epicardial EMT may then act as a trigger for its release into the extracellular space, where it can undergo rapid proteolysis to generate bioactive peptides. Several of these peptides were shown to bear a Cu^{2+}-binding KGHK motif, a well-characterised domain that has been shown to induce angiogenesis, when complexed with Cu^{2+}, *ex vivo* and *in vitro*, [122]. Therefore, SPARC released from EPDCs can support coronary vessel growth, consistent with the *in vivo* developmental remodelling of the epicardial ECM, which has been proposed to facilitate coronary vessel development [174].

Consistent with this, conditioned media derived from mouse embryonic epicardial cells cultured for 48 hours under epithelial conditions significantly enhanced sprouting in SV explants, associated with significantly increased endothelial proliferation, likely within the stalk cell compartment of sprouts, driving their elongation. Contrastingly, mesenchymal-conditioned media did not support any angiogenic features, despite containing greater levels of secreted SPARC protein relative to the epithelial state, which, upon cleavage, can generate pro-angiogenic motif-bearing fragments [107]. Paradoxically, proteolysis of SPARC by MMP-3 also yields cleavage products that inhibit endothelial proliferation [107], suggesting that the net angiogenic output of SPARC processing in the ECM may rely on its protease profile and substrate abundance, especially given that MMP-3 increases its proteolytic activity on SPARC with increasing concentration *in vitro* [107]. For instance, epicardial EMT is regulated by the induction of transcription factors such as Snail, Zeb1/2 and Twist, which repress the expression of epithelial markers like E-cadherin and drive the expression of mesenchymal markers, which include MMPs [73]. Furthermore, SPARC enhances the expression of stromelysins [102], a specific group of MMPs that includes MMP-3, establishing a positive-feedback loop in which SPARC promotes its own proteolytic turnover. The dominance of SPARC protein within the mesenchymal epicardial matrix, with which the expression of MMP-3, capable of generating anti-angiogenic fragments, increases, positions induction of epicardial EMT as an attenuator of sprouting angiogenesis. The absence of a pro-angiogenic response under mesenchymal conditions might reflect a transition towards an extracellular milieu that promotes endothelial quiescence and subsequent arterial specification. On this basis, we reasoned that SPARC, combined with growth factors, most enriched in the mesenchymal state, may support coronary arterialisation, leading us to investigate their combined effects on our SV explants.

4.2 SPARC may promote VEGF-A-driven angiogenesis

The receptor-ligand inference analysis performed on epicardial lineage-traced hearts by our group highlighted the relevance of VEGF-A-VEGFR2 signalling between mesenchymal

epicardial cells and SV-derived coronary endothelium. Combined with the known role of VEGF-A in arterial specification of CECs [51], we reasoned that the combined application of these two mesenchymal-associated factors might promote the arterialisation of SV-derived sprouts.

Contrary to this hypothesis, we found that co-stimulation of SPARC and VEGF-A, at the concentrations tested, did not promote the arterialisation of SV-derived sprouts, but rather induced angiogenic sprouting, both of which are likely shaped by multiple factors. To begin with, our observation of increased sprouting contrasts with findings from Cydzik et al. [125], who reported that SPARC combined with VEGF-A reduced angiogenesis in HUVECs, which was further corroborated *in vivo* [125]. This discrepancy may arise from pre-incubation of SPARC and VEGF-A for 45 minutes prior to application, guided by their finding that SPARC binds VEGF-A with slow association kinetics. This pre-incubation likely ensured that any sprouting effects reflected the action of the SPARC-VEGF-A complex itself. On the contrary, in our study, these factors were added without prior pre-incubation to the SV explants, rendering it plausible that the significant increase in sprouting largely reflected the independent effects of SPARC and VEGF-A. This interpretation is consistent with reports showing that VEGF-A phosphorylation of VEGFR2, its primary receptor for mediating pro-angiogenic activity, is rapid, occurring under five minutes of exposure to VEGF-A [182-184]. Therefore, in our culture conditions, VEGF-A is likely to have activated VEGFR2 before a SPARC-VEGF-A complex was allowed to form. Supporting this, VEGF-A alone significantly increased sprouting, exceeding that with SPARC, whereas SPARC alone significantly reduced proliferation of endothelial sprouts, in line with reports describing its anti-proliferative role across various contexts [107, 113, 122, 127]. Therefore, the combined treatment of SPARC and VEGF-A produced an intermediate sprouting response with proliferation nearly identical to that observed with VEGF-A alone. This suggests an additive, rather than a synergistic, interaction of the two factors in our assay, likely dominated by the rapid receptor activation by VEGF-A.

Further complexity to the dynamics of SPARC-VEGF-A binding arises from the fact that they bind at a 2:1 molar ratio under physiological conditions [125]. Our experimental design used near-

equimolar concentrations, meaning that approximately half of the exogenous VEGF-A would remain unbound by SPARC, favouring VEGF-A-driven sprouting. Moreover, VEGF-A has been reported to elicit a biphasic phosphorylation response on VEGFR2 in HUVECs [125], a cell model that might recapitulate the milieu of SV explants to the closest degree among other cell models currently available. With maximal VEGFR2 phosphorylation reported at 10 ng/mL, a ten-fold lower concentration than that used in our assay, it remains possible that VEGFR2 molecules on CEC membranes were already saturated by VEGF-A, leaving a proportion of VEGF-A unbound to potentially associate with SPARC.

Under physiological conditions, SPARC secreted into the extracellular space is likely tethered to matrix components such as collagens, many types of which have been shown to bind to SPARC [185]. Collagen type III, which is abundant in the vascular ECM, especially in association with collagen type I [186], was found to bind SPARC at its C-terminal extracellular domain, specifically involving the αA helix and adjacent αE-αF loop [187]. Interestingly, VEGF-A also binds SPARC at this C-terminal domain [125], although the precise residues or secondary structure elements facilitating the binding remain undefined. Regardless, this shared binding region suggests potential competition between VEGF-A and collagen when binding SPARC. At high local VEGF-A concentrations, VEGF-A, due to having a higher affinity for SPARC (K_d ~150 nM) than collagen (K_d 2 μM) [125], may outcompete collagen binding to SPARC, favouring the formation of SPARC-VEGF-A complexes that are released from the ECM. This mechanism, however, would not apply to VEGF-A molecules already tethered to the ECM via heparan sulphate proteoglycans, as the heparin-binding domain of VEGF-A does not affect its ability to bind SPARC [125]. However, since we used the VEGF-A_{165} isoform in our assay, which, while largely ECM-bound, also exists in a soluble form [188], some VEGF-A would remain available for SPARC binding. The resulting SPARC-VEGF-A complexes can then act as extracellular reservoirs of VEGF-A, modulating its local availability to activate VEGFR2 at the CEC surface. However, when bound to SPARC, VEGF-A may remain functionally sequestered until SPARC undergoes proteolytic cleavage, which can result in, directly or indirectly, the dissociation of VEGF-A from SPARC, rendering it available for VEGFR2 activation. In our system, the use of a non-physiological concentration of exogenous SPARC,

capable of sequestering VEGF-A, could have impeded a VEGF-A gradient, with higher concentrations around the VEGFR2- expressing membrane of endothelial tip cells, from establishing. Given that high VEGF-A- VEGFR2 signalling is required to induce EC cycle arrest and subsequent arterial differentiation [51], insufficient sequestering of VEGF-A by SPARC could have buffered the VEGF-A concentration near tip cells, attenuating VEGFR2 activation to below the threshold necessary for triggering arterialisation. This may further explain why, in our assay, SPARC promoted VEGF-A-driven sprouting rather than arterialisation, as only moderate VEGF-A levels are required for sprouting [54].

An additional methodological difference from Cydzik et al. [125] is that our explants were exposed to SPARC and VEGF-A for only 24 hours before medium replacement with new factors, likely washing away any SPARC-VEGF-A complexes that might have formed. By contrast, their HUVECs remained exposed to the pre-incubated complex for two days, over which they did not report any replacement of media, ultimately observing significantly reduced proliferation. Although arterialisation was not assessed in this study, reduced EC proliferation is a recently recognised prerequisite for arterial specification [51], supporting the possibility that SPARC-VEGF-A complexes, had they been present in culture beyond 24 hours, might have similarly driven arterialisation. Given that SPARC-VEGF-A complexes have slow dissociation kinetics, highly stabilised in the Ca^{2+}-rich vascular ECM (~1 mM Ca^{2+}) via hydrophobic and electrostatic interactions within the N-terminal and EF-hand-containing C-terminal domains [125], a prolonged incubation of the two factors may be required for their complex-mediated effects to emerge. This is notable considering Su et al. [46] showed that the majority of embryonic coronary arteries are specified between E12.5 and E14.5, corresponding to a 48-hour window, implying that persistence of SPARC-VEGF-A complexes in culture beyond 24 hours may establish an arterial identity in endothelial sprouts.

Nevertheless, VEGF-A alone induced a significant increase in arterialised endothelial sprouts relative to control, consistent with *in vivo* studies [51], thereby affirming the physiological relevance of our SV explants as a model for coronary arteriogenesis. Collectively, the stabilising of the SPARC-VEGF-A complex in the Ca^{2+}-rich environment of the ECM indicates

that SPARC modulates VEGF-A activity primarily in the extracellular space, which is likely associated with the mesenchymal state of the epicardium. The lack of arterialisation under combined SPARC and VEGF-A treatment, therefore, likely reflects experimental conditions that did not reproduce the biochemical properties required for their interaction, rather than an intrinsic limitation in their ability to influence arterial specification.

4.3 SPARC promotes arterial specification via TGF-β1 during coronary vessel development and may support vessel growth and arterialisation post-myocardial infarction

A previous study localised SPARC to developing cerebral vessels undergoing angiogenesis *in vivo* [189], while TGF-β1 has similarly been shown to promote endothelial sprouting via the ALK1- TGβRII receptor complex [190]. Nevertheless, the interplay between SPARC and TGF-β1, although extensively examined in fibrotic contexts [191], has been largely overlooked within the vascular setting, particularly during development. Addressing this gap, we demonstrated that SPARC and TGF-β1 together do not support angiogenesis of SV-derived endothelial sprouts.

Unexpectedly, SPARC alone elicited the greatest sprouting, with vessel elongation, relative to control, exceeding that observed with TGF-β1 or the two factors combined. This was not seen in the SPARC-VEGF-A regime, despite similar control conditions. In fact, in that context, SPARC significantly reduced the proliferation of SV-derived ECs, which is required for sprout elongation. The opposing outcomes between the two regimes can be explained by the tenfold higher concentration of SPARC used in the VEGF-A assay, consistent with previous reports of SPARC exerting a biphasic effect on proliferation [191-193].

Contrastingly, SPARC and TGF-β1 together significantly promoted arterialisation of SV-derived ECs. The same combination also produced a near-significant reduction in proliferating sprouts, likely underpowered in our study, suggesting that SPARC and TGF-β1 act cooperatively to drive arterialisation through a proliferation-dependent mechanism. This aligns

with the established model, in which the acquisition of arterial identity in CECs is coupled to cell cycle inhibition [51]. In the context of canonical TGF-β signalling, cell cycle arrest is only achieved through the Smad2/3-mediated activation of p21, an inhibitor of cyclin-dependent kinase 1 [194]. The same effector can be activated by high MAPK/ERK activity downstream of VEGF-A–VEGFR2 signalling, which correlates with increased formation of coronary arteries [51]. Beyond these, TGF-β1 can selectively induce arterial gene expression (*Efnb2*) via Smad2/3 activation exclusively in ECs undergoing cell cycle arrest [49]. These commonalities strengthen the interpretation that SPARC and TGF-β1 promote arterialisation by decreasing the proliferation of SV-derived sprouts.

While our data may define an effector outcome of SPARC and TGF-β1, they do not explain how SPARC modulates TGF-β1 signalling to elicit this arteriogenic response. Previous work has shown that SPARC does not directly bind TGF-β1 in glomerular mesangial cells but instead associates with the TGF-β1–bound TβRII [138]. Given that our *in vivo* data implicate SPARC as a common feature of mesothelium, owing to its broad expression across mesoderm-derived tissues, the findings from mesangial cells may be relevant for understanding how matricellular SPARC transduces cues in its extracellular environment.

Building on this, SPARC has been shown to bind endoglin, an accessory receptor that associates with the heteromeric TβRII–TβRI complex [142]. Since the co- immunoprecipitation assays were performed in 10T1/2 cells, an embryonic murine line that can be differentiated into pericytes, endoglin in this context likely interacts with the ALK5–TβRII complex, as pericytes express ALK5 but not ALK1 [195]. In this study, pericytes from *Sparc*-null mice exhibited dissociated focal adhesion complexes (FACs) associated with endoglin, in contrast with wild-type cells [142]. Furthermore, exogenous SPARC treatment reduced endoglin-associated αV integrins [142], which are contained within the FACs and have well-established roles in activating latent TGF-β1 to enable its downstream signalling, although the precise activation mechanisms vary by cell type [145]. Exogenous SPARC was therefore proposed to impair the presentation of active TGF-β1 to its receptor, leading the authors to conclude that SPARC negatively regulates ALK5–TβRII signalling via the Smad2/3 pathway.

This discrepancy with our findings, where exogenous SPARC and TGF-β1 reduce EC proliferation, likely as an effector of Smad2/3 activity, to promote arterialisation, can be explained by several factors. To begin with, the dissociation of endoglin-FAC and endoglin-αV integrin complexes occurred only at high SPARC concentrations ranging between 50 µg/mL and 150 µg/mL [142], 500- to 1500-fold greater than those used in our assay. Indeed, the same study reported almost identical levels of endoglin-αV integrin complexes at a lower SPARC dose of 10 µg/mL in *Sparc*-null relative to wild-type pericytes and further observed that knocking down endoglin in wild-type pericytes did not alter baseline phosphorylation of Smad2 [142]. Corroborating this, another study reported *Sparc* knockdown in fibroblasts was shown to reduce the phospho-Smad2/Smad3 ratio following TGF-β1 stimulation [141]. Collectively, these data suggest that SPARC does not antagonise TGF-β1 signalling, which is mediated via the ALK5-TβRII-Smad2/3 axis and may instead modulate it in a concentration-dependent manner.

It is important to note that these studies were not performed in ECs, which, unlike fibroblasts and pericytes, express both ALK1 and ALK5 receptors. This dual receptor system adds complexity to how SPARC might regulate the arteriogenic output from TGF-β1 signalling Endoglin, primarily its long form, can bias signalling toward ALK1 and downstream Smad1/5 activation, promoting endothelial proliferation while counteracting the cell cycle arrest-promoting ALK5-TβRII-Smad2/3 activation [196]. The differential outputs favoured by ALK1 and ALK5-TβRII signalling mirror our proposed model in which the epithelial epicardial state promotes angiogenesis, while the mesenchymal transition favours arterialisation, consistent with the mesenchymal association of SPARC and TGF-β1. Interestingly, ALK1 is preferentially expressed in the arterial endothelium and silencing ALK1 expression in cultured ECs enhances vascular sprouting while reducing the expression of the early arterial marker, *EphrinB2*. Loss of *Alk1* in mice results in AVMs, underscoring its role in establishing arteriovenous identity [197]. We therefore propose that SPARC accumulation within the extracellular space during the mesenchymal state may either mediate the receptor preference of endoglin, favouring ALK5–TβRII activation, or bind TβRII, both of which can culminate in Smad2/3 phosphorylation shown to favour the acquisition of arterial identity in arrested ECs [49] **(Fig. 11)**.

This mechanism may extend to the post-injury setting as Smad3 is heavily implicated in post-MI cardiac repair, owing to reports describing its activation of reparative myofibroblasts and promotion of the anti-inflammatory, reparative M2 phenotype of macrophages [198], all of which can foster neovascularisation. In line with this, vascular coverage of SMCs within the infarct/border zone region at 7 days post-MI increased following SPARC and TGF-β1 administration, relative to vehicle. Although the effects of TGF-β1 on SMC proliferation appear concentration-dependent *in vitro*, *in vivo* evidence identifies it as a potent stimulator of arterial SMC growth through Smad3-dependent mechanisms [199-202]. Similarly, TGF-β1 also promotes SMC migration, which, together with its proliferation, is required for the maturation of newly formed arteries. For instance, inhibition of ALK5 or short hairpin RNA-mediated knockdown of its downstream effectors, Smad2 or Smad3, was shown to reduce SMC migration [203]. Therefore, our proposed model, whereby SPARC augments TGF-β1-mediated Smad2/3 activation to drive arterial specification of ECs, may also extend to the post-MI arterial remodelling.

Consistent with this, SPARC and TGF-β1-treated post-MI hearts displayed significantly greater arterialisation compared to vehicle controls. The absence of a corresponding increase in total coronary vessel growth likely reflects both underpowered analysis and methodological limitations, as AngioTool [155] was optimised for explant sprouting rather than quantifying vessels in transverse-cut tissue sections. Nevertheless, since endothelial proliferation peaks within four days of infarction [90], later phases (> 4 days) may inherently favour arteriogenesis over angiogenesis, a pattern recapitulated by SPARC and TGF-β1 in the coronary vessel sprouting assay. Interestingly, *Sparc* expression rises as early as day 3 post-MI, coinciding with reduced CD31 protein levels in wild-type hearts. This reduction was attenuated in *Sparc*-null mice, suggesting that the absence of SPARC preserves vessel numbers [135]. Together, these findings raise the possibility that temporally regulated SPARC expression mediates a switch in TGF- β1 signalling, from inhibiting to promoting coronary vessel growth and arteriogenesis, as the heart transitions from the inflammatory to the proliferative phase of repair.

Nevertheless, the lack of a TGF-β1-only group in our post-MI study prevents us from distinguishing the additive from synergistic effects of SPARC and TGF-β1. Schellings et al. [134] reported increased coronary growth in *Sparc*-null infarcted hearts treated with TGF-β1 relative to wild-type controls, although their dosage, 13.3-fold higher and delivered continuously via osmotic minipumps, exceeded ours. Even after accounting for this, their cumulative exposure per day remained substantially greater than our single administration, which may explain their more pronounced angiogenic response. Therefore, it remains plausible that combined SPARC and TGF-β1 treatment could outperform either factor alone when dose-matched with their study.

Notably, we have also shown that SPARC and TGF-β1 administration may increase collagen deposition within the infarct/border zone at day 7 post-MI, although this was a moderate increase due to the limited sample size. Previous studies have largely focused on whether *Sparc* deficiency impairs infarct healing and whether this dependency involves TGF-β1, investigating either early post-MI phases (≤ 3 days) or late scar maturation (≥ 14 days) [134, 135]. The role of SPARC appears temporally dichotomous as *Sparc*-null mice have shown improved cardiac function at an early stage, evidenced by attenuated decrease in ejection fraction and a lower increase in end-diastolic volume [135]. In a separate study, these *Sparc*-null mice were shown to exhibit a fourfold increase over 14 days post-MI in mortality due to increased rupture and heart failure, owing to disorganised and immature collagen [134]. These opposing outcomes suggest that SPARC–TGF-β1 signalling may shift from maladaptive to reparative across phases of infarct healing.

Mechanistically, TGF-β1 can enhance fibroblast activity by stimulating proliferation and migration, primarily through ALK5–Smad2/3 signalling. It also promotes differentiation into myofibroblasts that secrete ECM proteins such as collagens [198], many of which directly bind SPARC [175]. Here, SPARC functions as a cofactor of collagen assembly by binding newly secreted procollagen in the ECM and shielding collagen from premature engagement with cell-surface receptors such as discoidin domain receptors, which have recently been characterised to engage the SPARC binding site on fibrillar collagen [187]. This prevents the deposition of

premature fibrils, allowing procollagen to be properly processed prior to its spatiotemporal deposition in the infarct zone. This can stabilise the scar, preventing myocardial rupture. Accordingly, *Sparc*-null dermal tissues exhibit thin, poorly cross-linked fibrils with reduced tensile strength [128], which can render them more prone to degradation by collagenases. In addition, increased maturation and deposition of collagen through SPARC-mediated TGF-β1–ALK5–Smad2/3 signalling may facilitate vessel stabilisation, consistent with the greater arteriogenesis observed following SPARC and TGF-β1 co-treatment in our infarcted hearts. Evidence from *Sparc-null* mice supports this interpretation as disrupted pancreatic tumour vascularisation in these animals increased in invasion and metastasis, which was accompanied by diminished vessel maturation and pericyte recruitment [121]. Moreover, the vascular basement membrane in *Sparc-null* mice was thinner and more permeable than in wild-type counterparts, a phenotype attributed to altered collagen deposition and maturation [121]. Therefore, the augmented arteriogenesis observed post-MI with SPARC and TGF-β1 infusion may also be mediated indirectly, by promoting collagen-driven stabilisation of nascent vascular basement membranes, which in turn may provide a scaffold for coronary arterial remodelling **(Fig. 12)**.

Interestingly, although exogenous TGF-β1 infusion in *Sparc*-null mice decreased rupture incidence and increased collagen content, it failed to restore full infarct healing by day 14 [134], hinting that the cooperation of SPARC and TGF-β1 may be a requirement for proper infarct healing. As our hearts were collected at day 7, later timepoints will be required to evaluate this phase of fibrotic maturation.

At day 7 post-MI, no difference was observed in CD45-positive leukocyte numbers between wild-type and *Sparc*-null hearts, whereas by day 14, *Sparc*-null hearts contained fewer leukocytes [134], suggesting that SPARC supports leukocyte viability and prevents chronic immune responses at later times post-MI. Since fibrosis often precedes inflammatory expansion, it will also be valuable to determine whether immune cells represent a cellular source of SPARC during repair. Indeed, macrophages have been shown to express SPARC in pressure-overload-induced hypertrophy [204], an observation which may be relevant here, as

cardiac hypertrophy is a major predictor of CAD [205], the underlying cause of myocardial infarction.

4.4 Limitations and future directions

Our study has several limitations. To start with, since the coronary arteries are not found superficially in mice, their complete visualisation in whole-mount hearts requires an antibody and light penetration through the entire myocardial wall. We attempted to achieve the latter using light-sheet fluorescence microscopy, yet our antibody penetration was suboptimal. The attenuation of endomucin and SPARC signals in deeper regions likely reflects limited penetration rather than true expression of the proteins. Prolonged incubation, extending beyond five days at 37°C, replacing it every day, in 100% CUBIC-R2 to achieve optical clearing, may also have contributed to fluorophore quenching. Increasing the concentration and incubation times of both primary and secondary antibodies and switching to an organic-solvent rather than aqueous tissue-clearing method, such as iDISCO, might improve the reliability of our signals, especially because iDISCO is recognised to favour robust immunohistochemistry [206].

EMT *in vitro* can take more than 72 hours, and our analysis of *Sparc* mRNA, intracellular and secreted proteins was only captured up to 48 hours post-EMT induction. Particularly because SPARC secretion in the mesenchymal state plateaued between 24+8 and 48+8 hours, it may be interesting to see whether this would increase beyond 48+8 hours.

Since SPARC undergoes proteolytic cleavage upon secretion into the ECM, it results in peptides which exhibit distinct activities. Peptide containing aa 113-130, which contains the copper-binding KGHK motif, is strongly pro-angiogenic [102], whereas peptides bearing aa 5-23 [207] and 254-273 [113] inhibit cell spreading, with the latter also preventing VEGF binding and downstream ERK activation [113]. However, these effects were largely studied using excessive molar concentrations of the peptides, which were 166- [102], 266- [207] and 500- times [113] higher compared to the molar concentration of full-length SPARC. Future assays should compare biologically relevant concentrations of full-length SPARC and its major peptides, which may

provide insight into whether SPARC cleavage adds another layer of control in the switch between pro- and anti- angiogenic activity during epiEMT. Nevertheless, these are not commercially available, requiring isolation from full-length SPARC [208].

Moreover, our *in vitro* sprouting assays employed a single VEGF-A concentration (100 ng/mL). *In vivo* work, which has demonstrated that moderate VEGF-A promotes angiogenesis, whereas higher levels favour endothelial quiescence and subsequent arterialisation, relied on inducible fluorescent genetic mosaic mouse lines, which enabled conditional activation or inhibition of *Vegfr2* and ERK signalling at a single-cell resolution in their experimental model, angiogenic retinal ECs [54]. To establish dose–response relationships relevant to our assay, future studies should first derive bell-shaped curves for VEGF-A (10–100 ng/mL), alone and in combination with graded ratios of SPARC and TGF-β1. This should similarly be performed for SPARC and TGF-β1 individually, given their reported biphasic actions on endothelial proliferation in other systems [107, 134, 135, 139, 140].

Importantly, variability between SV explants represents an additional limitation of our *in vitro* model. Differences in explant size and occasional underpowered experimental conditions likely contributed to heterogeneous sprouting responses, such that explants exposed to identical treatments could exhibit markedly different degrees of outgrowth. This inter-explant variability is therefore likely to contribute to the wide standard deviations observed in sprouting metrics and may obscure more subtle treatment effects. Although we attempted to mitigate this by normalising sprouting parameters to explant area, this may not fully account for the intrinsic biological heterogeneity between explants. Future studies should therefore increase the number of biological replicates and incorporate stratification by explant size.

Future studies should quantify the downstream mediators of TGF-β1 signalling, rather than its final effect (proliferation), especially because ECs express ALK1 and ALK5, which often have opposing effects on angiogenesis [196]. This can therefore shed light on whether SPARC promotes a switch between sprouting angiogenesis and arterialisation via a differential activation of the two TGF-βR receptors. In addition, the use of recombinant TGF-β1 in its active form, *in vitro*, might have enabled rapid activation of its receptors rather than replicating the

spatial and temporal constraints of intrinsic, matrix-bound TGF-β1 activation. Analogous to thrombospondin-1, which releases active TGF-β1 from its latency complex [209, 210], SPARC may also function as a stimulator of latent TGF-β1, which can be explored using commercially available latent recombinant TGF-β1.

Arguably, the largest limitation in our study was that our pilot MI investigation was under-powered and lacked several essential control groups, including a TGF-β1-only and a sham-operated cohort, due to which we were unable to deduce whether the pro-arteriogenic effect of SPARC and TGF-β1 in the infarct/border zone region arose from additive or antagonistic interaction between the two. Furthermore, the size of infarct across our treatments was very variable, which normalisation may not have fully corrected for. Increasing sample size and standardising infarct size can ensure the reproducibility of our results. Furthermore, future work should also explore how the arteriogenic effect under SPARC and TGF-β1 co-stimulation at 7 days post-MI relates to earlier and later timepoints. Also, delivery of these factors via prolonged release through osmotic minipumps should be explored to determine whether it changes the bioavailability of the factors. Given the evidence that *Sparc* deletion attenuates ageing in periodontal ligaments [99], age is a likely confounder in modulating cardiac outcomes. Future experiments should therefore explore age-dependent differences in SPARC/TGF-β1-mediated arteriogenesis and potential fibrosis following MI, as this could provide insights into their therapeutic relevance for older patients recovering from MI.

Lastly, SPARC acts at multiple levels after myocardial infarction: it can modulate collagen deposition by myofibroblasts [134], influence macrophage recruitment and polarisation [127, 133], and may indirectly affect cardiomyocyte survival and proliferation [211]. Comprehensive immunohistochemical characterisation of post-MI hearts should therefore be conducted to, for instance, include inflammatory dynamics, neutrophil (myeloperoxidase) and macrophage (CD68) recruitment and resolution [212]; cardiomyocyte survival and proliferation indices (P-AKT, FoxO1/3, EdU, p-Histone H3). Such analyses will clarify whether SPARC and TGF-β1 enhance arterialisation through secondary mechanisms rather than direct endothelial effects.

5 Conclusions

Taken together, the findings of this thesis demonstrate that epicardial EMT induces the secretion of the matricellular protein SPARC into the extracellular milieu of mesenchymal-derived epicardial cells, where it modulates endothelial responses to growth factors. Specifically, SPARC acts in concert with TGF-β1, which is also upregulated in the mesenchymal state, to bias sinus venosus–derived ECs toward an arterial fate during coronary vessel development. Their interaction persists in the infarcted heart, suggesting that SPARC–TGF-β1 signalling reactivates developmental programmes of arteriogenesis to support post-injury revascularisation. However, future work should investigate the mechanisms underlying arterialisation induced by the combined effect of these two factors during coronary vessel development, as well as following MI.

To design effective strategies for stimulating endogenous coronary neovascularisation after myocardial infarction, it is essential first to understand the mechanisms by which coronary vessels grow and arterialise during development. The failure of clinical trials, which involved infusing infarcted hearts with pro-angiogenic growth factors, like VEGF-A, to promote revascularisation, highlights that growth factor delivery alone is insufficient, and that the extracellular environments in which these cues act can also influence neovascularisation. By identifying SPARC as a mediator of arterialisation in ECs, our work establishes a conceptual framework for modulating the extracellular cues to promote angiogenesis and arteriogenesis, offering therapeutic potential for myocardial repair and other conditions characterised by impaired vascular remodelling.

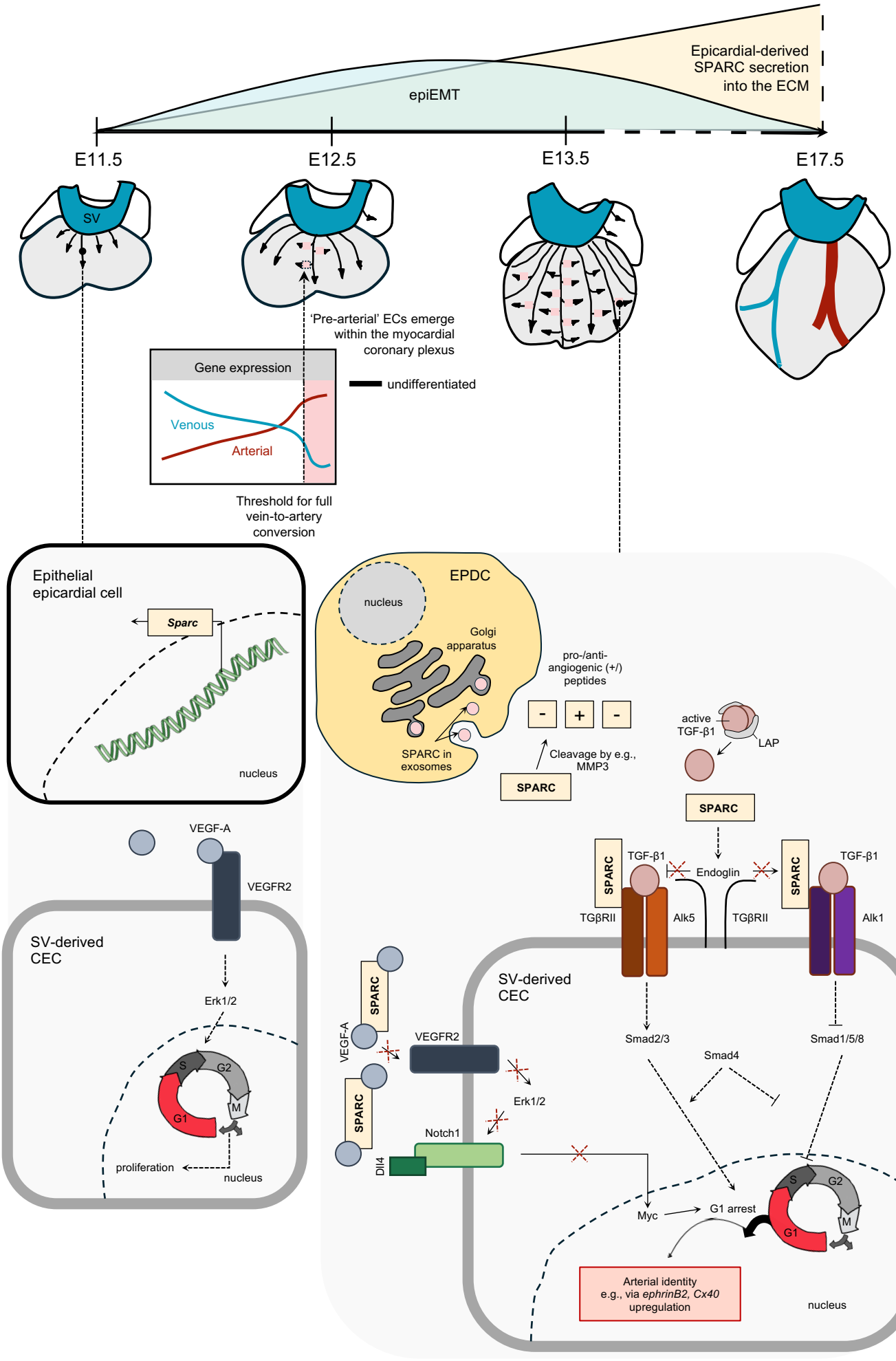

Epicardial-derived
SPARC secretion
into the ECM
epiEMT
E11.5
E12.5
E13.5
E17.5
SV
'Pre-arterial' ECs emerge
within the myocardial
coronary plexus
Gene expression
undifferentiated
Venous
Arterial
Threshold for full
vein-to-artery
conversion
Epithelial
epicardial cell
Sparc
nucleus
EPDC
nucleus
Golgi
apparatus
SPARC in
exosomes
pro-/anti-
angiogenic (+/)
peptides
-
+
-
Cleavage by e.g.,
MMP3
SPARC
active
TGF-β1
LAP
SPARC
VEGF-A
VEGFR2
SV-derived
CEC
Erk1/2
S
G2
M
G1
proliferation
nucleus
SPARC
TGF-β1
Endoglin
TGF-β1
TGβRII
Alk5
TGβRII
Alk1
SPARC
SV-derived
CEC
Smad2/3
Smad1/5/8
Smad4
VEGF-A
SPARC
VEGFR2
Erk1/2
SPARC
Notch1
Dll4
Myc
G1 arrest
S
G2
M
G1
Arterial identity
e.g., via ephrinB2, Cx40
upregulation
nucleus

Figure 11. Proposed model of SPARC and TGFβ-1-induced arterialisation of sinus-venosus-derived coronary vessel sprout

Schematic summarising the pro-arteriogenic role of SPARC across the time window of epiEMT, which coincides with coronary arteriovenous specification. At E12.5, expression of arterial-specific genes surpasses a threshold within the myocardial coronary plexus, committing ECs to an arterial fate. We propose that SPARC expression in the epicardium is initiated during the epithelial state, where it is transcribed and translated to build an intracellular reservoir primed for secretion upon EMT induction. In the mesenchymal state, SPARC is actively secreted into the extracellular matrix, which might be via exocytosis. Once secreted, SPARC can undergo proteolytic cleavage to generate bioactive fragments capable of interacting with endoglin on SV-derived CECs. Endoglin normally facilitates ALK1–Smad1/5/8 signalling, promoting proliferation. We, however, propose that SPARC binding to endoglin inhibits this pathway, thereby favouring ALK5–Smad2/3 activation, which induces G1-phase cell-cycle arrest, a prerequisite for arterial specification. Alternatively, SPARC can also bind to TβRII, activating the downstream Smad2/3-mediated pathway that may culminate in cell cycle arrest. In parallel, we considered whether SPARC might modulate VEGF-A–VEGFR2 signalling. While SPARC binding was hypothesised to enhance VEGFR2-dependent ERK1/2 activation and downstream Notch-mediated repression of Myc, for the acquisition of arterial identity, our data did not support this mechanism. Instead, we propose that during the epithelial stage of the epicardium, moderate VEGFR2 activation and intermediate ERK1/2 phosphorylation promote angiogenic sprouting and proliferation.

ALK1/5, activin receptor-like kinase 1/5; CEC, coronary endothelial cell; ECM, extracellular matrix; EC, endothelial cell; ENG, endoglin; epiEMT, epicardial epithelial-to-mesenchymal transition; EPDC, epicardium-derived cell; ERK1/2, extracellular signal-regulated kinase 1/2; E, embryonic day; Myc, myelocytomatosis oncogene; Notch1, neurogenic locus notch homolog protein 1; Smad, mothers against decapentaplegic homolog; SPARC, secreted

protein acidic and rich in cysteine; SV, sinus venosus; TGF-β1, transforming growth factor beta 1; VEGF-A, vascular endothelial growth factor A; VEGFR2, vascular endothelial growth factor receptor 2

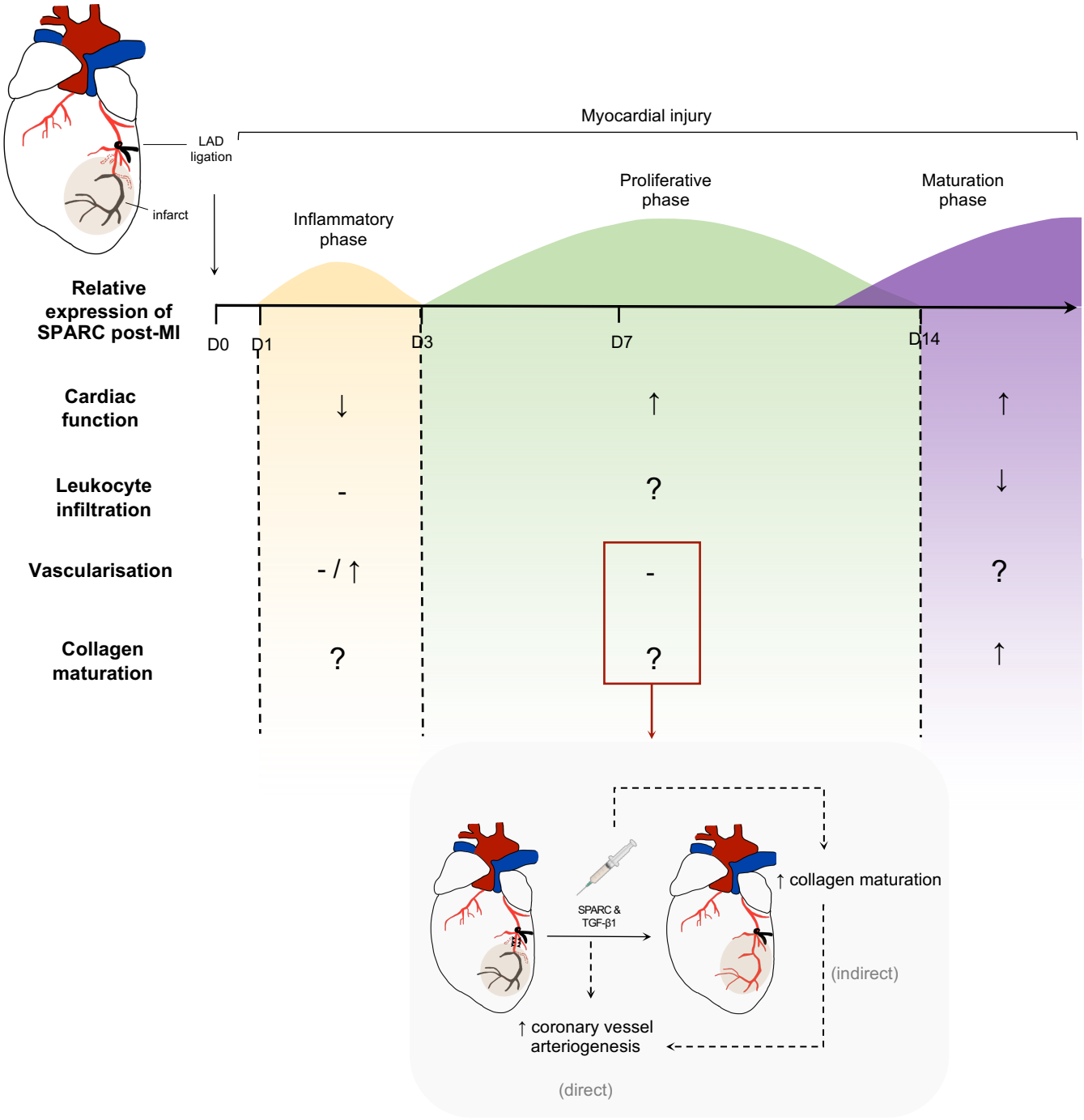

LAD ligation
infarct
Myocardial injury
Inflammatory phase
Proliferative phase
Maturation phase
Relative expression of SPARC post-MI
D0
D1
D3
D7
D14
Cardiac function
Leukocyte infiltration
Vascularisation
Collagen maturation
↓
-
- / ↑
?
↑
?
-
?
↑
↓
?
↑
SPARC & TGF-β1
↑ collagen maturation
(indirect)
↑ coronary vessel arteriogenesis
(direct)

Figure 12. Summary of current evidence on the role of SPARC in cardiac repair post-myocardial infarction and proposed model of SPARC and TGFβ-1-induced arteriogenesis in the infarcted heart

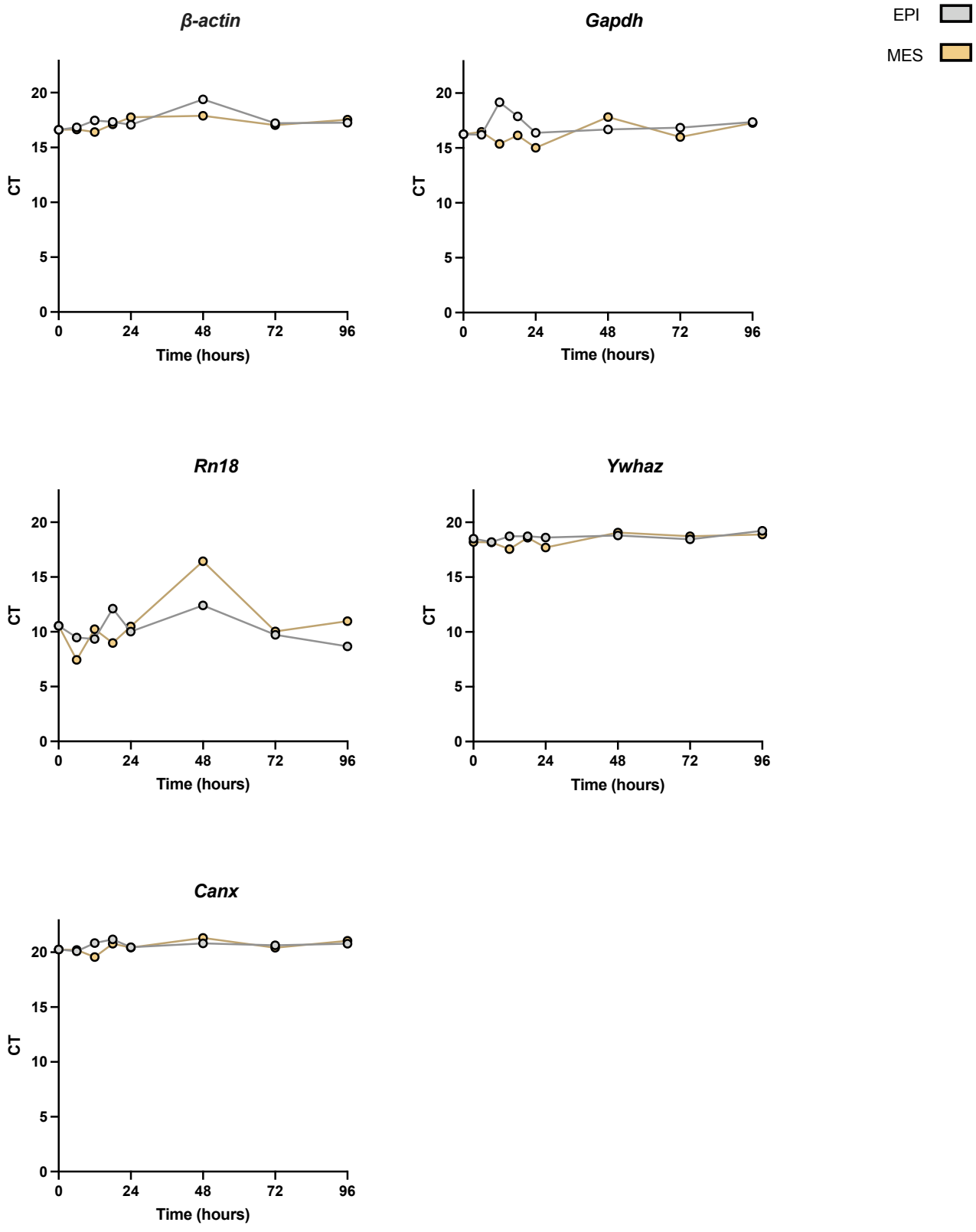
Schematic illustrating the temporal dynamics of SPARC expression during different phases of cardiac repair following myocardial infarction, as well as its differential effects on these phases. During the early inflammatory phase (days 0-3), SPARC exhibits deleterious effects as its presence correlates with reduced cardiac function and decreased vessel density within the infarct zone. However, beyond this phase, SPARC adopts a reparative role. In the proliferative and maturation stages (days 7-14), *Sparc*-null mice display impaired cardiac function and increased risk of rupture, attributed to disorganised collagen fibril assembly and defective matrix maturation [134]. Regarding leukocyte infiltration, *Sparc*-null mice had a greater number of macrophages in the infarcted heart compared to wild-type infarcts at 14 days post-MI [134], although no difference was observed at 3 days post-MI [134, 135]. Although evidence remains limited, SPARC has also been implicated in promoting revascularisation, with one study reporting that in *Sparc*-null mice, the decline in blood vessel numbers was attenuated compared to wild-type mice at 3 days post-MI [135]. However, another study did not find any significant difference in coronary growth between these genotypes at 7 days post-MI [134]. Building on this, we show that combined SPARC and TGF-β1 infusion may augment coronary arteriogenesis and collagen deposition, possibly through activation of the TGF-β1–ALK5–Smad2/3 pathway. This pathway, previously associated with collagen maturation and scar stabilisation, may also reinforce stabilisation of the vascular basement membranes in newly formed vessels [121], thereby supporting their subsequent arterial remodelling in the post-infarct myocardium.

ALK5, activin receptor-like kinase 5; D, day; LAD, left anterior descending coronary artery; MI, myocardial infarction; Smad2/3, mothers against decapentaplegic homolog 2/3; SPARC, secreted protein acidic and rich in cysteine; TGF-β1, transforming growth factor beta 1; WT, wild type.

6 Supplementary materials

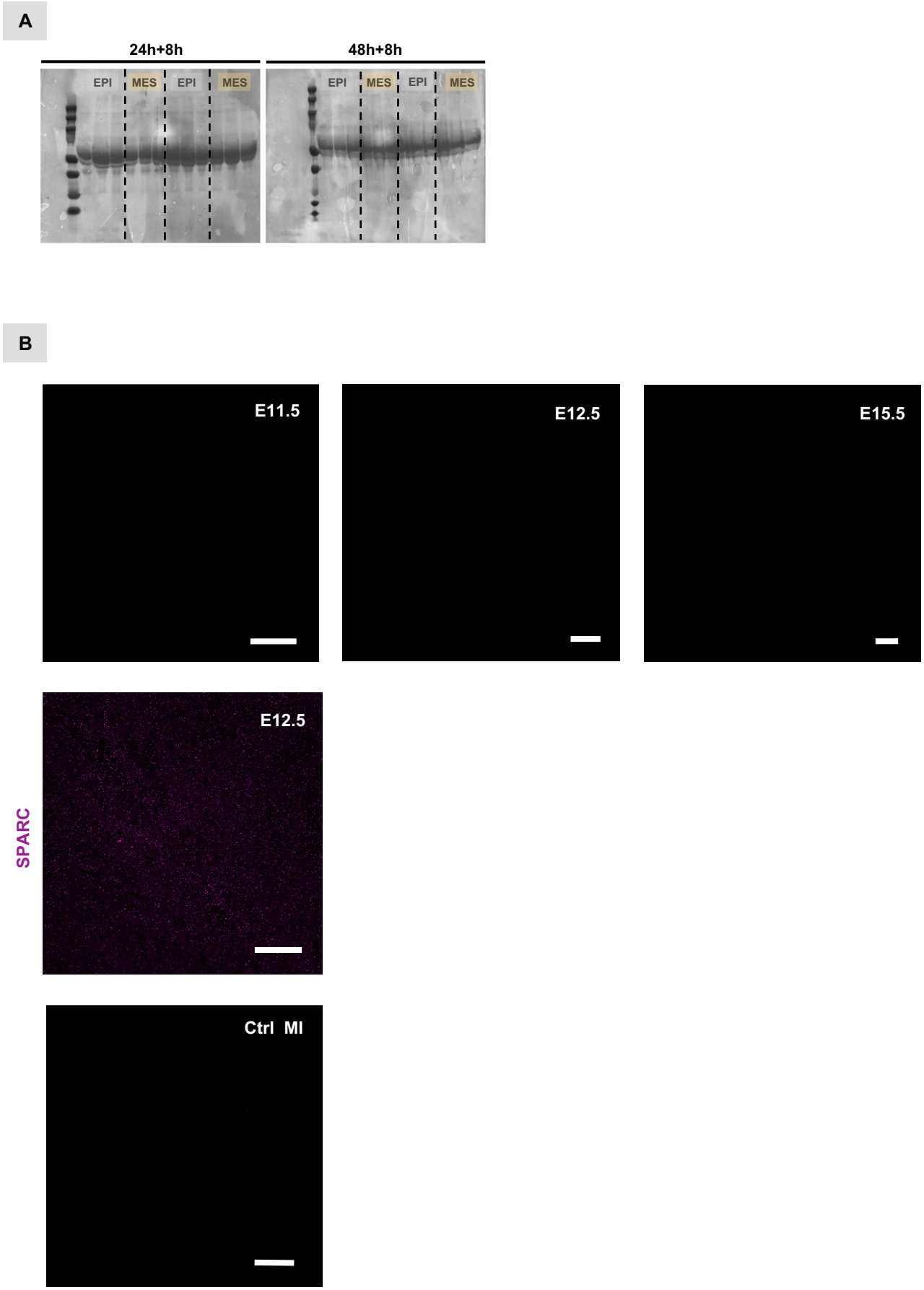
Gene	Forward sequence (5’ → 3’)	Reverse sequence (5’ → 3’)
β-actin	CTGTCGAGTCGCGTCCACC	GCTTTGCACATGCCGGAGC
Gapdh	AGGTCGGTGTGAACGGATTTG	TGTAGACCATGTAGTTGAGGTCA
Rn18	GTAACCCGTTGAACCCCATT	CCATCCAATCGGTAGTAGCG
Canx	ATGGAAGGGAAGTGGTTACTGT	GCTTTGTAGGTGACCTTTGGAG

Appendix Table 1. Primers used for testing housekeeping genes for RT-qPCR


EPI
MES
β-actin
Gapdh
Rn18
Ywhaz
Canx
CT
Time (hours)
0
5
10
15
20
24
48
72
96

Appendix Figure 1. Expression profiles of candidate housekeeping genes in the mouse epicardial cell (MEC1) line during epicardial epithelial-to-mesenchymal transition

β-actin, Gapdh, Rn18, Ywhaz and *Canx* gene expression was measured using RT-qPCR in MEC1 cells cultured under epithelial (EPI) or mesenchymal (MES) conditions from 0 to 96 hours after EMT induction. Data are presented as mean cycle threshold (CT) values. Among the tested genes, *Ywhaz* and *canx* showed the most consistent expression across timepoints and EPI versus MES conditions. Since *Ywhaz* was more abundantly expressed than *Canx* in the MEC1 line, as indicated by lower CT values, it was selected as the housekeeping gene for normalisation in subsequent RT-qPCR experiments. Data are presented as individual points (n=1 experiment).


A
24h+8h
48h+8h
EPI
MES
EPI
MES
EPI
MES
EPI
MES
B
E11.5
E12.5
E15.5
SPARC
E12.5
Ctrl MI

Appendix Figure 2.

(A) Ponceau S staining of conditioned media samples. Total protein levels in conditioned media collected from MEC1 epicardial cells cultured in epithelial (EPI) or mesenchymal (MES) states. Media was refreshed at either 24 hours (left) or 48 hours (right) and collected 8 hours later (24h+8h, 48h+8h). These stains were used to normalise Western blot analysis of secreted SPARC (see Fig. 4E-F). Images of n=3-4 experiments.

(B) Secondary antibody–only immunostaining controls for SPARC performed on E11.5, E12.5 and E15.5 coronal heart sections, E12.5 sagittal whole-embryo section, and saline-treated (ctrl) axial MI heart section, demonstrating the absence of non-specific secondary antibody signal. Images of n=1 experiment.

7 References

1. Udan RS, Culver JC, Dickinson ME. Understanding vascular development. Wiley Interdiscip Rev Dev Biol. 2013;2(3):327–46.

2. Folkman J. Tumor angiogenesis: therapeutic implications. N Engl J Med. 1971;285(21):1182–6.

3. Droste P, Wong DWL, Hohl M, von Stillfried S, Klinkhammer BM, Boor P. Semiautomated pipeline for quantitative analysis of heart histopathology. Journal of Translational Medicine. 2023;21(1):666.

4. Sheikh AM, Yano S, Tabassum S, Nagai A. The Role of the Vascular System in Degenerative Diseases: Mechanisms and Implications. Int J Mol Sci. 2024;25(4).

5. Reese DE, Mikawa T, Bader DM. Development of the Coronary Vessel System. Circulation Research. 2002;91(9):761–8.

6. Saitoh S, Zhang C, Tune JD, Potter B, Kiyooka T, Rogers PA, et al. Hydrogen peroxide: a feed-forward dilator that couples myocardial metabolism to coronary blood flow. Arterioscler Thromb Vasc Biol. 2006;26(12):2614–21.

7. Laflamme MA, Murry CE. Regenerating the heart. Nat Biotechnol. 2005;23(7):845–56.

8. Wu X, Reboll MR, Korf-Klingebiel M, Wollert KC. Angiogenesis after acute myocardial infarction. Cardiovasc Res. 2021;117(5):1257–73.

9. Doost Hosseiny A, Moloi S, Chandrasekhar J, Farshid A. Mortality pattern and cause of death in a long-term follow-up of patients with STEMI treated with primary PCI. Open

Heart. 2016;3(1):e000405.

10. Reffelmann T, Kloner RA. The no-reflow phenomenon: A basic mechanism of myocardial ischemia and reperfusion. Basic Res Cardiol. 2006;101(5):359–72.

11. Regenfus M, Schlundt C, Krähner R, Schönegger C, Adler W, Ludwig J, et al. Six-Year Prognostic Value of Microvascular Obstruction After Reperfused ST-Elevation Myocardial Infarction as Assessed by Contrast-Enhanced Cardiovascular Magnetic Resonance. Am J Cardiol. 2015;116(7):1022–7.

12. Reinstadler SJ, Stiermaier T, Reindl M, Feistritzer HJ, Fuernau G, Eitel C, et al. Intramyocardial haemorrhage and prognosis after ST-elevation myocardial infarction. Eur Heart J Cardiovasc Imaging. 2019;20(2):138–46.

13. van Kranenburg M, Magro M, Thiele H, de Waha S, Eitel I, Cochet A, et al. Prognostic value of microvascular obstruction and infarct size, as measured by CMR in STEMI patients. JACC Cardiovasc Imaging. 2014;7(9):930–9.

14. Lupu IE, De Val S, Smart N. Coronary vessel formation in development and disease: mechanisms and insights for therapy. Nat Rev Cardiol. 2020;17(12):790–806.

15. Henry TD, Annex BH, McKendall GR, Azrin MA, Lopez JJ, Giordano FJ, et al. The VIVA trial: Vascular endothelial growth factor in Ischemia for Vascular Angiogenesis. Circulation. 2003;107(10):1359–65.

16. Simons M, Annex BH, Laham RJ, Kleiman N, Henry T, Dauerman H, et al. Pharmacological treatment of coronary artery disease with recombinant fibroblast growth factor-2: double-blind, randomized, controlled clinical trial. Circulation. 2002;105(7):788–93.

17. Red-Horse K, Ueno H, Weissman IL, Krasnow MA. Coronary arteries form by developmental reprogramming of venous cells. Nature. 2010;464(7288):549–53.

18. Zeini M, Hang CT, Lehrer-Graiwer J, Dao T, Zhou B, Chang CP. Spatial and temporal regulation of coronary vessel formation by calcineurin-NFAT signaling. Development. 2009;136(19):3335–45.

19. Sadler T. Langman's Medical Embryology. 14th ed. Philadelphia: Wolters Kluwer; 2019.

20. Pugsley MK, Tabrizchi R. The vascular system. An overview of structure and function. J Pharmacol Toxicol Methods. 2000;44(2):333–40.

21. Baeyens N, Bandyopadhyay C, Coon BG, Yun S, Schwartz MA. Endothelial fluid shear stress sensing in vascular health and disease. J Clin Invest. 2016;126(3):821–8.

22. Xu J, Shi GP. Vascular wall extracellular matrix proteins and vascular diseases. Biochim Biophys Acta. 2014;1842(11):2106–19.

23. Armulik A, Genové G, Betsholtz C. Pericytes: developmental, physiological, and pathological perspectives, problems, and promises. Dev Cell. 2011;21(2):193–215.

24. Passman JN, Dong XR, Wu SP, Maguire CT, Hogan KA, Bautch VL, et al. A sonic hedgehog signaling domain in the arterial adventitia supports resident Sca1+ smooth muscle progenitor cells. Proc Natl Acad Sci U S A. 2008;105(27):9349–54.

25. Stenmark KR, Yeager ME, El Kasmi KC, Nozik-Grayck E, Gerasimovskaya EV, Li M, et al. The adventitia: essential regulator of vascular wall structure and function. Annu Rev Physiol. 2013;75:23–47.

26. Uyttendaele H, Ho J, Rossant J, Kitajewski J. Vascular patterning defects associated with expression of activated Notch4 in embryonic endothelium. Proceedings of the National Academy of Sciences. 2001;98(10):5643–8.

27. McCracken IR, Dobie R, Bennett M, Passi R, Beqqali A, Henderson NC, et al.

Mapping the developing human cardiac endothelium at single-cell resolution identifies MECOM as a regulator of arteriovenous gene expression. Cardiovasc Res. 2022;118(14):2960–72.

28. Phansalkar R, Krieger J, Zhao M, Kolluru SS, Jones RC, Quake SR, et al. Coronary blood vessels from distinct origins converge to equivalent states during mouse and human development. eLife. 2021;10:e70246.

29. Hutchins GM, Kessler-Hanna A, Moore GW. Development of the coronary arteries in the embryonic human heart. Circulation. 1988;77(6):1250–7.

30. Bogers AJ, Gittenberger-de Groot AC, Poelmann RE, Péault BM, Huysmans HA. Development of the origin of the coronary arteries, a matter of ingrowth or outgrowth? Anat Embryol (Berl). 1989;180(5):437–41.

31. Mikawa T, Fischman DA. Retroviral analysis of cardiac morphogenesis: discontinuous formation of coronary vessels. Proceedings of the National Academy of Sciences. 1992;89(20):9504–8.

32. Poelmann RE, Gittenberger-de Groot AC, Mentink MM, Bökenkamp R, Hogers B. Development of the cardiac coronary vascular endothelium, studied with antiendothelial antibodies, in chicken-quail chimeras. Circ Res. 1993;73(3):559–68.

33. Vrancken Peeters MP, Gittenberger-de Groot AC, Mentink MM, Hungerford JE, Little CD, Poelmann RE. The development of the coronary vessels and their differentiation into arteries and veins in the embryonic quail heart. Dev Dyn. 1997;208(3):338–48.

34. Tian X, Hu T, He L, Zhang H, Huang X, Poelmann RE, et al. Peritruncal Coronary Endothelial Cells Contribute to Proximal Coronary Artery Stems and Their Aortic Orifices in the Mouse Heart. PLOS ONE. 2013;8(11):e80857.

35. Guadix JA, Carmona R, Muñoz-Chápuli R, Pérez-Pomares JM. In vivo and in vitro

analysis of the vasculogenic potential of avian proepicardial and epicardial cells. Dev Dyn. 2006;235(4):1014–26.

36. Pérez-Pomares JM, Carmona R, González-Iriarte M, Atencia G, Wessels A, Muñoz-Chápuli R. Origin of coronary endothelial cells from epicardial mesothelium in avian embryos. Int J Dev Biol. 2002;46(8):1005–13.

37. Cai CL, Martin JC, Sun Y, Cui L, Wang L, Ouyang K, et al. A myocardial lineage derives from Tbx18 epicardial cells. Nature. 2008;454(7200):104–8.

38. Zhou B, Ma Q, Rajagopal S, Wu SM, Domian I, Rivera-Feliciano J, et al. Epicardial progenitors contribute to the cardiomyocyte lineage in the developing heart. Nature. 2008;454(7200):109–13.

39. Wu B, Zhang Z, Lui W, Chen X, Wang Y, Chamberlain AA, et al. Endocardial cells form the coronary arteries by angiogenesis through myocardial-endocardial VEGF signaling. Cell. 2012;151(5):1083–96.

40. Chen HI, Sharma B, Akerberg BN, Numi HJ, Kivelä R, Saharinen P, et al. The sinus venosus contributes to coronary vasculature through VEGFC-stimulated angiogenesis. Development. 2014;141(23):4500–12.

41. Tian X, Hu T, Zhang H, He L, Huang X, Liu Q, et al. De novo formation of a distinct coronary vascular population in neonatal heart. Science. 2014;345(6192):90–4.

42. Zhang H, Pu W, Li G, Huang X, He L, Tian X, et al. Endocardium Minimally Contributes to Coronary Endothelium in the Embryonic Ventricular Free Walls. Circulation Research. 2016;118(12):1880–93.

43. Lu P, Wang Y, Liu Y, Wang Y, Wu B, Zheng D, et al. Perinatal angiogenesis from pre-existing coronary vessels via DLL4–NOTCH1 signalling. Nature Cell Biology. 2021;23(9):967–77.

44. Claxton S, Fruttiger M. Oxygen modifies artery differentiation and network morphogenesis in the retinal vasculature. Dev Dyn. 2005;233(3):822–8.

45. le Noble F, Moyon D, Pardanaud L, Yuan L, Djonov V, Matthijsen R, et al. Flow regulates arterial-venous differentiation in the chick embryo yolk sac. Development. 2004;131(2):361–75.

46. Su T, Stanley G, Sinha R, D'Amato G, Das S, Rhee S, et al. Single-cell analysis of early progenitor cells that build coronary arteries. Nature. 2018;559(7714):356–62.

47. Mack JJ, Mosqueiro TS, Archer BJ, Jones WM, Sunshine H, Faas GC, et al. NOTCH1 is a mechanosensor in adult arteries. Nature Communications. 2017;8(1):1620.

48. Payne S, Gunadasa-Rohling M, Neal A, Redpath AN, Patel J, Chouliaras KM, et al. Regulatory pathways governing murine coronary vessel formation are dysregulated in the injured adult heart. Nat Commun. 2019;10(1):3276.

49. Chavkin NW, Genet G, Poulet M, Jeffery ED, Marziano C, Genet N, et al. Endothelial cell cycle state determines propensity for arterial-venous fate. Nature Communications. 2022;13(1):5891.

50. Fang JS, Coon BG, Gillis N, Chen Z, Qiu J, Chittenden TW, et al. Shear-induced Notch-Cx37-p27 axis arrests endothelial cell cycle to enable arterial specification. Nature Communications. 2017;8(1):2149.

51. Luo W, Garcia-Gonzalez I, Fernández-Chacón M, Casquero-Garcia V, Sanchez-Muñoz MS, Mühleder S, et al. Arterialization requires the timely suppression of cell growth. Nature. 2021;589(7842):437–41.

52. Farber G, Parks MM, Lustgarten Guahmich N, Zhang Y, Monette S, Blanchard SC, et al. ADAM10 controls the differentiation of the coronary arterial endothelium. Angiogenesis. 2019;22(2):237–50.

53. Fish JE, Wythe JD. The molecular regulation of arteriovenous specification and maintenance. Dev Dyn. 2015;244(3):391–409.

54. Pontes-Quero S, Fernández-Chacón M, Luo W, Lunella FF, Casquero-Garcia V, Garcia-Gonzalez I, et al. High mitogenic stimulation arrests angiogenesis. Nature Communications. 2019;10(1):2016.

55. Lee T, Yao G, Nevins J, You L. Sensing and integration of Erk and PI3K signals by Myc. PLoS Comput Biol. 2008;4(2):e1000013.

56. Oh SP, Seki T, Goss KA, Imamura T, Yi Y, Donahoe PK, et al. Activin receptor-like kinase 1 modulates transforming growth factor-beta 1 signaling in the regulation of angiogenesis. Proc Natl Acad Sci U S A. 2000;97(6):2626–31.

57. Urness LD, Sorensen LK, Li DY. Arteriovenous malformations in mice lacking activin receptor-like kinase-1. Nat Genet. 2000;26(3):328–31.

58. Ang LT, Nguyen AT, Liu KJ, Chen A, Xiong X, Curtis M, et al. Generating human artery and vein cells from pluripotent stem cells highlights the arterial tropism of Nipah and Hendra viruses. Cell. 2022;185(14):2523–41.e30.

59. Männer J, Pérez-Pomares JM, Macías D, Muñoz-Chápuli R. The origin, formation and developmental significance of the epicardium: a review. Cells Tissues Organs. 2001;169(2):89–103.

60. Sanchez-Fernandez C, Rodriguez-Outeiriño L, Matias-Valiente L, Ramirez de Acuña F, Hernandez-Torres F, Lozano-Velasco E, et al. Regulation of Epicardial Cell Fate during Cardiac Development and Disease: An Overview. Int J Mol Sci. 2022;23(6).

61. Smits AM, Dronkers E, Goumans MJ. The epicardium as a source of multipotent adult cardiac progenitor cells: Their origin, role and fate. Pharmacol Res. 2018;127:129–40.

62. Cao Y, Duca S, Cao J. Epicardium in Heart Development. Cold Spring Harb Perspect Biol. 2020;12(2).

63. Pérez-Pomares JM, de la Pompa JL. Signaling during epicardium and coronary vessel development. Circ Res. 2011;109(12):1429–42.

64. Risebro CA, Vieira JM, Klotz L, Riley PR. Characterisation of the human embryonic and foetal epicardium during heart development. Development. 2015;142(21):3630–6.

65. Lupu IE, Redpath AN, Smart N. Spatiotemporal Analysis Reveals Overlap of Key Proepicardial Markers in the Developing Murine Heart. Stem Cell Reports. 2020;14(5):770–87.

66. Redpath AN, Smart N. Recapturing embryonic potential in the adult epicardium: Prospects for cardiac repair. Stem Cells Transl Med. 2021;10(4):511–21.

67. Joukov V, Sorsa T, Kumar V, Jeltsch M, Claesson-Welsh L, Cao Y, et al. Proteolytic processing regulates receptor specificity and activity of VEGF-C. Embo j. 1997;16(13):3898–911.

68. Tammela T, Zarkada G, Wallgard E, Murtomäki A, Suchting S, Wirzenius M, et al. Blocking VEGFR-3 suppresses angiogenic sprouting and vascular network formation. Nature. 2008;454(7204):656–60.

69. Chen T, Chang TC, Kang JO, Choudhary B, Makita T, Tran CM, et al. Epicardial induction of fetal cardiomyocyte proliferation via a retinoic acid-inducible trophic factor. Dev Biol. 2002;250(1):198–207.

70. Velecela V, Torres-Cano A, García-Melero A, Ramiro-Pareta M, Müller-Sánchez C, Segarra-Mondejar M, et al. Epicardial cell shape and maturation are regulated by Wt1 via transcriptional control of Bmp4. Development. 2019;146(20).

71. Debnath P, Huirem RS, Dutta P, Palchaudhuri S. Epithelial-mesenchymal transition and its transcription factors. Biosci Rep. 2022;42(1).

72. Kalluri R, Weinberg RA. The basics of epithelial-mesenchymal transition. J Clin Invest. 2009;119(6):1420–8.

73. Foglio E, D'Avorio E, Nieri R, Russo MA, Limana F. Epicardial EMT and cardiac repair: an update. Stem Cell Research & Therapy. 2024;15(1):219.

74. Meilhac SM, Buckingham ME. The deployment of cell lineages that form the mammalian heart. Nat Rev Cardiol. 2018;15(11):705–24.

75. Kattan J, Dettman RW, Bristow J. Formation and remodeling of the coronary vascular bed in the embryonic avian heart. Dev Dyn. 2004;230(1):34–43.

76. Lavine KJ, White AC, Park C, Smith CS, Choi K, Long F, et al. Fibroblast growth factor signals regulate a wave of Hedgehog activation that is essential for coronary vascular development. Genes Dev. 2006;20(12):1651–66.

77. Bonet F, Inácio JM, Bover O, Añez SB, Belo JA. CCBE1 in Cardiac Development and Disease. Front Genet. 2022;13:836694.

78. Bonet F, Pereira PNG, Bover O, Marques S, Inácio JM, Belo JA. CCBE1 is required for coronary vessel development and proper coronary artery stem formation in the mouse heart. Dev Dyn. 2018;247(10):1135–45.

79. Tyagi SC. Vasculogenesis and angiogenesis: extracellular matrix remodeling in coronary collateral arteries and the ischemic heart. J Cell Biochem. 1997;65(3):388–94.

80. Liu Y, Xu J, Wu M, Kang L, Xu B. The effector cells and cellular mediators of immune system involved in cardiac inflammation and fibrosis after myocardial infarction. J Cell Physiol. 2020;235(12):8996–9004.

81. Swirski FK, Nahrendorf M. Cardioimmunology: the immune system in cardiac homeostasis and disease. Nat Rev Immunol. 2018;18(12):733–44.

82. Horckmans M, Ring L, Duchene J, Santovito D, Schloss MJ, Drechsler M, et al. Neutrophils orchestrate post-myocardial infarction healing by polarizing macrophages towards a reparative phenotype. Eur Heart J. 2017;38(3):187–97.

83. Fröhlich GM, Meier P, White SK, Yellon DM, Hausenloy DJ. Myocardial reperfusion injury: looking beyond primary PCI. Eur Heart J. 2013;34(23):1714–22.

84. Grines CL, Watkins MW, Helmer G, Penny W, Brinker J, Marmur JD, et al. Angiogenic Gene Therapy (AGENT) Trial in Patients With Stable Angina Pectoris. Circulation. 2002;105(11):1291–7.

85. Aviles RJ, Annex BH, Lederman RJ. Testing clinical therapeutic angiogenesis using basic fibroblast growth factor (FGF-2). British Journal of Pharmacology. 2003;140(4):637–46.

86. Hedman M, Hartikainen J, Syvänne M, Stjernvall J, Hedman A, Kivelä A, et al. Safety and Feasibility of Catheter-Based Local Intracoronary Vascular Endothelial Growth Factor Gene Transfer in the Prevention of Postangioplasty and In-Stent Restenosis and in the Treatment of Chronic Myocardial Ischemia. Circulation. 2003;107(21):2677–83.

87. Kukuła K, Chojnowska L, Dąbrowski M, Witkowski A, Chmielak Z, Skwarek M, et al. Intramyocardial plasmid-encoding human vascular endothelial growth factor A165/basic fibroblast growth factor therapy using percutaneous transcatheter approach in patients with refractory coronary artery disease (VIF-CAD). Am Heart J. 2011;161(3):581–9.

88. McCracken IR, Smart N. Control of coronary vascular cell fate in development and regeneration. Semin Cell Dev Biol. 2024;155(Pt C):50–61.

89. Tian X, Zhou B. Coronary vessel formation in development and regeneration: origins

and mechanisms. Journal of Molecular and Cellular Cardiology. 2022;167:67–82.

90. Dubé KN, Thomas TM, Munshaw S, Rohling M, Riley PR, Smart N. Recapitulation of developmental mechanisms to revascularize the ischemic heart. JCI Insight. 2017;2(22).

91. He L, Huang X, Kanisicak O, Li Y, Wang Y, Li Y, et al. Preexisting endothelial cells mediate cardiac neovascularization after injury. J Clin Invest. 2017;127(8):2968–81.

92. Li Z, Solomonidis EG, Berkeley B, Tang MNH, Stewart KR, Perez-Vicencio D, et al. Multi-species meta-analysis identifies transcriptional signatures associated with cardiac endothelial responses in the ischaemic heart. Cardiovasc Res. 2023;119(1):136–54.

93. Li Z, Solomonidis EG, Meloni M, Taylor RS, Duffin R, Dobie R, et al. Single-cell transcriptome analyses reveal novel targets modulating cardiac neovascularization by resident endothelial cells following myocardial infarction. Eur Heart J. 2019;40(30):2507–20.

94. Tombor LS, John D, Glaser SF, Luxán G, Forte E, Furtado M, et al. Single cell sequencing reveals endothelial plasticity with transient mesenchymal activation after myocardial infarction. Nat Commun. 2021;12(1):681.

95. Manavski Y, Lucas T, Glaser SF, Dorsheimer L, Günther S, Braun T, et al. Clonal Expansion of Endothelial Cells Contributes to Ischemia-Induced Neovascularization. Circ Res. 2018;122(5):670–7.

96. Jin S, Guerrero-Juarez CF, Zhang L, Chang I, Ramos R, Kuan C-H, et al. Inference and analysis of cell-cell communication using CellChat. Nature Communications. 2021;12(1):1088.

97. Pellet-Many C, Frankel P, Jia H, Zachary I. Neuropilins: structure, function and role in disease. Biochem J. 2008;411(2):211–26.

98. Yan Q, Sage EH. SPARC, a matricellular glycoprotein with important biological

functions. J Histochem Cytochem. 1999;47(12):1495–506.

99. Trombetta JM, Bradshaw AD. SPARC/osteonectin functions to maintain homeostasis of the collagenous extracellular matrix in the periodontal ligament. J Histochem Cytochem. 2010;58(10):871–9.

100. Chlenski A, Cohn SL. Modulation of matrix remodeling by SPARC in neoplastic progression. Seminars in Cell & Developmental Biology. 2010;21(1):55–65.

101. Thomas R, True LD, Bassuk JA, Lange PH, Vessella RL. Differential Expression of Osteonectin/SPARC during Human Prostate Cancer Progression1. Clinical Cancer Research. 2000;6(3):1140–9.

102. Lane TF, Iruela-Arispe ML, Johnson RS, Sage EH. SPARC is a source of copper-binding peptides that stimulate angiogenesis. J Cell Biol. 1994;125(4):929–43.

103. Hirota S, Imakita M, Kohri K, Ito A, Morii E, Adachi S, et al. Expression of osteopontin messenger RNA by macrophages in atherosclerotic plaques. A possible association with calcification. Am J Pathol. 1993;143(4):1003–8.

104. Rivera LB, Bradshaw AD, Brekken RA. The regulatory function of SPARC in vascular biology. Cell Mol Life Sci. 2011;68(19):3165–73.

105. Jin Y, Kim HP, Cao J, Zhang M, Ifedigbo E, Choi AM. Caveolin-1 regulates the secretion and cytoprotection of Cyr61 in hyperoxic cell death. Faseb j. 2009;23(2):341–50.

106. Albacete-Albacete L, Sánchez-Álvarez M, del Pozo MA. Extracellular Vesicles: An Emerging Mechanism Governing the Secretion and Biological Roles of Tenascin-C. Frontiers in Immunology. 2021;Volume 12 - 2021.

107. Sage EH, Reed M, Funk SE, Truong T, Steadele M, Puolakkainen P, et al. Cleavage of the matricellular protein SPARC by matrix metalloproteinase 3 produces polypeptides that

influence angiogenesis. J Biol Chem. 2003;278(39):37849–57.

108. Zhong ME, Chen Y, Xiao Y, Xu L, Zhang G, Lu J, et al. Serum extracellular vesicles contain SPARC and LRG1 as biomarkers of colon cancer and differ by tumour primary location. EBioMedicine. 2019;50:211–23.

109. Zivko C, Fuhrmann K, Fuhrmann G, Luciani P. Tracking matricellular protein SPARC in extracellular vesicles as a non-destructive method to evaluate lipid-based antifibrotic treatments. Communications Biology. 2022;5(1):1155.

110. Peng C, Xu H, Zhuang Q, Liu J, Ding Y, Tang Q, et al. Placenta-derived mesenchymal stem cells promote diabetic wound healing via exosomal protein interaction networks. Wound Repair Regen. 2024;32(5):638–51.

111. Rabouille C. Pathways of Unconventional Protein Secretion. Trends Cell Biol. 2017;27(3):230–40.

112. Suzuki J, Jin Z-G, Meoli DF, Matoba T, Berk BC. Cyclophilin A Is Secreted by a Vesicular Pathway in Vascular Smooth Muscle Cells. Circulation Research. 2006;98(6):811–7.

113. Kupprion C, Motamed K, Sage EH. SPARC (BM-40, osteonectin) inhibits the mitogenic effect of vascular endothelial growth factor on microvascular endothelial cells. J Biol Chem. 1998;273(45):29635–40.

114. Chlenski A, Liu S, Guerrero LJ, Yang Q, Tian Y, Salwen HR, et al. SPARC expression is associated with impaired tumor growth, inhibited angiogenesis and changes in the extracellular matrix. Int J Cancer. 2006;118(2):310–6.

115. Yunker CK, Golembieski W, Lemke N, Schultz CR, Cazacu S, Brodie C, et al. SPARC-induced increase in glioma matrix and decrease in vascularity are associated with reduced VEGF expression and secretion. Int J Cancer. 2008;122(12):2735–43.

116. Bhoopathi P, Chetty C, Gujrati M, Dinh DH, Rao JS, Lakka SS. The role of MMP-9 in the anti-angiogenic effect of secreted protein acidic and rich in cysteine. British Journal of Cancer. 2010;102(3):530–40.

117. Zhang JL, Chen GW, Liu YC, Wang PY, Wang X, Wan YL, et al. Secreted protein acidic and rich in cysteine (SPARC) suppresses angiogenesis by down-regulating the expression of VEGF and MMP-7 in gastric cancer. PLoS One. 2012;7(9):e44618.

118. Gorantla B, Bhoopathi P, Chetty C, Gogineni VR, Sailaja GS, Gondi CS, et al. Notch signaling regulates tumor-induced angiogenesis in SPARC-overexpressed neuroblastoma. Angiogenesis. 2013;16(1):85–100.

119. Boyineni J, Tanpure S, Gnanamony M, Antony R, Fernández KS, Lin J, et al. SPARC overexpression combined with radiation retards angiogenesis by suppressing VEGF-A via miR-410 in human neuroblastoma cells. Int J Oncol. 2016;49(4):1394–406.

120. Arnold S, Mira E, Muneer S, Korpanty G, Beck AW, Holloway SE, et al. Forced expression of MMP9 rescues the loss of angiogenesis and abrogates metastasis of pancreatic tumors triggered by the absence of host SPARC. Exp Biol Med (Maywood). 2008;233(7):860–73.

121. Arnold SA, Rivera LB, Miller AF, Carbon JG, Dineen SP, Xie Y, et al. Lack of host SPARC enhances vascular function and tumor spread in an orthotopic murine model of pancreatic carcinoma. Dis Model Mech. 2010;3(1-2):57–72.

122. Iruela-Arispe ML, Lane TF, Redmond D, Reilly M, Bolender RP, Kavanagh TJ, et al. Expression of SPARC during development of the chicken chorioallantoic membrane: evidence for regulated proteolysis in vivo. Molecular Biology of the Cell. 1995;6(3):327–43.

123. Nozaki M, Sakurai E, Raisler BJ, Baffi JZ, Witta J, Ogura Y, et al. Loss of SPARC-mediated VEGFR-1 suppression after injury reveals a novel antiangiogenic activity of VEGF-

A. J Clin Invest. 2006;116(2):422–9.

124. Takahashi M, Nagaretani H, Funahashi T, Nishizawa H, Maeda N, Kishida K, et al. The expression of SPARC in adipose tissue and its increased plasma concentration in patients with coronary artery disease. Obes Res. 2001;9(7):388–93.

125. Cydzik M, Abdul-Wahid A, Park S, Bourdeau A, Bowden K, Prodeus A, et al. Slow binding kinetics of secreted protein, acidic, rich in cysteine-VEGF interaction limit VEGF activation of VEGF receptor 2 and attenuate angiogenesis. The FASEB Journal. 2015;29(8):3493–505.

126. Fu Y, Tang M, Xiang X, Liu K, Xu X. Glucose affects cell viability, migration, angiogenesis and cellular adhesion of human retinal capillary endothelial cells via SPARC. Exp Ther Med. 2019;17(1):273–83.

127. Deng SK, Jin Y, Jin Y, Wang JF. SPARC induces M2 polarization of macrophages to promote proliferation, migration, and angiogenesis of cholangiocarcinoma cells. Neoplasma. 2022;69(5):1101–7.

128. Bradshaw AD, Puolakkainen P, Dasgupta J, Davidson JM, Wight TN, Helene Sage E. SPARC-null mice display abnormalities in the dermis characterized by decreased collagen fibril diameter and reduced tensile strength. J Invest Dermatol. 2003;120(6):949–55.

129. Reed MJ, Puolakkainen P, Lane TF, Dickerson D, Bornstein P, Sage EH. Differential expression of SPARC and thrombospondin 1 in wound repair: immunolocalization and in situ hybridization. J Histochem Cytochem. 1993;41(10):1467–77.

130. Sage H, Vernon RB, Decker J, Funk S, Iruela-Arispe ML. Distribution of the calcium-binding protein SPARC in tissues of embryonic and adult mice. J Histochem Cytochem. 1989;37(6):819–29.

131. Agah A, Kyriakides TR, Lawler J, Bornstein P. The lack of thrombospondin-1 (TSP1) dictates the course of wound healing in double-TSP1/TSP2-null mice. Am J Pathol. 2002;161(3):831–9.

132. Bornstein P, Agah A, Kyriakides TR. The role of thrombospondins 1 and 2 in the regulation of cell-matrix interactions, collagen fibril formation, and the response to injury. Int J Biochem Cell Biol. 2004;36(6):1115–25.

133. Dobaczewski M, Bujak M, Zymek P, Ren G, Entman ML, Frangogiannis NG. Extracellular matrix remodeling in canine and mouse myocardial infarcts. Cell Tissue Res. 2006;324(3):475–88.

134. Schellings MW, Vanhoutte D, Swinnen M, Cleutjens JP, Debets J, van Leeuwen RE, et al. Absence of SPARC results in increased cardiac rupture and dysfunction after acute myocardial infarction. J Exp Med. 2009;206(1):113–23.

135. McCurdy SM, Dai Q, Zhang J, Zamilpa R, Ramirez TA, Dayah T, et al. SPARC mediates early extracellular matrix remodeling following myocardial infarction. Am J Physiol Heart Circ Physiol. 2011;301(2):H497–505.

136. Komatsubara I, Murakami T, Kusachi S, Nakamura K, Hirohata S, Hayashi J, et al. Spatially and temporally different expression of osteonectin and osteopontin in the infarct zone of experimentally induced myocardial infarction in rats. Cardiovasc Pathol. 2003;12(4):186–94.

137. Hess A, Thackeray JT, Wollert KC, Bengel FM. Radionuclide Image-Guided Repair of the Heart. JACC: Cardiovascular Imaging. 2020;13(11):2415–29.

138. Francki A, McClure TD, Brekken RA, Motamed K, Murri C, Wang T, et al. SPARC regulates TGF-beta1-dependent signaling in primary glomerular mesangial cells. J Cell Biochem. 2004;91(5):915–25.

139. Ikeuchi M, Tsutsui H, Shiomi T, Matsusaka H, Matsushima S, Wen J, et al. Inhibition of TGF-beta signaling exacerbates early cardiac dysfunction but prevents late remodeling after infarction. Cardiovasc Res. 2004;64(3):526–35.

140. Okada H, Takemura G, Kosai K, Li Y, Takahashi T, Esaki M, et al. Postinfarction gene therapy against transforming growth factor-beta signal modulates infarct tissue dynamics and attenuates left ventricular remodeling and heart failure. Circulation. 2005;111(19):2430–7.

141. Wrana JL, Overall CM, Sodek J. Regulation of the expression of a secreted acidic protein rich in cysteine (SPARC) in human fibroblasts by transforming growth factor beta. Comparison of transcriptional and post-transcriptional control with fibronectin and type I collagen. Eur J Biochem. 1991;197(2):519–28.

142. Rivera LB, Brekken RA. SPARC promotes pericyte recruitment via inhibition of endoglin-dependent TGF-β1 activity. J Cell Biol. 2011;193(7):1305–19.

143. Cunha SI, Magnusson PU, Dejana E, Lampugnani MG. Deregulated TGF-β/BMP Signaling in Vascular Malformations. Circulation Research. 2017;121(8):981–99.

144. Goumans M-J, Liu Z, ten Dijke P. TGF-β signaling in vascular biology and dysfunction. Cell Research. 2009;19(1):116–27.

145. Deng Z, Fan T, Xiao C, Tian H, Zheng Y, Li C, et al. TGF-β signaling in health, disease and therapeutics. Signal Transduction and Targeted Therapy. 2024;9(1):61.

146. Sorensen LK, Brooke BS, Li DY, Urness LD. Loss of distinct arterial and venous boundaries in mice lacking endoglin, a vascular-specific TGFbeta coreceptor. Dev Biol. 2003;261(1):235–50.

147. Miquerol L, Meysen S, Mangoni M, Bois P, van Rijen HV, Abran P, et al. Architectural and functional asymmetry of the His-Purkinje system of the murine heart. Cardiovasc Res.

2004;63(1):77–86.

148. Large CL, Vitali HE, Whatley JD, Red-Horse K, Sharma B. In Vitro Model of Coronary Angiogenesis. J Vis Exp. 2020(157).

149. Maruyama K, Naemura K, Yoshihara K, Imanaka-Yoshida K, Kurihara H, Miyagawa-Tomita S. Surgical protocol for permanent ligation of the left anterior descending coronary artery in mice to generate a model of myocardial infarction. STAR Protoc. 2021;2(3):100775.

150. Livak KJ, Schmittgen TD. Analysis of relative gene expression data using real-time quantitative PCR and the 2(-Delta Delta C(T)) Method. Methods. 2001;25(4):402–8.

151. Mazzolini G, Atorrasagasti C, Onorato A, Peixoto E, Schlattjan M, Sowa J-P, et al. SPARC expression is associated with hepatic injury in rodents and humans with non-alcoholic fatty liver disease. Scientific Reports. 2018;8(1):725.

152. Bio-Rad. Image Analysis and Quantitation for Western Blotting 2021 [cited 2025. Available from: https://www.bio-rad.com/en-uk/applications-technologies/image-analysis-quantitation-for-western-blotting?ID=PQEERM9V5F6X.

153. Schindelin J, Arganda-Carreras I, Frise E, Kaynig V, Longair M, Pietzsch T, et al. Fiji: an open-source platform for biological-image analysis. Nat Methods. 2012;9(7):676–82.

154. Musy M, Flaherty K, Raspopovic J, Robert-Moreno A, Richtsmeier JT, Sharpe J. A quantitative method for staging mouse embryos based on limb morphometry. Development. 2018;145(7).

155. Zudaire E, Gambardella L, Kurcz C, Vermeren S. A Computational Tool for Quantitative Analysis of Vascular Networks. PLOS ONE. 2011;6(11):e27385.

156. Calcagno DM, Taghdiri N, Ninh VK, Mesfin JM, Toomu A, Sehgal R, et al. Single-cell and spatial transcriptomics of the infarcted heart define the dynamic onset of the border

zone in response to mechanical destabilization. Nat Cardiovasc Res. 2022;1(11):1039–55.

157. Lumanto P. MS, Nakib D. QuPath Stain Quantification of Whole Tissue by Percent Area: protocols.io; 2025 [Available from: https://www.protocols.io/view/qupath-stain-quantification-of-whole-tissue-by-per-6qpvrw64olmk/v1?step=5.

158. Beyer S, Kelly RG, Miquerol L. Inducible Cx40-Cre expression in the cardiac conduction system and arterial endothelial cells. Genesis. 2011;49(2):83–91.

159. Zhou B, Pu WT. Genetic Cre-loxP assessment of epicardial cell fate using Wt1-driven Cre alleles. Circ Res. 2012;111(11):e276–80.

160. Li P, Cavallero S, Gu Y, Chen TH, Hughes J, Hassan AB, et al. IGF signaling directs ventricular cardiomyocyte proliferation during embryonic heart development. Development. 2011;138(9):1795–805.

161. Bienz M. beta-Catenin: a pivot between cell adhesion and Wnt signalling. Curr Biol. 2005;15(2):R64–7.

162. Zeisberg M, Neilson EG. Biomarkers for epithelial-mesenchymal transitions. J Clin Invest. 2009;119(6):1429–37.

163. Hay ED. The mesenchymal cell, its role in the embryo, and the remarkable signaling mechanisms that create it. Dev Dyn. 2005;233(3):706–20.

164. von Gise A, Zhou B, Honor LB, Ma Q, Petryk A, Pu WT. WT1 regulates epicardial epithelial to mesenchymal transition through β-catenin and retinoic acid signaling pathways. Dev Biol. 2011;356(2):421–31.

165. Lane TF, Sage EH. The biology of SPARC, a protein that modulates cell-matrix interactions. Faseb j. 1994;8(2):163–73.

166. Herbert SP, Stainier DY. Molecular control of endothelial cell behaviour during blood

vessel morphogenesis. Nat Rev Mol Cell Biol. 2011;12(9):551–64.

167. Phng LK, Gerhardt H. Angiogenesis: a team effort coordinated by notch. Dev Cell. 2009;16(2):196–208.

168. Kato Y, Lewalle JM, Baba Y, Tsukuda M, Sakai N, Baba M, et al. Induction of SPARC by VEGF in human vascular endothelial cells. Biochem Biophys Res Commun. 2001;287(2):422–6.

169. Virag JI, Murry CE. Myofibroblast and Endothelial Cell Proliferation during Murine Myocardial Infarct Repair. The American Journal of Pathology. 2003;163(6):2433–40.

170. Wei K, Serpooshan V, Hurtado C, Diez-Cuñado M, Zhao M, Maruyama S, et al. Epicardial FSTL1 reconstitution regenerates the adult mammalian heart. Nature. 2015;525(7570):479–85.

171. Schiemann BJ, Neil JR, Schiemann WP. SPARC inhibits epithelial cell proliferation in part through stimulation of the transforming growth factor-beta-signaling system. Mol Biol Cell. 2003;14(10):3977–88.

172. Cleutjens JP, Verluyten MJ, Smiths JF, Daemen MJ. Collagen remodeling after myocardial infarction in the rat heart. Am J Pathol. 1995;147(2):325–38.

173. Venugopal H, Hanna A, Humeres C, Frangogiannis NG. Properties and Functions of Fibroblasts and Myofibroblasts in Myocardial Infarction. Cells. 2022;11(9).

174. Smart N, Riley PR. The epicardium as a candidate for heart regeneration. Future Cardiol. 2012;8(1):53–69.

175. Bradshaw AD, Sage EH. SPARC, a matricellular protein that functions in cellular differentiation and tissue response to injury. J Clin Invest. 2001;107(9):1049–54.

176. Dronkers E, Wauters MMM, Goumans MJ, Smits AM. Epicardial TGFβ and BMP

Signaling in Cardiac Regeneration: What Lesson Can We Learn from the Developing Heart? Biomolecules. 2020;10(3).

177. Stary M, Pasteiner W, Summer A, Hrdina A, Eger A, Weitzer G. Parietal endoderm secreted SPARC promotes early cardiomyogenesis in vitro. Exp Cell Res. 2005;310(2):331–43.

178. Sage H, Johnson C, Bornstein P. Characterization of a novel serum albumin-binding glycoprotein secreted by endothelial cells in culture. J Biol Chem. 1984;259(6):3993–4007.

179. Tyree B. The partial degradation of osteonectin by a bone-derived metalloprotease enhances binding to type I collagen. J Bone Miner Res. 1989;4(6):877–83.

180. Page AE, Hayman AR, Andersson LMB, Chambers TJ, Warburton MJ. Degradation of bone matrix proteins by osteoclast cathepsins. International Journal of Biochemistry. 1993;25(4):545–50.

181. Sundberg M. Mass Spectrometry and Affinity Based Methods for Analysis of Proteins and Proteomes: Uppsala Universitet; 2015.

182. Ewan LC, Jopling HM, Jia H, Mittar S, Bagherzadeh A, Howell GJ, et al. Intrinsic tyrosine kinase activity is required for vascular endothelial growth factor receptor 2 ubiquitination, sorting and degradation in endothelial cells. Traffic. 2006;7(9):1270–82.

183. Lamalice L, Houle F, Huot J. Phosphorylation of Tyr1214 within VEGFR-2 triggers the recruitment of Nck and activation of Fyn leading to SAPK2/p38 activation and endothelial cell migration in response to VEGF. J Biol Chem. 2006;281(45):34009–20.

184. Yao X, Ping Y, Liu Y, Chen K, Yoshimura T, Liu M, et al. Vascular endothelial growth factor receptor 2 (VEGFR-2) plays a key role in vasculogenic mimicry formation, neovascularization and tumor initiation by Glioma stem-like cells. PLoS One. 2013;8(3):e57188.

185. Bradshaw AD. The role of SPARC in extracellular matrix assembly. J Cell Commun Signal. 2009;3(3-4):239–46.

186. Ponticos M, Smith BD. Extracellular matrix synthesis in vascular disease: hypertension, and atherosclerosis. J Biomed Res. 2014;28(1):25–39.

187. Hohenester E, Sasaki T, Giudici C, Farndale RW, Bächinger HP. Structural basis of sequence-specific collagen recognition by SPARC. Proceedings of the National Academy of Sciences. 2008;105(47):18273–7.

188. Houck KA, Leung DW, Rowland AM, Winer J, Ferrara N. Dual regulation of vascular endothelial growth factor bioavailability by genetic and proteolytic mechanisms. J Biol Chem. 1992;267(36):26031–7.

189. Alkabie S, Basivireddy J, Zhou L, Roskams J, Rieckmann P, Quandt JA. SPARC expression by cerebral microvascular endothelial cells in vitro and its influence on blood-brain barrier properties. Journal of Neuroinflammation. 2016;13(1):225.

190. Goumans M-J, Zwijsen A, Rooijen MAv, Huylebroeck D, Roelen BAJ, Mummery CL. Transforming Growth Factor-β signalling in extraembryonic mesoderm is required for yolk sac vasculogenesis in mice. Development. 1999;126(16):3473–83.

191. Trombetta-Esilva J, Bradshaw AD. The Function of SPARC as a Mediator of Fibrosis. Open Rheumatol J. 2012;6:146–55.

192. Tai IT, Tang MJ. SPARC in cancer biology: its role in cancer progression and potential for therapy. Drug Resist Updat. 2008;11(6):231–46.

193. Brown TJ, Shaw PA, Karp X, Huynh MH, Begley H, Ringuette MJ. Activation of SPARC expression in reactive stroma associated with human epithelial ovarian cancer. Gynecol Oncol. 1999;75(1):25–33.

194. Guerrero P, McCarty J. TGF-β Activation and Signaling in Angiogenesis. In: Simionescu DT, Simionescu A, editors. Physiologic and Pathologic Angiogenesis - Signaling Mechanisms and Targeted Therapy. London: IntechOpen; 2017.

195. Van Geest RJ, Klaassen I, Vogels IM, Van Noorden CJ, Schlingemann RO. Differential TGF-{beta} signaling in retinal vascular cells: a role in diabetic retinopathy? Invest Ophthalmol Vis Sci. 2010;51(4):1857–65.

196. Tual-Chalot S, Mahmoud M, Allinson KR, Redgrave RE, Zhai Z, Oh SP, et al. Endothelial Depletion of Acvrl1 in Mice Leads to Arteriovenous Malformations Associated with Reduced Endoglin Expression. PLOS ONE. 2014;9(6):e98646.

197. Larrivée B, Prahst C, Gordon E, del Toro R, Mathivet T, Duarte A, et al. ALK1 signaling inhibits angiogenesis by cooperating with the Notch pathway. Dev Cell. 2012;22(3):489–500.

198. Humeres C, Venugopal H, Frangogiannis NG. Smad-dependent pathways in the infarcted and failing heart. Curr Opin Pharmacol. 2022;64:102207.

199. Majesky MW, Lindner V, Twardzik DR, Schwartz SM, Reidy MA. Production of transforming growth factor beta 1 during repair of arterial injury. The Journal of clinical investigation. 1991;88(3):904–10.

200. Schulick AH, Taylor AJ, Zuo W, Qiu C-b, Dong G, Woodward RN, et al. Overexpression of transforming growth factor β1 in arterial endothelium causes hyperplasia, apoptosis, and cartilaginous metaplasia. Proceedings of the National Academy of Sciences. 1998;95(12):6983–8.

201. Suwanabol PA, Seedial SM, Shi X, Zhang F, Yamanouchi D, Roenneburg D, et al. Transforming growth factor-β increases vascular smooth muscle cell proliferation through the Smad3 and extracellular signal-regulated kinase mitogen-activated protein kinases

pathways. Journal of vascular surgery. 2012;56(2):446–54. e1.

202. Tsai S, Hollenbeck ST, Ryer EJ, Edlin R, Yamanouchi D, Kundi R, et al. TGF-β through Smad3 signaling stimulates vascular smooth muscle cell proliferation and neointimal formation. American Journal of Physiology-Heart and Circulatory Physiology. 2009;297(2):H540–H9.

203. Mao X, DeBenedittis P, Sun Y, Chen J, Yuan K, Jiao K, et al. Vascular smooth muscle cell Smad4 gene is important for mouse vascular development. Arteriosclerosis, thrombosis, and vascular biology. 2012;32(9):2171–7.

204. McDonald LT, Zile MR, Zhang Y, Van Laer AO, Baicu CF, Stroud RE, et al. Increased macrophage-derived SPARC precedes collagen deposition in myocardial fibrosis. Am J Physiol Heart Circ Physiol. 2018;315(1):H92–h100.

205. Schirmer H, Lunde P, Rasmussen K. Prevalence of left ventricular hypertrophy in a general population; The Tromsø Study. Eur Heart J. 1999;20(6):429–38.

206. Renier N, Wu Z, Simon David J, Yang J, Ariel P, Tessier-Lavigne M. iDISCO: A Simple, Rapid Method to Immunolabel Large Tissue Samples for Volume Imaging. Cell. 2014;159(4):896–910.

207. Lane TF, Sage EH. Functional mapping of SPARC: peptides from two distinct Ca+(+)-binding sites modulate cell shape. J Cell Biol. 1990;111(6 Pt 2):3065–76.

208. McCluskey AJ, Poon GM, Gariépy J. A rapid and universal tandem-purification strategy for recombinant proteins. Protein Sci. 2007;16(12):2726–32.

209. Ribeiro SM, Poczatek M, Schultz-Cherry S, Villain M, Murphy-Ullrich JE. The activation sequence of thrombospondin-1 interacts with the latency-associated peptide to regulate activation of latent transforming growth factor-beta. J Biol Chem. 1999;274(19):13586–93.

210. Schultz-Cherry S, Chen H, Mosher DF, Misenheimer TM, Krutzsch HC, Roberts DD, et al. Regulation of Transforming Growth Factor-β Activation by Discrete Sequences of Thrombospondin 1 (∗). Journal of Biological Chemistry. 1995;270(13):7304–10.

211. Deckx S, Johnson DM, Rienks M, Carai P, Van Deel E, Van der Velden J, et al. Extracellular SPARC increases cardiomyocyte contraction during health and disease. PLoS One. 2019;14(4):e0209534.

212. Farache Trajano L, Smart N. Immunomodulation for optimal cardiac regeneration: insights from comparative analyses. npj Regenerative Medicine. 2021;6(1):8.